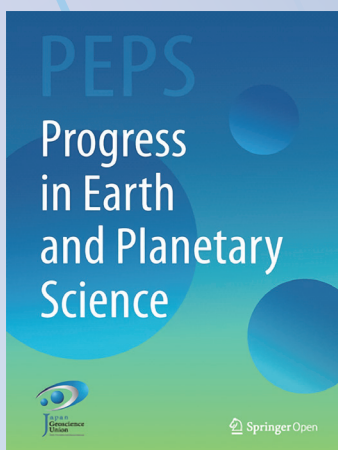


The collection of review articles

Progress in Earth and Planetary Science

(the 1st edition: published from April 2014 to January 2021)



Japan Geoscience Union (JpGU) Open Access journal

<https://progearthplanetsci.springeropen.com/>



CONTENTS

1. Space and planetary sciences

Review of the accomplishments of Mid-latitude Super Dual Auroral Radar Network (SuperDARN) HF Radars	2
Scientific innovations from the Mars aerosol optical depth based on satellite data with a temporal resolution of hours	3
Simulation study of near-Earth space disturbances: 1. Magnetic storms	4
Simulation study of near-Earth space disturbances: 2. Auroral substorms	5
Day-to-day and short-term variabilities in the equatorial plasma bubble/spread F irregularity seeding and development	6
Asteroid Ryugu before the Hayabusa2 encounter	7
Review of the generation mechanisms of post-midnight irregularities in the equatorial and low-latitude ionosphere	8
Lightning detection on Venus: a critical review	9
Post-sunset rise of equatorial <i>F</i> layer—or upwelling growth?	10
Effects of the postsunset vertical plasma drift on the generation of equatorial spread F	11
A review on the numerical simulation of equatorial plasma bubbles toward scintillation evaluation and forecasting	12
Mars core structure — concise review and anticipated insights from InSight	13
Extreme geomagnetically induced currents	14
Magnetohydrodynamics Modeling of Coronal Magnetic Field and Solar Eruptions Based on the Photospheric Magnetic Field	15
MF and HF radar techniques for investigating the dynamics and structure of the 50 to 110 km height region: a review	16
Advancing the understanding of the Sun-Earth interaction - the Climate and Weather of the Sun-Earth System (CAWSES) II Program	17
The science case for the EISCAT_3D radar	18
Short-term variability of the Sun-Earth system: an overview of progress made during the CAWSES-II period	19
eScience and Informatics for International Science Programs	20
What is the solar influence on climate? Overview of activities during CAWSES-II	21
Response of the mesosphere-thermosphere-ionosphere system to global change – CAWSES-II contribution	22
The geospace response to variable inputs from the lower atmosphere: A review of the progress made by Task Group 4 of CAWSES-II	23

2. Atmospheric and hydrospheric sciences

Marine microplastics as vectors of major ocean pollutants and its hazards to the marine ecosystem and humans	26
Applications of soft computing models for predicting sea surface temperature: a comprehensive review and assessment	27
Two decades of Earth system modeling with an emphasis on Model for Interdisciplinary Research on Climate (MIROC)	28
d4PDF: large-ensemble and high-resolution climate simulations for global warming risk assessment	29

DYAMOND: The DYNAMICS of the Atmospheric general circulation Modeled On Non-hydrostatic Domains ...	30
Toward reduction of the uncertainties in climate sensitivity due to cloud processes using a global non-hydrostatic atmospheric model	31
Maritime continent coastlines controlling Earth's climate	32
Outcomes and challenges of global high-resolution non-hydrostatic atmospheric simulations using the K computer	33
A review of atmospheric chemistry observation at mountain sites	34
A review of progress towards understanding the transient global mean surface temperature response to radiative perturbation	35
Overview of the development of the Aerosol Loading Interface for Cloud microphysics In Simulation (ALICIS)	36
The dynamics of the mesosphere and lower thermosphere: a brief review	37
Modeling in Earth system science up to and beyond IPCC AR5	38
The Non-hydrostatic Icosahedral Atmospheric Model: Description and Development	39

3. Human geosciences • Biogeosciences

Arsenic cycling in the Earth's crust and hydrosphere: interaction between naturally occurring arsenic and human activities	42
Perspective on the response of marine calcifiers to global warming and ocean acidification – Behavior of corals and foraminifera in a high CO ₂ world “hot house”	43
Theoretical constraints of physical and chemical properties of hydrothermal fluids on variations in chemolithotrophic microbial communities in seafloor hydrothermal systems.	44
Biochemical and physiological bases for the use of carbon and nitrogen isotopes in environmental and ecological studies	45

4. Solid earth sciences

Visualizing heterogeneities of earthquake hypocenter catalogs: modeling, analysis, and compensation	48
Strength models of the terrestrial planets and implications for their lithospheric structure and evolution	49
Deep mantle melting, global water circulation and its implications for the stability of the ocean mass	50
A coupled core-mantle evolution: Review and future prospects	51
Some remarks on hydrogen-assisted electrical conductivity in olivine and other minerals	52
Detection of repeating earthquakes and their application in characterizing slow fault slip	53
Nitrogen in the Earth: abundance and transport	54
Earthquake Early Warning: what does “seconds before a strong hit” mean?	55
Redox-controlled mechanisms of C and H isotope fractionation between silicate melt and COH fluid in the Earth's interior	56
Nonlinear dynamical analysis of GNSS data: quantification, precursors and synchronization	57
Structural context and variation of ocean plate stratigraphy, Franciscan Complex, California: insight into mélange origins and subduction-accretion processes	58
Seismic imaging of slab metamorphism and genesis of intermediate-depth intraslab earthquakes	59
Imaging in 3D under pressure: a decade of high-pressure X-ray microtomography development at GSECARS	60
Philippine Sea Plate inception, evolution and consumption with special emphasis on the early stages of Izu-Bonin-Mariana subduction	61
Mantle hydration and Cl-rich fluids in the subduction forearc	62

Iron snow, crystal floats, and inner-core growth: modes of core solidification and implications for dynamos in terrestrial planets and moons	63
Liquid Sodium Models of the Earth's Core	64
Towards more realistic core-mantle boundary heat flux patterns: a source of diversity in planetary dynamos	65
Sound velocity of hcp-Fe at high pressure: experimental constraints, extrapolations and comparison with seismic models	66
Earthquake faulting in subduction zones: insights from fault rocks in accretionary prisms	67
Water-melt interaction in hydrous magmatic systems at high temperature and pressure	68

5. Interdisciplinary research

Coupling library Jcup3: its philosophy and application	70
Morphometric measurements of bedrock rivers at different spatial scales and applications to geomorphological heritage research	71
Northern Eurasia Future Initiative (NEFI): facing the challenges and pathways of global change in the twenty-first century	72
Cenozoic sedimentary records of climate-tectonic coupling in the Western Himalaya	73
Transitional changes in microfossil assemblages in the Japan Sea from the Late Pliocene to Early Pleistocene related to global climatic and local tectonic events	74
Evolution and variability of the Asian monsoon and its potential linkage with uplift of the Himalaya and Tibetan Plateau	75
Geochemical approaches to the quantification of dispersed volcanic ash in marine sediment	76
Sea surface temperature proxies (alkenones, foraminiferal Mg/Ca, and planktonic foraminiferal assemblage) and their implications in the Okinawa Trough	77
Marine tephra in the Japan Sea sediments as a tool for paleoceanography and paleoclimatology	78
The Pliocene to Recent History of the Kuroshio and Tsushima Currents: a multi-proxy approach	79

Review

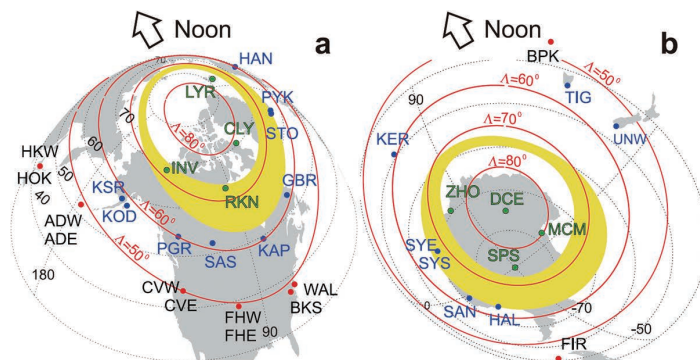
Space and planetary sciences

Review of the accomplishments of Mid-latitude Super Dual Auroral Radar Network (SuperDARN) HF Radars

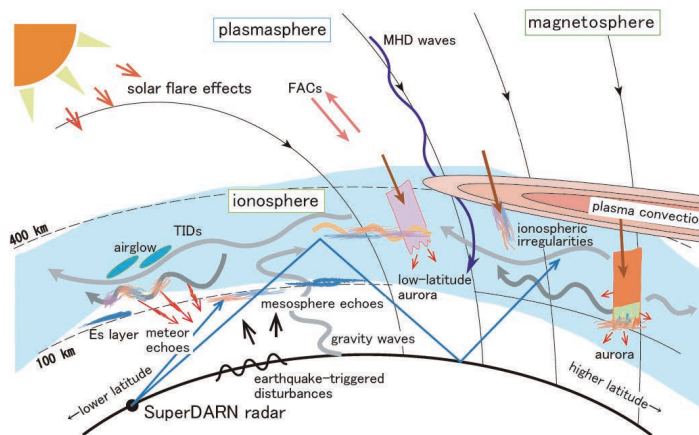
Nishitani N, Ruohoniemi JM, Lester M, Baker JBH, Koustov AV, Shepherd SG, Chisham G, Hori T, Thomas EG, Makarevich RA, Marchaudon A, Ponomarenko P, Wild JA, Milan SE, Bristow WA, Devlin J, Miller E, Greenwald RA, Ogawa T, Kikuchi T

[Keywords] Mid-latitude SuperDARN, Ionosphere, Magnetosphere, Convection, Ionospheric irregularities, HF propagation analysis, Ion-neutral interactions, MHD waves

The Super Dual Auroral Radar Network (SuperDARN) is a network of high-frequency (HF) radars located in the high- and mid-latitude regions of both hemispheres that is operated under international cooperation. The network was originally designed for monitoring the dynamics of the ionosphere and upper atmosphere in the high-latitude regions. However, over the last approximately 15 years, SuperDARN has expanded into the mid-latitude regions. With radar coverage that now extends continuously from auroral to sub-auroral and mid-latitudes, a wide variety of new scientific findings have been obtained. In this paper, the background of mid-latitude SuperDARN is presented at first. Then, the accomplishments made with mid-latitude SuperDARN radars are reviewed in five specified scientific and technical areas: convection, ionospheric irregularities, HF propagation analysis, ion-neutral interactions, and magnetohydrodynamic (MHD) waves. Finally, the present status of mid-latitude SuperDARN is updated and directions for future research are discussed.



Schematic plots showing the a Northern and b Southern Hemisphere SuperDARN radar locations with respect to the auroral oval. The model auroral oval (yellow) for moderately disturbed conditions is plotted with the SuperDARN radar locations identified in green type and green closed circles (polar cap latitudes), blue type and blue closed circles (auroral latitudes), and black type and red closed circles (mid-latitude radars).



Schematic illustration of natural phenomena which can be studied by SuperDARN radars.

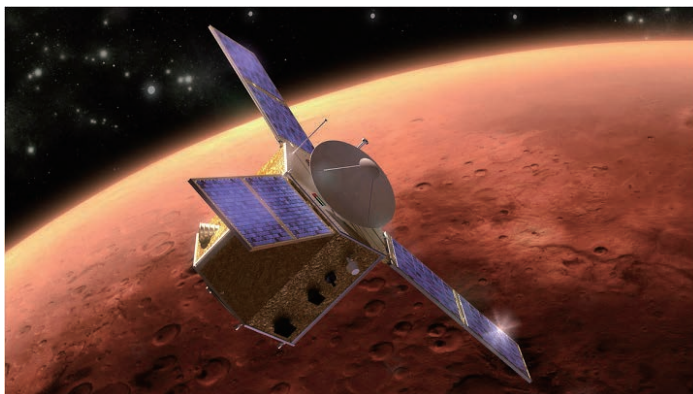


Scientific innovations from the Mars aerosol optical depth based on satellite data with a temporal resolution of hours

Gebhardt C, Abuelgasim A.

[Keywords] ExoMars Trace Gas Orbiter (TGO), Emirates Mars Mission (EMM), Mars stationary satellites, Mars atmosphere, Aerosol optical depth, Dust, Water ice clouds, Mars climatology, Mars numerical weather forecasting, Data assimilation

The ExoMars Trace Gas Orbiter (TGO), Emirates Mars Mission (EMM), and possible future Mars stationary satellite(s) will provide innovative data products on the optical depth of dust and water ice clouds in the Martian atmosphere with a temporal resolution of hours. The science phase of TGO has begun in April 2018, and the EMM science operation is scheduled to start in 2021. In this work, the relationship between TGO, EMM, and precursor missions/instruments is analyzed based on the obtained data products. This is followed by discussing



the foreseen innovation from the latter in the fields of Martian climatology and numerical weather forecasting.

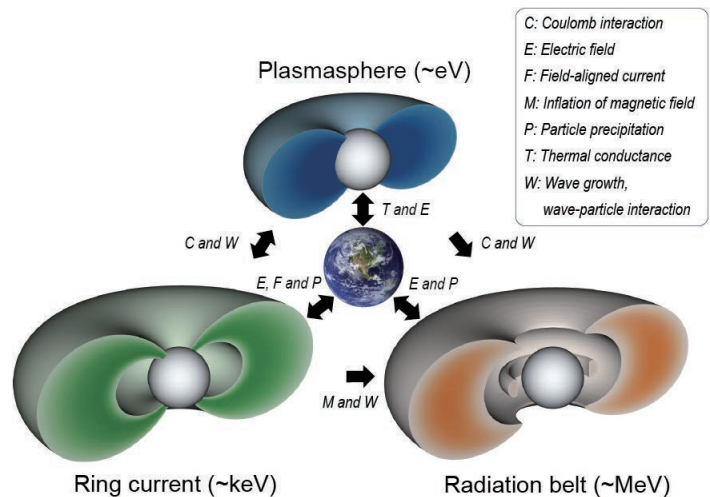


Simulation study of near-Earth space disturbances: 1. Magnetic storms

Ebihara Y.

[Keywords] Magnetic storms, Computer simulation, Magnetosphere, Ionosphere, Inner magnetosphere, and Ring current.

A magnetic storm is the world-wide geomagnetic disturbance taking place in near-Earth space environment, lasting for a few days. Geomagnetic fields can be depressed by $\sim 1\%$ on the ground for large magnetic storms. The prime cause of the long-lasting, world-wide geomagnetic disturbance is the development of the ring current that surrounds the Earth. The ring current is an electric current carried by charged particles. Thus, the growth and decay of the ring current correspond to accumulation and loss of the ring current particles, respectively. The ring current is strong enough to modulate near-Earth space environment, and leads to many observable effects. In this sense, the ring current can be regarded as an important mediator in the near-Earth space environment. Here, the dynamics and structure of the ring current and its active role are briefly reviewed on the basis of numerical simulation results.



Cross energy and cross region coupling in the inner magnetosphere and the ionosphere.

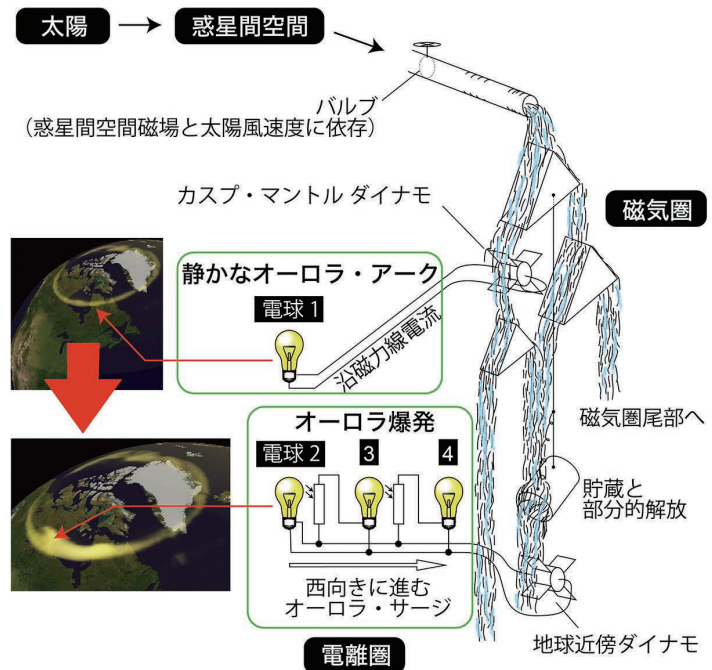


Simulation study of near-Earth space disturbances: 2. Auroral substorms

Yusuke Ebihara

[Keywords] Substorm, Aurora, Computer simulation, Magnetosphere, and Ionosphere.

A substorm is a transient phenomenon that lasts for only 1–2 h. One significant manifestation of the substorm is a sudden brightening of the aurora on the nightside. Simultaneously, the auroral electrojets are abruptly intensified in the ionosphere, disturbing the geomagnetic field in the polar region. The near-Earth space environment is highly disturbed, which manifests as an earthward fast flow of plasma, a sudden change in the magnetic field, or a sudden increase in hot plasma. Such disturbances are known to severely affect human society. The ultimate cause of the disturbances is the solar wind, but an explanation of the chain of processes leading from solar wind to the ionosphere is problematic. Here, the evolution of the auroral substorm is reviewed based on the results of a global magnetohydrodynamics (MHD) simulation, called a REProduce Plasma Universe (REPPU) code. The REPPU code is shown to reproduce many aspects of the auroral substorms and to be useful for understanding the primary chain processes from the solar wind to the ionosphere.



Conceptual illustration of possible chain reaction of an auroral substorm in terms of energy transfer from the solar wind to the ionosphere.

The REPPU code is shown to reproduce many aspects of the auroral substorms and to be useful for understanding the primary chain processes from the solar wind to the ionosphere.



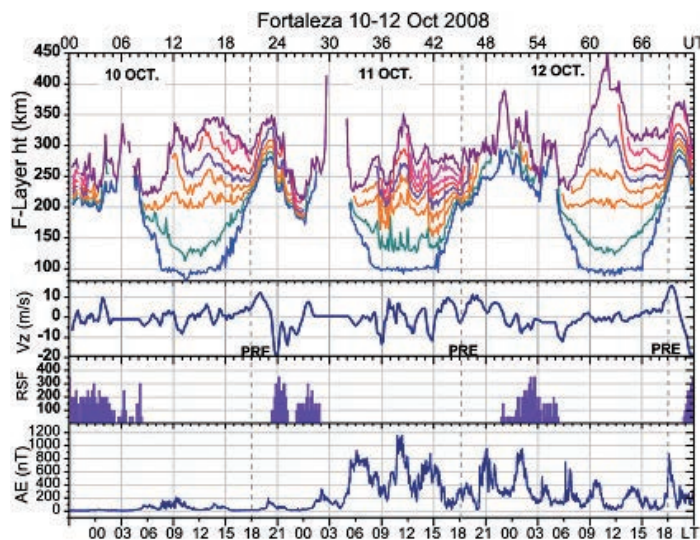
Day-to-day and short-term variabilities in the equatorial plasma bubble/spread F irregularity seeding and development

Mangalathayil Ali Abdu

[Keywords] Equatorial ionosphere, Plasma bubbles/spread F irregularities, Prereversal vertical drift, Prompt penetration electric field, Gravity waves, Trans-equatorial wind, Planetary/Kelvin waves, ESF/EPB short-term variability

The background ionospheric conditions shaped by sunset electrodynamic processes are responsible for the development of equatorial plasma bubble (EPB)/equatorial spread F (ESF) irregularities of the post-sunset ionosphere. Distinct conditions exist for the EPB/ESF development also at later hours of the night. The plasma instability growth leading to EPB generation is dependent on the basic precursor conditions defined by the well-known parameters: the evening prereversal enhancement in vertical plasma drift (PRE), wave structure in plasma density and polarization electric field required to initiate/seed the instability, and the F layer bottom side density gradient, as a

significant factor in controlling the growth rate. Competing roles of the zonal versus meridional thermospheric winds additionally control their development. Statistical as well as case studies have addressed aspects of the EPB development and occurrence under different geophysical conditions, generally focusing attention on any one of the above specific parameters. Little is known regarding the relative importance of concurrent presence of the precursor parameters (mentioned above) in shaping a given event. A large degree of day-to-day variability in these parameters arise from different sources of forcing, such as upward propagating atmospheric waves, and magnetic disturbance time electric fields in the form of prompt penetration and disturbance dynamo electric fields that often contribute to the widely observed short-term variabilities in EPB development and dynamics. In this paper, we will present and discuss some important aspects of the EPB/ESF short-term variability, focusing attention on their enhanced development, or suppression and, wherever possible, highlighting also the relative roles of the precursor parameters in such variability.

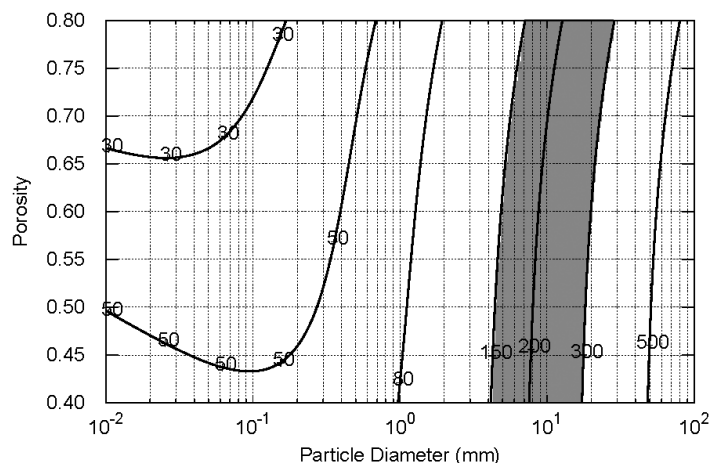


Asteroid Ryugu before the Hayabusa2 encounter

Wada K, Grott M, Michel P, Walsh K, Barucci A, Biele J, Blum J, Ernst C, Grundmann J, Gundlach B, Hagermann A, Hamm M, Jutzi M, Kim M, Kührt E, Le Corre L, Libourel G, Lichtenheldt R, Maturilli A, Messenger S, Michikami T, Miyamoto H, Mottola S, Müller T, Nakamura A, Nittler L, Ogawa K, Okada T, Palomba E, Sakatani N, Schröder S, Senshu H, Takir D, Zolensky M and International Regolith Science Group (IRSG) in Hayabusa2 project

[Keywords] Hayabusa2, Ryugu, Asteroids, Regolith, Physical properties

Asteroid (162173) Ryugu is the target object of Hayabusa2, an asteroid exploration and sample return mission led by Japan Aerospace Exploration Agency (JAXA). Ground-based observations indicate that Ryugu is a C-type near-Earth asteroid with a diameter of less than 1 km, but the knowledge of its detailed properties is very limited prior to Hayabusa2 observation. This paper summarizes our best understanding of the physical and dynamical properties of Ryugu based on ground-based remote sensing and theoretical modeling before the Hayabusa2's arrival at the asteroid. This information is used to construct a design reference model of the asteroid that is used for the formulation of mission operation plans in advance of asteroid arrival. Particular attention is given to the surface properties of Ryugu that are relevant to sample acquisition. This reference model helps readers to appropriately interpret the data that will be directly obtained by Hayabusa2 and promotes scientific studies not only for Ryugu itself and other small bodies but also for the solar system evolution that small bodies shed light on.



Contour plot of thermal inertia (in units of $J m^{-2} s^{-1/2} K^{-1}$) as a function of typical particle diameter and porosity (see text for the regolith parameters assumed in the calculation). The gray-filled region indicates the thermal inertia range estimated for Ryugu by ground-based observations (Müller et al. 2017). From this figure, we can estimate a typical particle size for the Ryugu regolith.

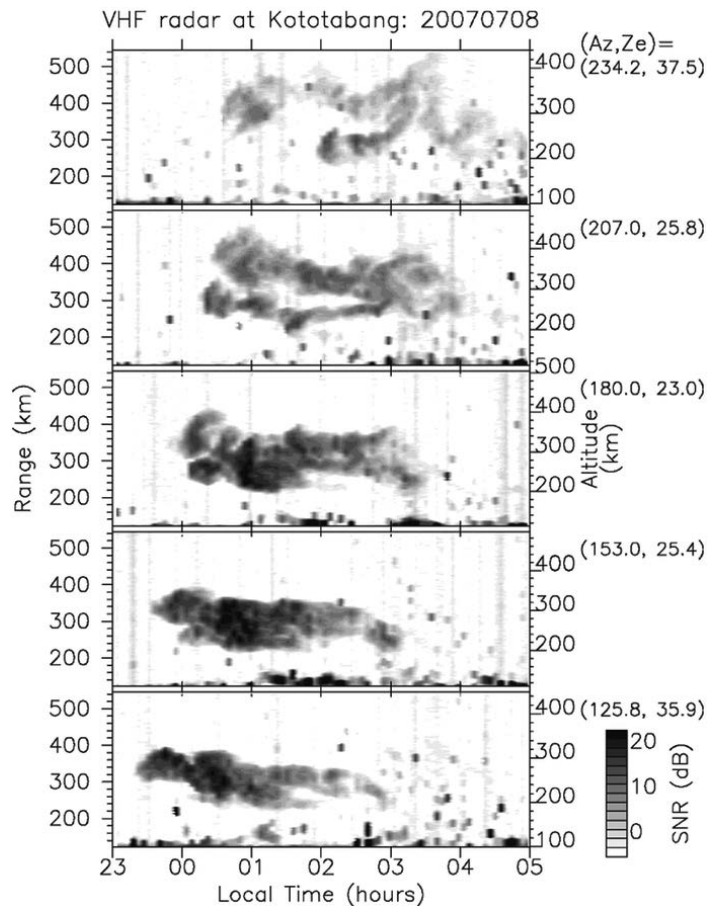


Review of the generation mechanisms of post-midnight irregularities in the equatorial and low-latitude ionosphere

Otsuka Y

[Keywords] Equatorial ionosphere, Ionospheric irregularity, Rayleigh–Taylor instability, Plasma bubble

This paper provides a brief review of ionospheric irregularities that occur in magnetically equatorial and low-latitude regions post-midnight during low solar activity periods. Ionospheric irregularities can occur in equatorial plasma bubbles. Plasma bubbles are well-known to frequently occur post-sunset when the solar terminator is nearly parallel to the geomagnetic field lines (during equinoxes at the longitude where the declination of the geomagnetic field is almost equal to zero and near the December solstice at the longitude where the declination is tilted westward), especially during high solar activity conditions via the Rayleigh–Taylor instability. However, recent observations during a solar minimum period show a high occurrence rate of irregularities post-midnight around the June solstice. The mechanisms for generating the post-midnight irregularities are still unknown, but two candidates have been proposed. One candidate is the seeding of the Rayleigh–Taylor instability by atmospheric gravity waves propagating from below into the ionosphere. The other candidate is the uplift of the *F* layer by the meridional neutral winds in the thermosphere, which may be associated with midnight temperature maximums in the thermosphere.



Range-time-intensity plot of the field-aligned irregularity (FAI) echo in the *F* region observed on the five beams of a VHF radar in Indonesia on the nights of August 21, 2007. (after Otsuka et al. 2009)



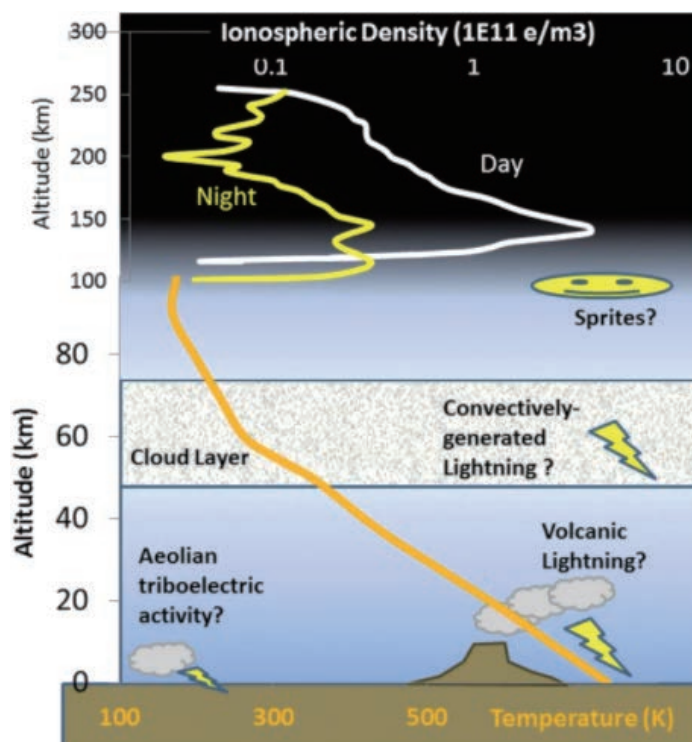
Lightning detection on Venus: a critical review

Ralph D. Lorenz

[Keywords] Venus, Lightning, Electromagnetic emission, Observation

Claimed detections and nondetections of lightning and related electromagnetic emissions on Venus are qualitatively contradictory. Here, motivated by the commencement of observations by the Akatsuki spacecraft and by studies of future missions, we critically review spacecraft and ground-based observations of the past 40 years, in an attempt to reconcile the discordant reports with a minimal number of assumptions. These include invoking alternative interpretations of individual reports, guided by sensitivity thresholds, controls, and other objective benchmarks of observation integrity. The most compelling evidence is in fact the first, the very low frequency (VLF) radio emissions recorded beneath the clouds by all four of the Veneras 11–13 landers, and those data are re-examined closely, finding power-law amplitude characteristics and substantial differences between the different profiles. It is concluded

that some kind of frequent electrical activity is supported by the preponderance of observations, but optical emissions are not consistent with terrestrial levels of activity. Venus' activity may, like Earth's, have strong temporal and/or spatial variability, which coupled with the relatively short accumulated observation time for optical measurements, can lead to qualitative discrepancies between observation reports. We note a number of previously unconsidered observations and outline some considerations for future observations.

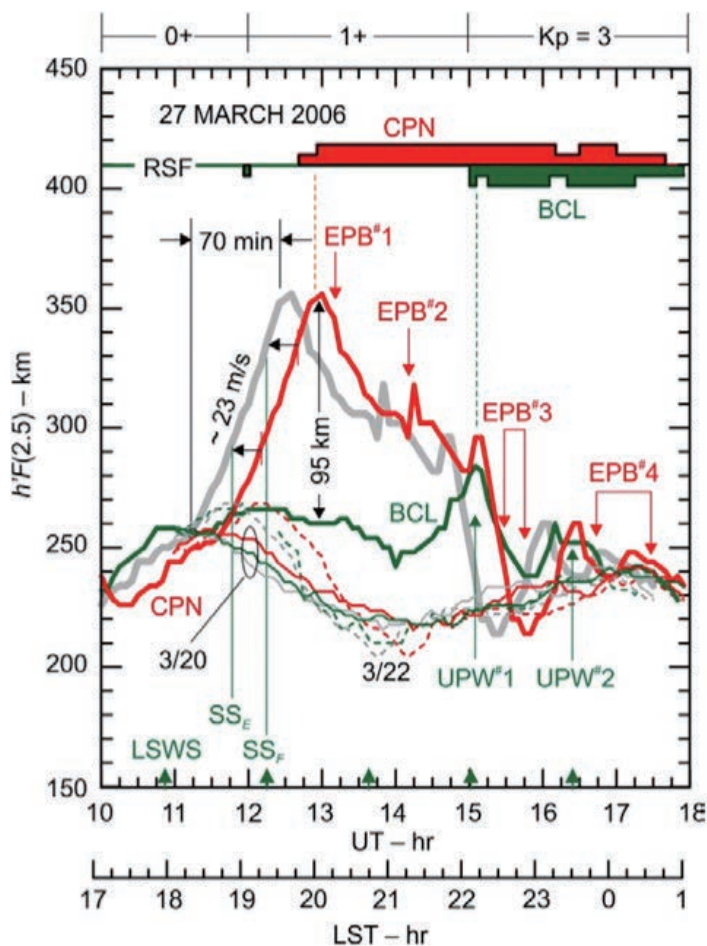


Post-sunset rise of equatorial F layer—or upwelling growth?

Tsunoda R T, Saito S, Nguyen T T

[Keywords] Equatorial plasma bubbles, Equatorial spread F , Day-to-day variability, Post-sunset rise of equatorial F layer, Large-scale wave structure, Upwelling paradigm, Upwelling growth, Pre-reversal enhancement, Electric field, Equatorial ionosphere

According to the so-called upwelling paradigm, development of equatorial plasma bubbles (EPBs) involves (1) appearance of an upwelling (i.e., local uplift with a zonal width of ~ 400 km) in the bottomside of the equatorial F layer, (2) its growth via the F -region interchange instability during the post-sunset rise (PSSR) of the F layer, and (3) launching of EPBs, which starts near the end of PSSR, from within the confines of the upwelling. In this description, the PSSR is presumed to be the primary driver of the paradigm, with upwelling growth dependent on PSSR strength. As constructed, the paradigm describes EPB development when PSSR is strong (i.e., high solar activity), but not when it is weak. We, show, for the first time, that when PSSR is weak (e.g., low solar activity), upwelling growth can still be comparable in strength to what would be considered a strong PSSR, and that this growth drives EPB development. Given that EPBs do not develop outside of upwellings, regardless of solar activity, we are led to conclude, against mainstream thinking, that the controlling driver for EPB development is upwelling growth, not PSSR. For continued progress toward understanding EPB development, a crucial next step is to identify the source mechanism for upwelling growth, especially when PSSR is weak, and to better understand the complexities of the underlying physics.



Curves of $h'F(2.5)$ vs UT, for two quiet nights (20 and 22 March 2006), and one disturbed night (27 March 2006). The green (red) curve is for BCL (CPN). The gray curve is $h'F(2.5)$ vs LST for CPN. Two levels for range type of ESF are shown, weak and strong; they should be used with the UT scale. Mean SSN for 2006 was 15.2.

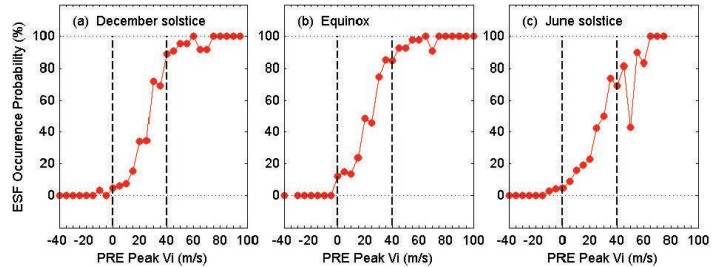


Effects of the postsunset vertical plasma drift on the generation of equatorial spread F

Huang C-S

[Keywords] Equatorial ionosphere, Equatorial spread F, Plasma bubbles, Rayleigh-Taylor instability, Vertical plasma drift, Prereversal enhancement

Equatorial spread F (ESF) irregularities are caused by plasma instability processes in the equatorial ionosphere and especially related to plasma bubble phenomena in the topside F region. Plasma bubbles result from nonlinear evolution of the Rayleigh-Taylor instability. The prereversal enhancement (PRE) of the postsunset vertical plasma drift increases the height of the equatorial F layer, creating conditions conducive to the growth of the Rayleigh-Taylor instability, and is an important factor that controls the generation of ESF. Three different relationships of the quantitative connection between the PRE and ESF occurrence have been derived. (1) A threshold PRE must be reached for the occurrence of ESF. ESF will be generated when the PRE is larger than the threshold and will not be generated when the PRE is smaller than the threshold. (2) The occurrence probability of ESF increases approximately linearly with the PRE. (3) The occurrence probability of ESF is characterized by a continuous probability distribution as a function of the PRE magnitude. The second and third relationships imply that the PRE can be used to specify the occurrence probability of ESF. This paper will review these relationships and discuss how these relationships are connected to each other. The effects of seeding perturbations on the generation and global distribution of ESF will be briefly discussed.



The dependence of the plasma bubble occurrence probability on the vertical ion drift at the PRE peak measured by C/NOFS during May 2008–June 2013 for different seasons.

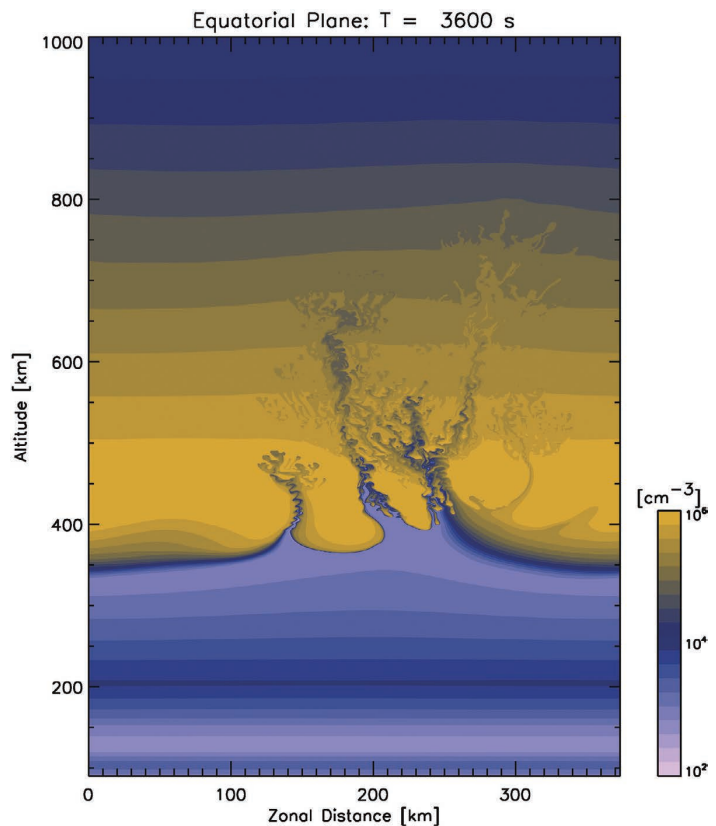


A review on the numerical simulation of equatorial plasma bubbles toward scintillation evaluation and forecasting

Yokoyama T

[Keywords] Equatorial ionosphere, Equatorial spread F, Equatorial plasma bubbles, Numerical simulation, Scintillation, High-performance computing, Space weather

Equatorial plasma bubbles (EPBs) have been a longstanding and increasingly important subject because they cause severe scintillations in radio waves from Global Navigation Satellite System satellites. The phenomenon was found in the 1930s as irregular ionosonde observations and was termed equatorial spread F (ESF). ESF is interpreted as plasma density irregularities associated with EPBs that have nonlinearly evolved into the topside ionosphere. Numerical simulations have been powerful tools to study the fully nonlinear evolution of EPBs, which cannot be wholly understood from theoretical predictions. In this paper, historical achievements in the numerical simulation of EPBs are reviewed, and future directions toward scintillation evaluation and forecast are discussed.



An example of numerical simulation results of equatorial plasma bubbles

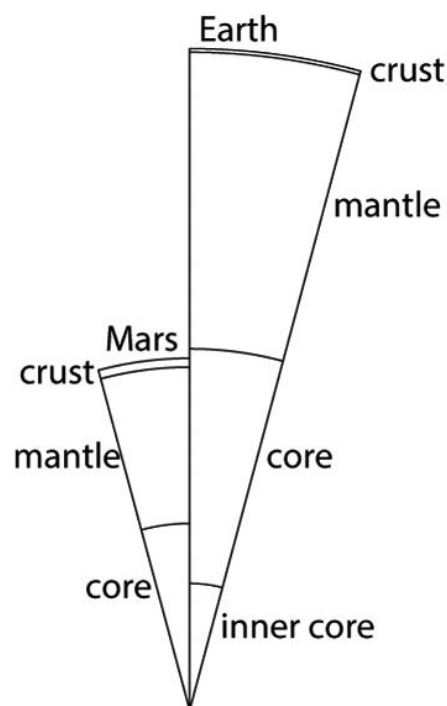


Mars core structure — concise review and anticipated insights from InSight

Helfrich G

[Keywords] Mars, InSight, Dynamo, Core, Fe-FeS phase relations, Stratification

This review summarizes the knowledge of Mars' interior structure, its inferred composition, and the anticipated seismological properties arising from its composition with particular focus on Mars' core. The emphasis on the core stems from the unusual morphology of the liquidus diagram of iron at moderate pressures when enriched in sulfur. From a fairly detailed liquidus diagram constructed from experimental studies, I identify a set of processes that could act within Mars' core: an iron "snow" from the core-mantle boundary's surface and a $\text{Fe}_{3-x}\text{S}_2$ "ground fog" forming at the base of the core. Depending on temperature and bulk sulfur composition, these could form an inner core or could stratify the outer core by enriching it in sulfur, or both. Core stratification could be one explanation for the extinction of Mars' magnetic field early in the planet's history, and I demonstrate the feasibility of this mechanism. The crystallization processes in the core could be observable in the seismic data that the future Mars geophysical mission, InSight, is planned to provide. The core size, the presence of an inner core, and the wavespeed profile of the outer core, whose radial derivative provides a proxy for changes in composition, are key observables to seek.



Comparison of sizes and interior features of Earth and Mars. Mars is almost a half-size scale model of the Earth, except for its thicker crust (Rivoldini et al., 2011) and its probable absence of an inner core. Core, Fe-FeS phase relations, Stratification

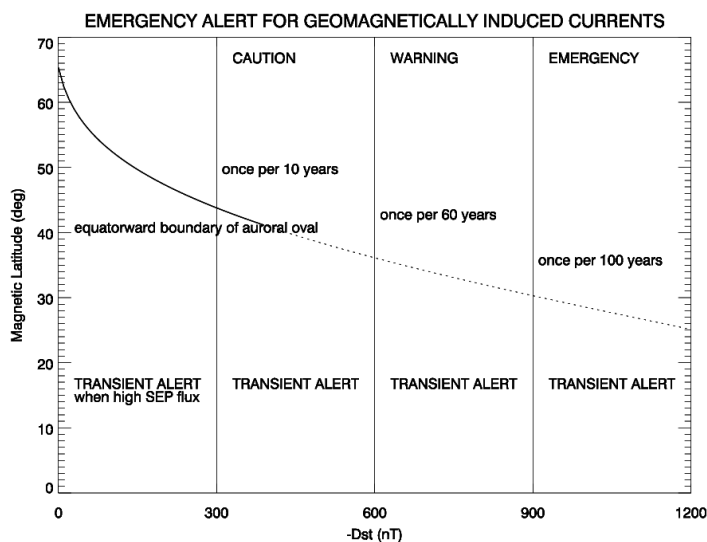


Extreme geomagnetically induced currents

Kataoka R, Ngwira C

[Keywords] Geomagnetically induced currents, Magnetic storms, Auroral substorms, Sudden commencements, Solar energetic particles

We propose an emergency alert framework for geomagnetically induced currents (GICs), based on the empirically extreme values and theoretical upper limits of the solar wind parameters and of dB/dt , the time derivative of magnetic field variations at ground. We expect this framework to be useful for preparing against extreme events. Our analysis is based on a review of various papers, including those presented during Extreme Space Weather Workshops held in Japan in 2011, 2012, 2013, and 2014. Large-amplitude dB/dt values are the major cause of hazards associated with three different types of GICs: (1) slow dB/dt with ring current evolution (RC-type), (2) fast dB/dt associated with auroral electrojet activity (AE-type), and (3) transient dB/dt of sudden commencements (SC-type). We set “caution,” “warning,” and “emergency” alert levels during the main phase of superstorms with the peak Dst index of less than -300 nT (once per 10 years), -600 nT (once per 60 years), or -900 nT (once per 100 years), respectively. The extreme dB/dt values of the AE-type GICs are 2000, 4000, and 6000 nT/min at caution, warning, and emergency levels, respectively. For the SC-type GICs, a “transient alert” is also proposed for dB/dt values of 40 nT/s at low latitudes and 110 nT/s at high latitudes, especially when the solar energetic particle flux is unusually high.



Emergency alert framework for geomagnetically induced currents. The equatorward boundary of the auroral oval according to the model of Yokoyama et al. (1998) is shown by the solid curve, and the dotted curve shows its theoretical extrapolation. It is important to update the possible extension of the auroral oval toward middle to low latitudes during extreme magnetic storms.

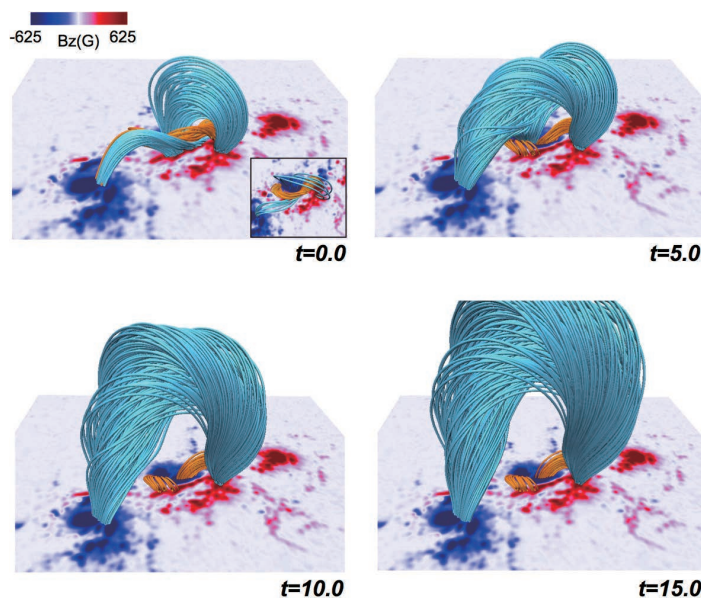


Magnetohydrodynamics Modeling of Coronal Magnetic Field and Solar Eruptions Based on the Photospheric Magnetic Field

Inoue S

[Keywords] Sun; Magnetic Field, Photosphere, Corona, Magnetohydrodynamics (MHD), Solar Active Region, Solar Flare, Coronal Mass Ejection (CME)

In this paper, we summarize current progress on using the observed magnetic fields for magnetohydrodynamics (MHD) modeling of the coronal magnetic field and of solar eruptions, including solar flares and coronal mass ejections (CMEs). Unfortunately, even with the existing state-of-the-art solar physics satellites, only the photospheric magnetic field can be measured. We first review the 3D extrapolation of the coronal magnetic fields from measurements of the photospheric field. Specifically, we focus on the nonlinear force-free field (NLFFF) approximation extrapolated from the three components of the photospheric magnetic field. On the other hand, because in the force-free approximation the NLFFF is reconstructed for equilibrium states, the onset and dynamics of solar flares and CMEs cannot be obtained from these calculations. Recently, MHD simulations using the NLFFF as an initial condition have been proposed for understanding these dynamics in a more realistic scenario. These results have begun to reveal complex dynamics, some of which have not been inferred from previous simulations of hypothetical situations, and they have also successfully reproduced some observed phenomena. Although MHD simulations play a vital role in explaining a number of observed phenomena, there still remains much to be understood. Herein, we review the results obtained by state-of-the-art MHD modeling combined with the NLFFF.



Three-dimensional dynamics of the flux tube during an X2.2-class flare obtained from our MHD simulation; the field lines with more (less) than one-turn at $t=0$ are depicted in orange (blue). The B_z distribution is shown in red and blue. The inset at $t=0$ shows the top view of the field lines; the number of field lines with less than one turn has been reduced. Eventually, the large highly twisted flux tube is formed through the magnetic reconnection between these twisted liens.

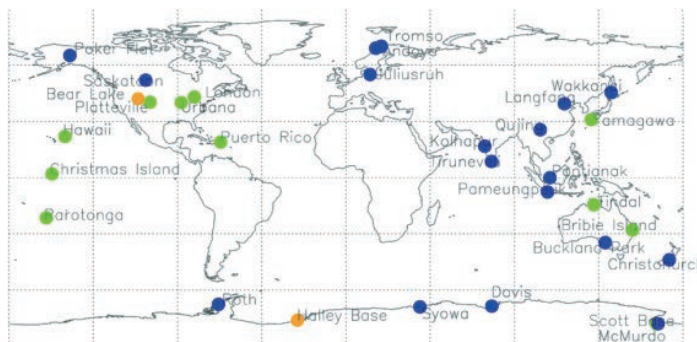


MF and HF radar techniques for investigating the dynamics and structure of the 50 to 110 km height region: a review

Reid I M

[Keywords] Medium-frequency radar techniques, High-frequency radar techniques, Partial reflection radar, Spaced antenna technique, Full correlation analysis, Mesosphere lower thermosphere region, D region, MLT region dynamics, Meteor radar, Imaging Doppler interferometer

The application of medium-frequency (MF) and high-frequency (HF) partial reflection radar to investigate the neutral upper atmosphere is one of the oldest such techniques still regularly in use. The techniques have been continuously improved and remain a robust and reliable method of obtaining wind velocities, turbulence intensities, electron densities, and measurements of atmospheric structure in the mesosphere lower thermosphere (MLT) region (50 to 110 km). In this paper, we review recent developments, discuss the strengths and weaknesses of the technique, and consider possible improvements.



MF and HF radars used to measure the MLT region. Green indicates retired radars, blue current radars, and yellow dynasondes that have operated as IDI radars. See text and Tables 2 and 3 for further details.

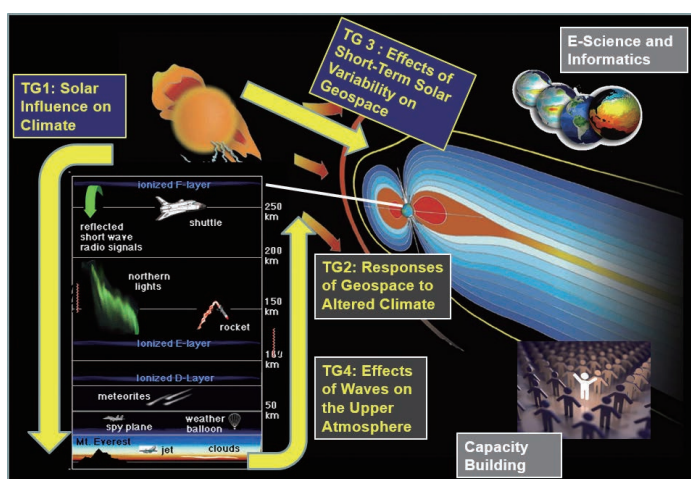


Advancing the understanding of the Sun-Earth interaction - the Climate and Weather of the Sun-Earth System (CAWSES) II Program

Tsuda T, Shepherd M G, Gopalswamy N

[Keywords] Coupled solar–terrestrial system, Solar activity, Space weather, Geospace, Atmospheric coupling, Trends, Global warming, Paleoclimatology

The Scientific Committee on Solar–Terrestrial Physics (SCOSTEP) of the International Council for Science (ICSU) implemented an international collaborative program called *Climate and Weather of the Sun–Earth System (CAWSES)*, which was active from 2004 to 2008; this was followed by the CAWSES II program during the period of 2009–2013. The CAWSES program was aimed at improving the understanding of the coupled solar–terrestrial system, with special emphasis placed on the short-term (weather) and long-term (climate) variability of solar activities and their effects on and responses of Geospace and Earth's environment. Following the successful implementation of CAWSES, the CAWSES II program pursued four fundamental questions addressing the way in which the coupled Sun–Earth system operates over time scales ranging from minutes to millennia, namely, (1) *What are the solar influences on the Earth's climate?* (2) *How will Geospace respond to an altered climate?* (3) *How does short-term solar variability affect the Geospace environment?* and (4) *What is the Geospace response to variable inputs from the lower atmosphere?* In addition to these four major tasks, the SCOSTEP and CAWSES promoted E-science and informatics activities including the creation of scientific databases and their effective utilization in solar–terrestrial physics research. Capacity building activities were also enhanced during CAWSES II, and this represented an important contribution of SCOSTEP to the world's solar–terrestrial physics community. This introductory paper provides an overview of CAWSES II activities and serves as a preface to the dedicated review papers summarizing the achievements of the program's four task groups (TGs) and the E-science component.



A schematic concept of CAWSES II with four task groups (TGs), E-science and capacity building.

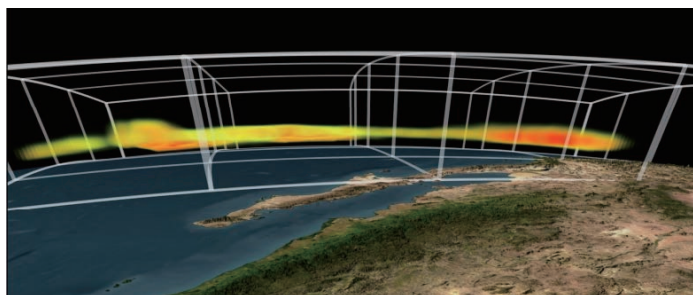


The science case for the EISCAT_3D radar

McCrea I, Aikio A, Alfonsi L, Belova E, Buchert S, Clilverd M, Engler N, Gustavsson B, Heinselman C, Kero J, Kosch M, Lamy H, Leyser T, Ogawa Y, Oksavik K, Pellinen-Wannberg A, Pitout F, Rapp M, Stanislawski I, Vierinen J

[Keywords] EISCAT, EISCAT_3D, Radar, Incoherent scatter, Atmospheric science, Space physics, Plasma physics, Solar system research, Space weather, Radar techniques

The EISCAT (European Incoherent SCATer) Scientific Association has provided versatile incoherent scatter (IS) radar facilities on the mainland of northern Scandinavia (the EISCAT UHF and VHF radar systems) and on Svalbard (the electronically scanning radar ESR (EISCAT Svalbard Radar) for studies of the high-latitude ionised upper atmosphere (the ionosphere). The mainland radars were constructed about 30 years ago, based on technological solutions of that time. The science drivers of today, however,



Schematic representation showing the volumetric imaging of an ionospheric layer above Scandinavia by EISCAT_3D. (Image courtesy of EISCAT Scientific Association)

require a more flexible instrument, which allows measurements to be made from the troposphere to the topside ionosphere and gives the measured parameters in three dimensions, not just along a single radar beam. The possibility for continuous operation is also an essential feature. To facilitate future science work with a world-leading IS radar facility, planning of a new radar system started first with an EU-funded Design Study (2005–2009) and has continued with a follow-up EU FP7 EISCAT_3D Preparatory Phase project (2010–2014). The radar facility will be realised by using phased arrays, and a key aspect is the use of advanced software and data processing techniques. This type of software radar will act as a pathfinder for other facilities worldwide. The new radar facility will enable the EISCAT_3D science community to address new, significant science questions as well as to serve society, which is increasingly dependent on space-based technology and issues related to space weather. The location of the radar within the auroral oval and at the edge of the stratospheric polar vortex is also ideal for studies of the long-term variability in the atmosphere and global change. This paper is a summary of the EISCAT_3D science case, which was prepared as part of the EU-funded Preparatory Phase project for the new facility. Three science working groups, drawn from the EISCAT user community, participated in preparing this document. In addition to these working group members, who are listed as authors, thanks are due to many others in the EISCAT scientific community for useful contributions, discussions, and support.

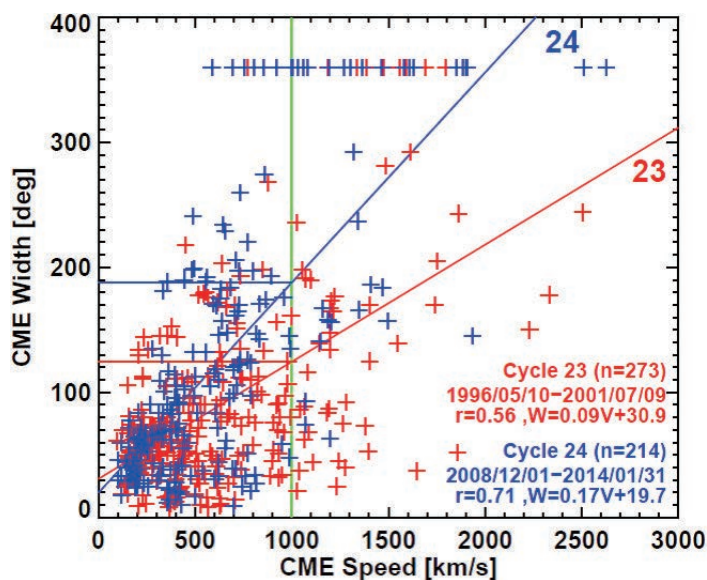


Short-term variability of the Sun-Earth system: an overview of progress made during the CAWSES-II period

Gopalswamy N, Tsurutani B, Yihua Y

[Keywords] Solar activity, Space weather, Coronal mass ejections, Flares, Solar energetic particle events, Geospace impact, Geomagnetic storms

This paper presents an overview of results obtained during the CAWSES-II period on the short-term variability of the Sun and how it affects the near-Earth space environment. CAWSES-II was planned to examine the behavior of the solar-terrestrial system as the solar activity climbed to its maximum phase in solar cycle 24. After a deep minimum following cycle 23, the Sun climbed to a very weak maximum in terms of the sunspot number in cycle 24 (MiniMax24), so many of the results presented here refer to this weak activity in comparison with cycle 23. The short-term variability that has immediate consequence to Earth and geospace manifests as solar eruptions from closed-field regions and high-speed streams from coronal holes. Both electromagnetic (flares) and mass emissions (coronal mass ejections - CMEs) are involved in solar eruptions, while coronal holes result in high-speed streams that collide with slow wind forming the so-called corotating interaction regions (CIRs). Fast CMEs affect Earth via leading shocks accelerating energetic particles and creating large geomagnetic storms. CIRs and their trailing high-speed streams (HSSs), on the other hand, are responsible for recurrent small geomagnetic storms and extended days of auroral zone activity, respectively. The latter leads to the acceleration of relativistic magnetospheric 'killer' electrons. One of the major consequences of the weak solar activity is the altered physical state of the heliosphere that has serious implications for the shock-driving and storm-causing properties of CMEs. Finally, a discussion is presented on extreme space weather events prompted by the 23 July 2012 super storm event that occurred on the backside of the Sun. Many of these studies were enabled by the simultaneous availability of remote sensing and *in situ* observations from multiple vantage points with respect to the Sun-Earth line.



Speed vs. width distributions of limb CMEs from cycles 23 and 24. Both cycles show a good correlation between speed and width, but the slopes are very different. The correlations coefficients (r) and the regression lines are given on the plot. Student's t-test confirms that the slope difference is statistically significant. The data points at width=360° are halo CMEs, which are mostly from cycle 24.



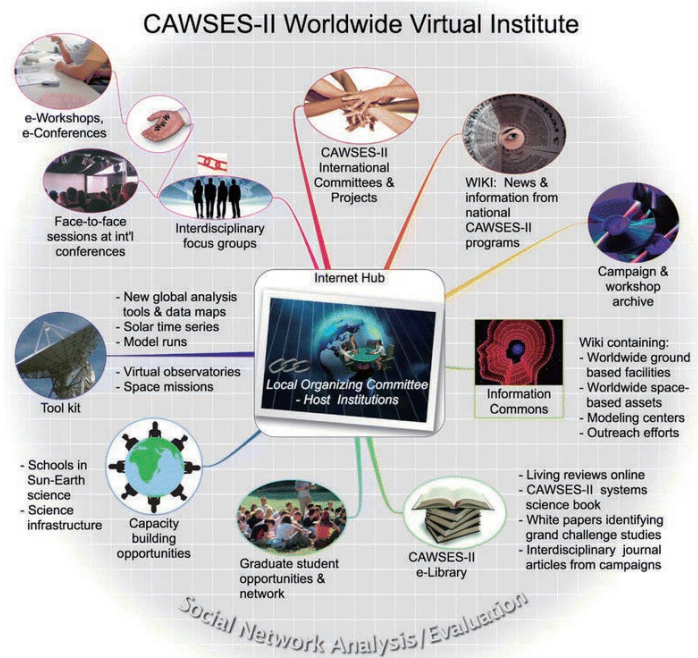
eScience and Informatics for International Science Programs

Fox P, Kozyra J

[Keywords] eScience, Informatics, Virtual observatory, Virtual organization, Collaboration, Interdisciplinary research

Both eScience and Informatics, their conceptual approaches, methods, and extant technical solutions, are still relatively new approaches in many science fields. Collectively, they intend to facilitate the electronic conduct of science (eScience) and the application of foundational principles drawn from experience in a number of fields of Informatics (e.g., helioinformatics, geoinformatics, and climateinformatics). The Climate and Weather of the Sun-Earth System II (CAWSES II) eScience and Informatics effort had the goal of promoting an international virtual institute and several virtual observatories in order to advance system-level science investigations aligned with the four CAWSES II Task Groups. This contribution elaborates on the key elements of eScience and Informatics applicable to CAWSES II as a virtual organization in the context of the current science-data landscape. We examine what was adopted for CAWSES

II and highlight the successes and challenges of the effort. Based on the lessons learned from this effort and other international communities, we present opportunities going forward that are relevant to both smaller collaborations and successor large-scale programs (such as the Variability of the Sun and Its Terrestrial Impact (VarSITI)) that are being recognized more as networks of science facilitated by a variety of modern information technologies.



CAWSES II program concept for virtual institute for collaborative knowledge development

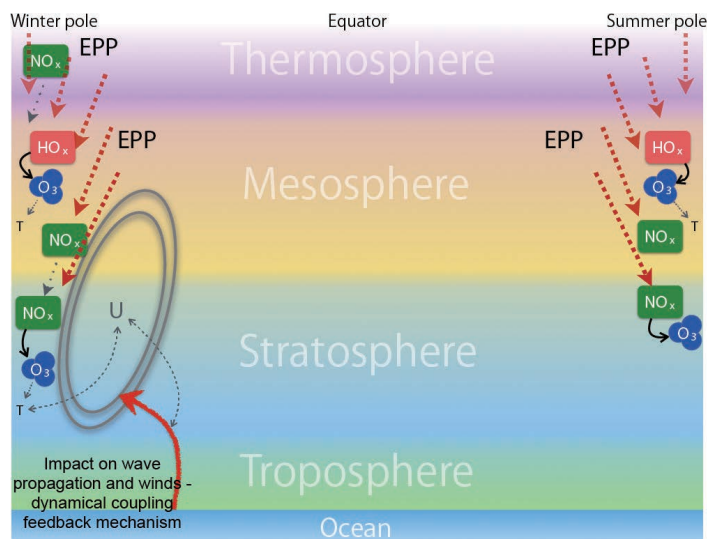


What is the solar influence on climate? Overview of activities during CAUSES-II

Seppälä A, Matthes K, Randall C E, Mironova I A

[Keywords] Climate, Atmosphere, Solar irradiance, Total solar irradiance, TSI, Solar spectral irradiance, SSI, Energetic particles, EPP, Cosmic rays

This paper presents an overview of the main advances in the Key Questions identified by the Task Group 'What is the Solar Influence on Climate' by the SCOSTEP CAUSES-II science program. We go through different aspects of solar forcing from solar irradiance, including total solar irradiance (TSI) and solar spectral irradiance (SSI), to energetic particle forcing, including energetic particle precipitation (EPP) and cosmic rays (CR). Besides discussing the main advances in the timeframe 2009 to 2013, we also illustrate the proposed mechanism for climate variability for the different solar variability sources listed above. The key questions are as follows: What is the importance of spectral variations to solar influences on climate? What is the effect of energetic particle forcing on the whole atmosphere and what are the implications for climate? How well do models reproduce and predict solar irradiance and energetic particle influences on the atmosphere and climate?



Energetic particle precipitation (EPP) impact on the atmosphere. Main direct and indirect impacts from EPP (including EEP and SPE). EPP ionisation is focused on the polar regions leading to production of HO_x and NO_x shown in the figure. Transport processes are shown with grey dotted lines, while coupling mechanisms are indicated with grey dashed lines. Direct chemical impacts are shown with black arrows.

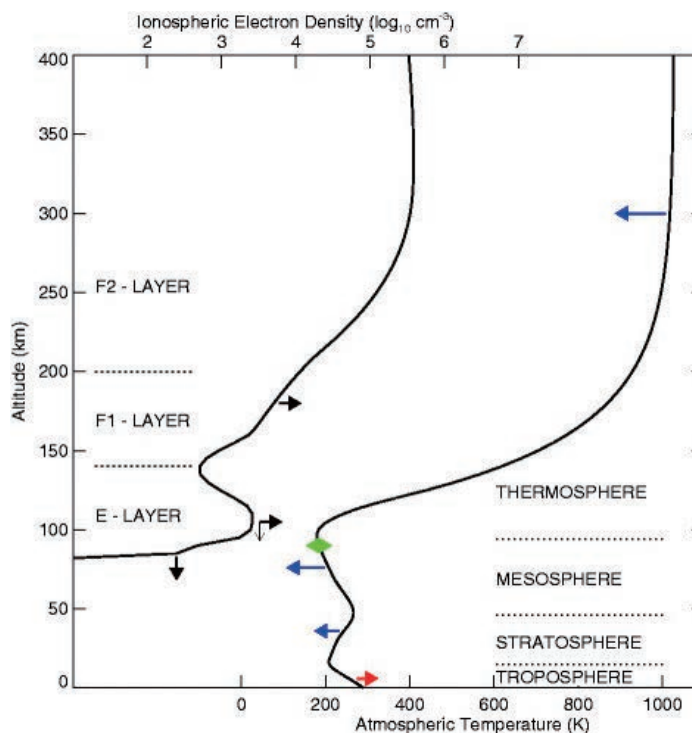


Response of the mesosphere-thermosphere-ionosphere system to global change – CAWSES-II contribution

Laštovička J, Beig G, Marsh D R

[Keywords] Mesosphere, Thermosphere, Ionosphere, Long-term trends, Climatic change

Long-term trends in the mesosphere, thermosphere, and ionosphere are areas of research of increasing importance both because they are sensitive indicators of climatic change and because they affect satellite-based technologies which are increasingly important to modern life. Their study was an important part of CAWSES-II project, as they were a topic of Task Group 2 (TG-2) 'How Will Geospace Respond to Changing Climate'. Three individual projects of TG-2 were focused on important problems in trend investigations. Significant progress was reached in several areas such as understanding and quantifying the role of stratospheric ozone changes in trends in the upper atmosphere, reaching reasonable agreement between observed and simulated trends in mesospheric temperatures and polar mesospheric clouds, or understanding of why the thermospheric density trends are much stronger under solar cycle minimum conditions. The TG-2 progress that is reviewed in this paper together with some results reached outside CAWSES-II so as to have the full context of progress in trends in the upper atmosphere and ionosphere.



Trends in the Earth's atmosphere. The atmospheric layers are defined by the temperature profile. The ionospheric layers are defined by the electron density profile (midnight at equator). Arrows indicate the direction of change. Red - warming, blue - cooling, green - no change of temperature, black - changes in electron density (horizontal) and heights of ionospheric layers (vertical).



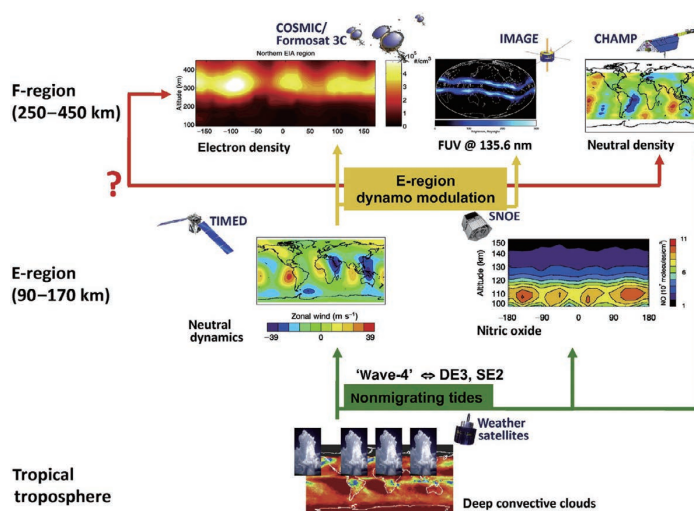
The geospace response to variable inputs from the lower atmosphere: A review of the progress made by Task Group 4 of CAWSES-II

Oberheide J, Kazuo S, Gurubaran S, Ward W E, Fujiwara H, Kosch M J, Makela J J, Takahashi H

[Keywords] Geospace, Thermosphere, Ionosphere, Tides, Planetary waves, Gravity waves, Traveling ionospheric disturbances, Traveling atmospheric disturbances

The advent of new satellite missions, ground-based instrumentation networks, and the development of whole atmosphere models over the past decade resulted in a paradigm shift in understanding the variability of geospace, that is, the region of the atmosphere between the stratosphere and several thousand kilometers above ground where atmosphere-ionosphere-magnetosphere interactions occur. It has now been realized that conditions in geospace are linked strongly to terrestrial weather and climate below, contradicting previous textbook knowledge that the space weather of Earth's near space environment is driven by energy injections at high latitudes connected with magnetosphere-ionosphere coupling and solar radiation variation at extreme ultraviolet wavelengths alone. The primary mechanism through which energy and momentum are transferred from the lower atmosphere is through the generation, propagation, and dissipation of atmospheric waves over a wide range of spatial

and temporal scales including electrodynamic coupling through dynamo processes and plasma bubble seeding. The main task of Task Group 4 of SCOSTEP's CAWSES-II program, 2009 to 2013, was to study the geospace response to waves generated by meteorological events, their interaction with the mean flow, and their impact on the ionosphere and their relation to competing thermospheric disturbances generated by energy inputs from above, such as auroral processes at high latitudes. This paper reviews the progress made during the CAWSES-II time period, emphasizing the role of gravity waves, planetary waves and tides, and their ionospheric impacts. Specific campaign contributions from Task Group 4 are highlighted, and future research directions are discussed.



Sketch of meteorological impacts on geospace due to non-Sun-synchronous (nonmigrating) tides as observed by different satellites in various neutral and plasma parameters. The COSMIC figure is adapted with permission from Lin et al. (2007), the IMAGE figure is adapted with permission from Immel et al. (2006), the TIMED figure uses data from Oberheide et al. (2006), and the SNOE figure is adapted with permission from Oberheide and Forbes (2008). Deep convective cloud data are from the ISCCP climatology. CHAMP neutral density data are provided by Dr X. Zhang and Dr. S. L. Bruinsma.



Review

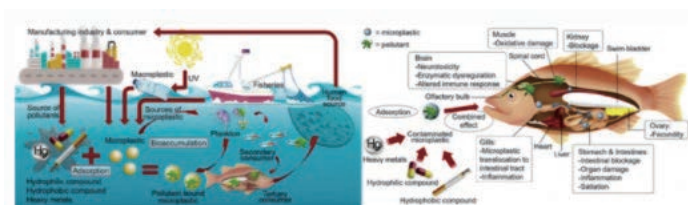
Atmospheric and hydrospheric sciences

Marine microplastics as vectors of major ocean pollutants and its hazards to the marine ecosystem and humans

Tan Suet May Amelia, Wan Mohd Afiq Wan Mohd Khalik, Meng Chuan Ong, Yi Ta Shao, Hui-Juan Pan, Kesaven Bhubalan

[Keywords] Adsorption, Bioaccumulation, Contaminant, Microplastic, Pollutant, Vector

Microplastic pollutes water, land, air, and groundwater environments not only visually but also ecologically for plants, animals, and humans. Microplastic has been reported to act as vectors by sorbing pollutants and contributing to the bioaccumulation of pollutants, particularly in marine ecosystems, organisms,



and subsequently food webs. The inevitable exposure of microplastic to humans emphasises the need to review the potential effects, exposure pathways, and toxicity of microplastic toward human health. Therefore, this review was aimed to reveal the risks of pollutant sorption and bioaccumulation by microplastic toward humans, as well as the dominant types of pollutants sorbed by microplastic, and the types of pollutants that are bioaccumulated by microplastic in the living organisms of the marine ecosystem. The possible factors influencing the sorption and bioaccumulation of pollutants by microplastic in marine ecosystems were also reviewed. The review also revealed the prevailing types of microplastic, abundance of microplastic, and geographical distribution of microplastic in the aquatic environment globally. The literature review revealed that microplastic characteristics, chemical interactions, and water properties played a role in the sorption of pollutants by microplastic. The evidence of microplastic posing a direct medical threat to humans is still lacking albeit substantial literature has reported the health hazards of microplastic-associated monomers, additives, and pollutants. This review recommends future research on the existing knowledge gaps in microplastic research, which include the toxicity of microplastic, particularly to humans, as well as the factors influencing the sorption and bioaccumulation of pollutants by microplastic.

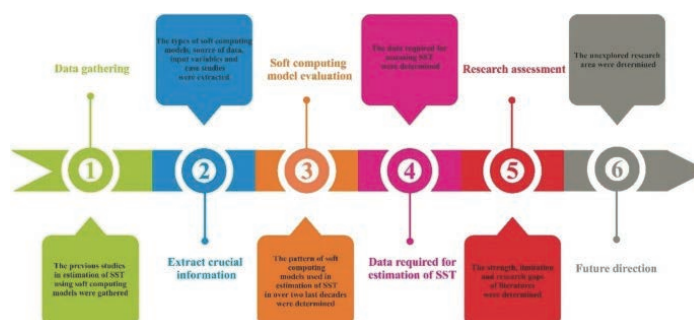


Applications of soft computing models for predicting sea surface temperature: a comprehensive review and assessment

Masoud Haghbin, Ahmad Sharafati, Davide Motta, Nadhir Al-Ansari, Mohamadreza Hosseinian Moghadam Noghani

[Keywords] Soft computing, Sea Surface Temperature, Prediction

The application of soft computing (SC) models for predicting environmental variables is widely gaining popularity, because of their capability to describe complex non-linear processes. The sea surface temperature (SST) is a key quantity in the analysis of sea and ocean systems, due to its relation with water quality, organisms, and hydrological events such as droughts and floods. This paper provides a comprehensive review of the SC model applications for estimating SST over the last two decades. Types of model (based on artificial neural networks, fuzzy logic, or other SC techniques), input variables, data sources, and performance indices are discussed. Existing trends of research in this field are identified, and possible directions for future investigation are suggested.

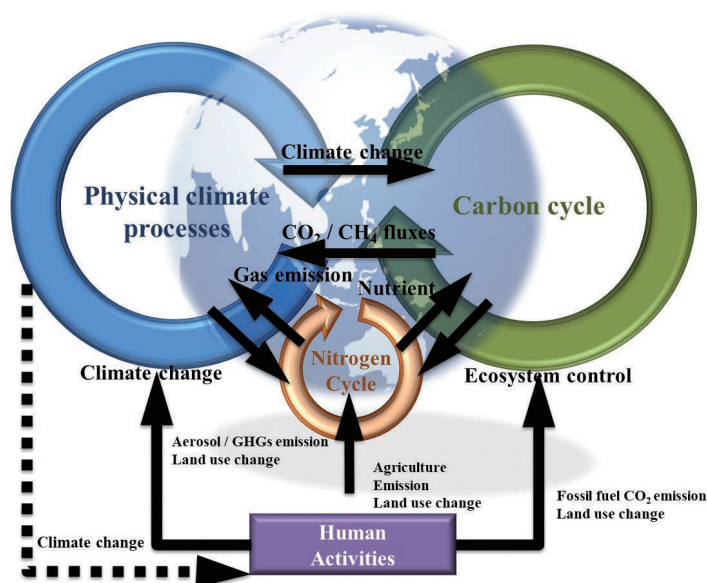


Two decades of Earth system modeling with an emphasis on Model for Interdisciplinary Research on Climate (MIROC)

Michio Kawamiya, Tomohiro Hajima, Kaoru Tachiiri, Shingo Watanabe, Tokuta Yokohata

[Keywords] Earth system model, Climate change, IPCC, Carbon cycle, Biogeochemistry, Interdisciplinary project, Remaining carbon budget, Socioeconomics, Nitrogen, Iron.

The past 20 years of research using Earth system models (ESMs) is reviewed with an emphasis on results from the ESM based on MIROC (Model for Interdisciplinary Research on Climate) developed in Japan. Earth system models are climate models incorporating biogeochemical processes such as the carbon cycle. The development of ESM was triggered by studies of the feedback between climate change and the carbon cycle. State-of-the-art ESMs are much more realistic than the first ESMs. They now include various biogeochemical processes other than carbon, such as atmospheric chemistry and the nitrogen and iron cycles as well as nutrient transport by atmospheric dust and rivers. They are used to address many practical issues, such as evaluating the amount of carbon dioxide emissions that is consistent with climate change mitigation targets, and are indispensable tools for the development of climate change mitigation policies. Novel, ambitious attempts to use ESMs include coupling socioeconomics with Earth systems, and projecting the carbon cycle on decadal timescales. Development of ESMs requires ongoing integration of multiple aspects of climate science. Emerging applications of ESMs can bring forth meaningful insights, and should be directed toward expanding connections with fields outside climate science, e.g., socioeconomics.



Conceptual diagram of Earth system model (ESM) projections of global change: Anthropogenic greenhouse gas emissions and nitrogen fixation are increasing; ESMs can model interactions between climate change and biogeochemical cycles.



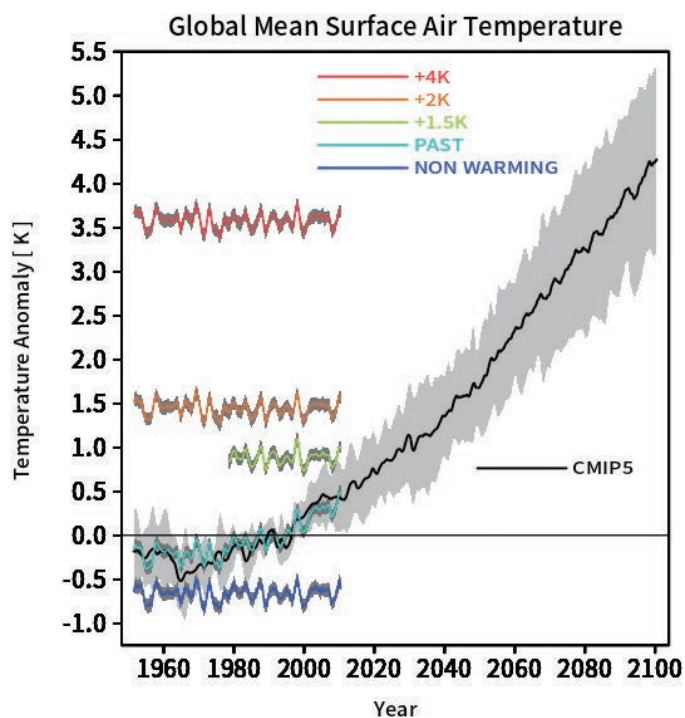
d4PDF: large-ensemble and high-resolution climate simulations for global warming risk assessment

Masayoshi Ishii, Nobuhito Mori

[Keywords] Global warming, d4PDF, ensemble climate simulation, atmospheric model, dynamical downscaling, detection and attribution, impact assessment, climate change adaptation, natural hazard, storm surge

A large-ensemble climate simulation database, which is known as the database for policy decision-making for future climate changes (d4PDF), was designed for climate change risk assessments. Since the completion of the first set of climate simulations in 2015, the database has been growing continuously. It contains the results of ensemble simulations conducted over a total of thousands years respectively for past and future climates using high-resolution global (60 km horizontal mesh) and regional (20 km mesh) atmospheric models. Several sets of future climate simulations are available, in which global mean surface air temperatures are forced to be higher by 4 K, 2 K, and 1.5 K relative to preindustrial levels. Nonwarming past climate simulations are incorporated in d4PDF along with the past climate simulations. The total data volume is approximately 2 petabytes. The atmospheric models satisfactorily simulate the past climate in terms of climatology, natural variations, and extreme events such as heavy precipitation and tropical cyclones. In addition, data users can obtain statistically significant

changes in mean states or weather and climate extremes of interest between the past and future climates via a simple arithmetic computation without any statistical assumptions. The database is helpful in understanding future changes in climate states and in attributing past climate events to global warming. Impact assessment studies for climate changes have concurrently been performed in various research areas such as natural hazard, hydrology, civil engineering, agriculture, health, and insurance. The database has now become essential for promoting climate and risk assessment studies and for devising climate adaptation policies. Moreover, it has helped in establishing an interdisciplinary research community on global warming across Japan.



Time series of global mean surface air temperature anomalies of d4PDF for past (light blue), nonwarming (blue), +1.5 K (green), +2 K (orange), and +4 K (red) climate simulations and CMIP5 historical and RCP8.5 experiments with six climate models. Shading indicates two-sigma uncertainties. Time series are drawn relative to the averages for the period from 1975 to 2005.

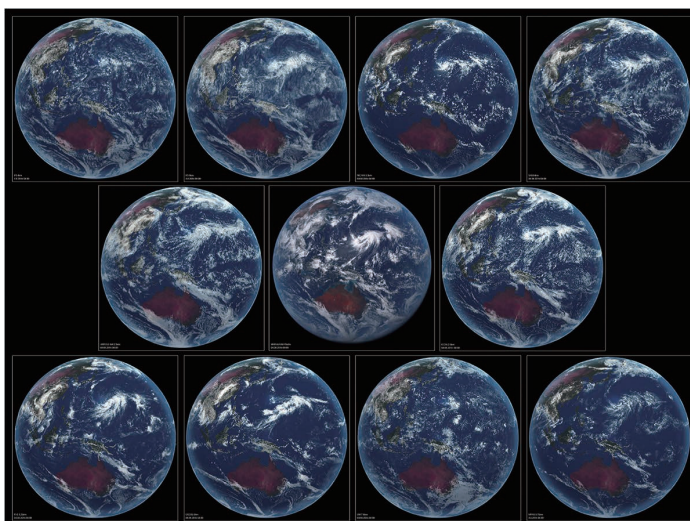


DYAMOND: The Dynamics of the Atmospheric general circulation Modeled On Non-hydrostatic Domains

Stevens B, Satoh M, Auger L, Biercamp J, Bretherton CS, Chen X, Duben P, Judt F, Khairoutdinov M, Klocke D, Kodama C, Kornblueh L, Lin SJ, Neumann P, Putman WM, Rober N, Shibuya R, Vanniere B, Vidale PL, Wedi N, Zhou L

[Keywords] Climate modelling, Model intercomparison project, Tropical Convection

A review of the experimental protocol and motivation for DYAMOND, the first intercomparison project of global storm-resolving models, is presented. Nine models submitted simulation output for a 40-day (1 August–10 September 2016) intercomparison period. Eight of these employed a tiling of the sphere that was uniformly less than 5 km. By resolving the transient dynamics of convective storms in the tropics, global storm-resolving models remove the need to parameterize tropical deep convection, providing a fundamentally more sound representation of the climate system and a more natural link to commensurately high-resolution data from satellite-borne sensors. The models and some basic characteristics of their output are described in more detail, as is the availability and planned use of this output for future scientific study. Tropically and zonally averaged energy budgets, precipitable water distributions, and precipitation from the model ensemble are evaluated, as is their representation of tropical cyclones and the predictability of column water vapor, the latter being important for tropical weather.



Snapshot of DYAMOND Models. Shown is a snapshot of the models taken from the perspective of the Himawari-8. The images are for the cloud scene on 4 August 2016, and are qualitatively rendered based on each model's condensate fields to illustrate the variety of convective structures resolved by the models, and difficulty of distinguishing them from actual observations. From left to right, the images are from IFS-4km, IFS-9km, NICAM, and SAM (top row); Arpege, Himawari, and ICON (middle row); FV3, GEOS5, UKMO and MPAS (bottom row).



Toward reduction of the uncertainties in climate sensitivity due to cloud processes using a global non-hydrostatic atmospheric model

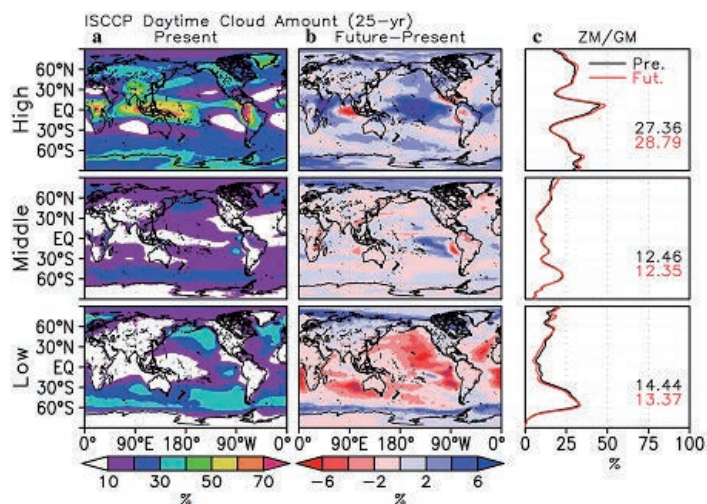
Satoh M, Noda A, Seiki T, Chen Y, Kodama C, Yamada Y, Kuba N, Sato Y

[Keywords] NICAM, Cloud microphysics scheme, Cloud changes, Cloud feedback, Global non-hydrostatic model, Global warming

In estimates of climate sensitivity obtained from global models, the need to represent clouds introduces a great deal of uncertainty. To address this issue, approaches using a high-resolution global non-hydrostatic model are promising: the model captures cloud structure by explicitly simulating meso-scale convective systems, and the results compare reasonably well with satellite observations. We review the outcomes of a 5-year project aimed at reducing the uncertainty in climate models due to cloud processes using a global non-hydrostatic model. In our project, which was conducted as a subgroup of the Program for Risk Information

on Climate Change, or SOUSEI, we use the non-hydrostatic icosahedral atmospheric model (NICAM) to study cloud processes related to climate change. NICAM performs numerical simulations with much higher resolution (about 7 km or 14 km mesh) than conventional global climate models (GCMs) using cloud microphysics schemes without a cumulus parameterization scheme, which causes uncertainties in climate projection.

The subgroup had three research targets: analyzing cloud changes in global warming simulations with NICAM with the time-slice approach, sensitivity of the results to the cloud microphysics scheme employed, and evaluating circulation changes due to global warming. The research project also implemented a double-moment bulk cloud microphysics scheme and evaluated its results using satellite observation, as well as comparing it with a bin cloud microphysics scheme. The future projection simulations show in general increase in high cloud coverage, contrary to results with other GCMs. Changes in cloud horizontal-size distribution size and structures of tropical/extratropical cyclones can be discussed with high resolution simulations. At the conclusion of our review, we also describe the future prospects of research for global warming using NICAM in the program that followed SOUSEI, known as TOUGOU.



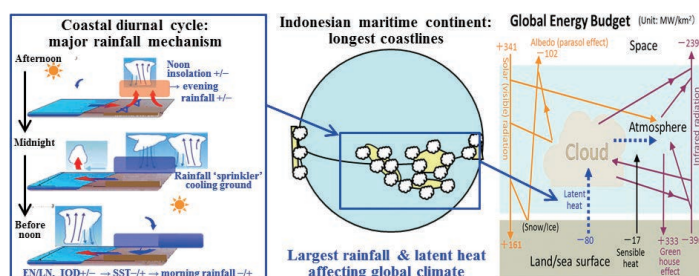
Maritime continent coastlines controlling Earth's climate

Yamanaka MD, Ogino SY, Wu PM, Hamada JI, Mori S, Matsumoto J, Syamsudin F

[Keywords] Indonesian maritime continent, Atmosphere–ocean–land interaction, Convective clouds, Multiple scales, Diurnal cycle, Sea–land breeze circulation

During the Monsoon Asian Hydro–Atmosphere Scientific Research and Prediction Initiative (MAHASRI; 2006–16), we carried out two projects over the Indonesian maritime continent (IMC), constructing the Hydrometeorological Array for Intraseasonal Variation–Monsoon Automonitoring (HARIMAU; 2005–10) radar network and setting up a prototype institute for climate studies, the Maritime Continent Center of Excellence (MCCOE; 2009–14). Here, we

review the climatological features of the world's largest “regional” rainfall over the IMC studied in these projects. The fundamental mode of atmospheric variability over the IMC is the diurnal cycle generated along coastlines by land–sea temperature contrast: afternoon land becomes hotter than sea by clear-sky insolation before noon, with the opposite contrast before sunrise caused by evening rainfall-induced “sprinkler”-like land cooling (different from the extratropical infrared cooling on clear nights). Thus, unlike the extratropics, the diurnal cycle over the IMC is more important in the rainy season. The intraseasonal, seasonal to annual, and interannual climate variabilities appear as amplitude modulations of the diurnal cycle. For example, in Jawa and Bali the rainy season is the southern hemispheric summer, because land heating in the clear morning and water vapor transport by afternoon sea breeze is strongest in the season of maximum insolation. During El Niño, cooler sea water surrounding the IMC makes morning maritime convection and rainfall weaker than normal. Because the diurnal cycle is almost the only mechanism generating convective clouds systematically near the equator with little cyclone activity, the local annual rainfall amount in the tropics is a steeply decreasing function of coastal distance (e -folding scale 100–300 km), and regional annual rainfall is an increasing function of “coastline density” (coastal length/land area) measured at a horizontal resolution of 100 km. The coastline density effect explains why rainfall and latent heating over the IMC are twice the global mean for an area that makes up only 4% of the Earth's surface. The diurnal cycles appearing almost synchronously over the whole IMC generate teleconnections between the IMC convection and the global climate. Thus, high-resolution ($\ll 100$ km; $\ll 1$ day) observations and models over the IMC are essential to improve both local disaster prevention and global climate prediction.



Maritime-continental diurnal-cycle rain and latent heat controlling global climate

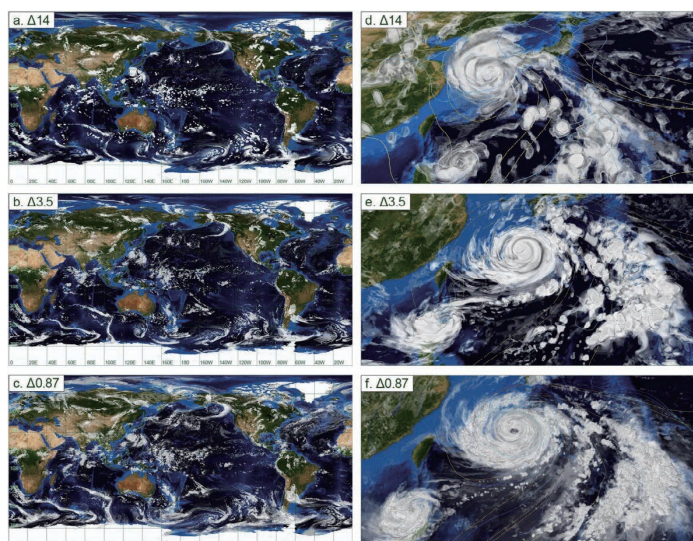


Outcomes and challenges of global high-resolution non-hydrostatic atmospheric simulations using the K computer

Satoh M, Tomita H, Yashiro H, Kajikawa Y, Miyamoto Y, Yamaura T, Miyakawa T, Nakano M, Kodama C, Noda A T, Nasuno T, Yamada Y, Fukutomi Y

[Keywords] K computer, NICAM, intra-seasonal oscillations, Madden-Julian oscillation, tropical cyclone, global non-hydrostatic model

This article reviews the major outcomes of a 5-year (2011–2016) project using the K computer to perform global numerical atmospheric simulations based on the non-hydrostatic icosahedral atmospheric model (NICAM). The K computer was made available to the public in September 2012 and was used as a primary resource for Japan's Strategic Programs for Innovative Research (SPIRE), an initiative to investigate five strategic research areas; the NICAM project fell under the research area of climate and weather simulation sciences. Combining NICAM with high-performance computing has created new opportunities in three areas of research: (1) higher resolution global simulations that produce more realistic representations of convective systems, (2) multi-member ensemble simulations that are able to perform extended-range forecasts 10–30 days in advance, and (3) multi-decadal simulations for climatology and variability. Before the K computer era, NICAM was used to demonstrate realistic simulations of intra-seasonal oscillations including the Madden-Julian oscillation (MJO), merely as a case study approach. Thanks to the big leap in computational performance of the K computer, we could greatly increase the number of cases of MJO events for numerical simulations, in addition to integrating time and horizontal resolution. We conclude that the high-resolution global non-hydrostatic model, as used in this five-year project, improves the ability to forecast intra-seasonal oscillations and associated tropical cyclogenesis compared with that of the relatively coarser operational models currently in use. The impacts of the sub-kilometer resolution simulation and the multi-decadal simulations using NICAM are also reviewed.



Resolution dependencies of simulated cloud distribution: mesh size 14 km, 3.5 km, and 870 m.

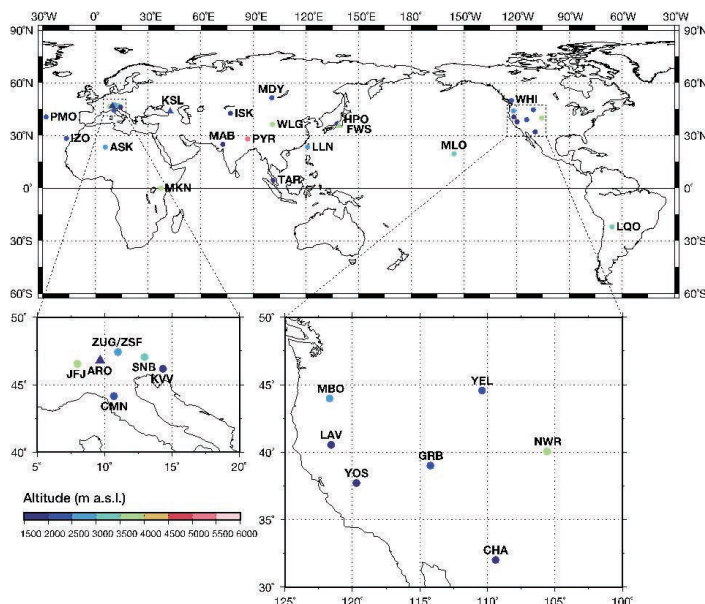


A review of atmospheric chemistry observation at mountain sites

Okamoto S, Tanimoto H

[Keywords] Atmospheric observation, High-altitude station, Long-range transport, Seasonal cycle, Long-term trend, Biomass burning, Anthropogenic pollution

Located far from anthropogenic emission sources, high-altitude mountain stations are considered to be ideal sites for monitoring climatic and environmentally important baseline changes in free tropospheric trace gases and aerosols. In addition, the observations taken at these stations are often used to study the long-range transport of dust as well as anthropogenic and biomass burning pollutants from source regions and to evaluate the performance of global and regional models. In this paper, we summarize the results from past and ongoing field measurements of atmospheric constituents at high-altitude stations across the globe, with particular emphasis on reactive trace species including tropospheric ozone, along with its precursors such as carbon monoxide, nitrogen oxides, total reactive nitrogen, and nonmethane hydrocarbons. Over the past decades, our understanding of the temporal variability and meteorological mechanisms of long-range transport has advanced in tandem with progress in instrumentation and modeling. Finally, the future needs of atmospheric chemistry observations at mountain sites are addressed.



Map showing the distribution of high-altitude mountain stations discussed in this paper. Circles with abbreviations denote stations providing the data presented in this paper. ASK Assekrem, CHA Chiricahua NM, CMN Monte Cimone, GRB Great Basin NP, HPO Mt. Haplo, ISK Issyk-Kul, IZO Izāna, JFJ Jungfrauoch, KVV Kravec, LAV Lassen Volcanic NP, LLN Lulin, LQO La Quiaca Observatorio, MBO Mt. Bachelor Observatory, MKN Mt. Kenya, MDY Mondy, MLO Mauna Loa, NWR Niwot Ridge, PMO Pico Mountain Observatory, PYR Nepal Climate Observatory–Pyramid, SNB Sonnblick, TAR Tanah Rata, WHI Whistler Mountain, WLG Mt. Waliguan, YEL Yellowstone NP, YOS Yosemite NP, ZSF Zugspitze–Schneefernerhaus, ZUG Zugspitze–Gipfel. Triangles with abbreviations denote stations for which data are not presented but are reviewed in this paper. ARO Arosa, FWS Mt. Fuji, KSL Kislovodsk.



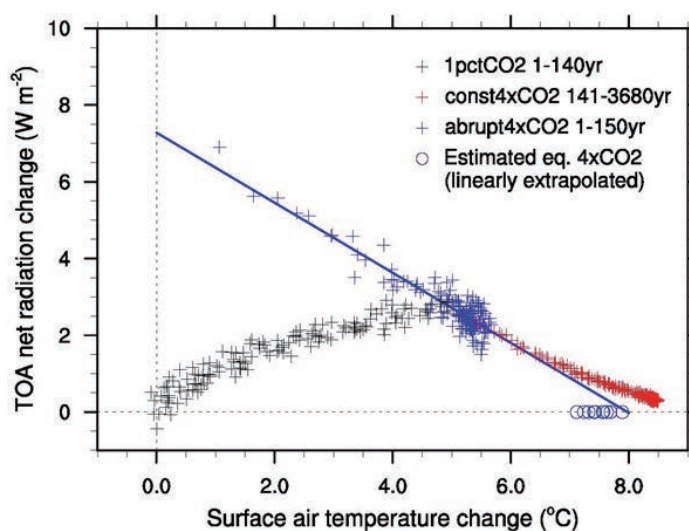
A review of progress towards understanding the transient global mean surface temperature response to radiative perturbation

Yoshimori M, Watanabe M, Shiogama H, Oka A, Abe-Ouchi A, Ohgaito R, Kamae Y

[Keywords] Transient climate response, Equilibrium climate sensitivity, Climate feedback, Ocean heat uptake efficacy, Efficacy of forcing

The correct understanding of the transient response to external radiative perturbation is important for the interpretation of observed climate change, the prediction of near-future climate change, and committed warming under climate stabilization scenarios, as well as the estimation of equilibrium climate sensitivity based on observation data. It has been known for some time that the radiative damping rate per unit of global mean surface temperature increase varies with time, and this inconstancy affects the transient response. Knowledge of the equilibrium response alone is insufficient, but understanding the transient response of the global mean surface temperature has made rapid progress. The recent progress accompanies the relatively new concept of the efficacies of ocean heat uptake and forcing. The ocean heat uptake efficacy associates the temperature response induced by ocean heat uptake with equilibrium temperature response, and the efficacy of forcing compares the temperature response caused by non-CO₂ forcing with that by CO₂ forcing.

In this review article, recent studies on these efficacies are discussed, starting from the classical global feedback framework and basis of the transient response. An attempt is made to structure different studies that emphasize different aspects of the transient response and to stress the relevance of those individual studies. The implications on the definition and computation of forcing and on the estimation of the equilibrium response in climate models are also discussed. Along with these discussions, examples are provided with MIROC climate model multi-millennial simulations



Relation between global mean surface air temperature and top-of-the-atmosphere net radiation changes from the preindustrial control simulation in the MIROC3.2 (medres) atmosphere-ocean general circulation model experiments. Black crosses: 1pctCO₂ experiment (every year for 1-140 years); blue crosses: abrupt4xCO₂ experiment (every year for 1-150 years), red crosses: const4xCO₂ experiment (every 20-year average for 141-3680 years); blue line: linear regression for the 150-year abrupt4xCO₂ experiment; Blue circles: equilibrium temperature response to 4xCO₂ estimated by Gregory's method for 10 abrupt4xCO₂ 20-year-long ensemble experiments (that start from different initial conditions in the preindustrial control simulation).

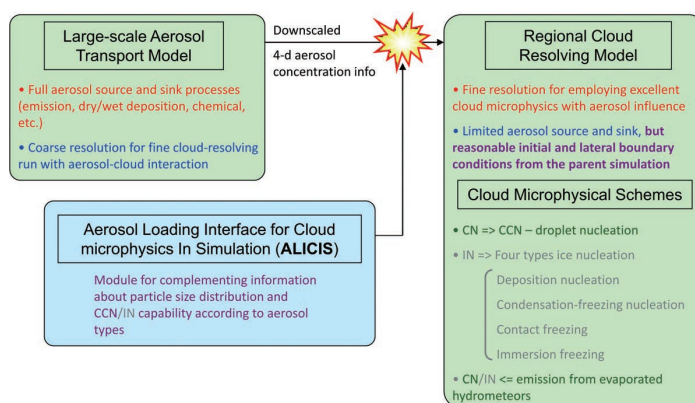


Overview of the development of the Aerosol Loading Interface for Cloud microphysics In Simulation (ALICIS)

Iguchi T, Choi I-J, Sato Y, Suzuki K, Nakajima T

[Keywords] Cloud microphysics, Cloud and aerosol, Regional modeling, Dynamical downscaling

This review summarizes the scientific background of and past/prospective update strategies for the development of the Aerosol Loading Interface for Cloud microphysics In Simulation (ALICIS). ALICIS provides a novel approach for coupling downscaled mesoscale cloud-resolving simulations to large-scale aerosol-transport simulations. Realistic aerosol loading, including spatio-temporal aerosol variations and particle-size spectra, is implemented in the cloud-resolving simulations. Prior studies employing ALICIS have demonstrated how the interface introduction significantly improves the reproducibility of the simulated microphysical cloud structure through better representation of aerosol effects on cloud.



Conceptual diagram of the coupling framework between a large-scale aerosol transport model and a regional-scale cloud resolving model using the ALICIS module.

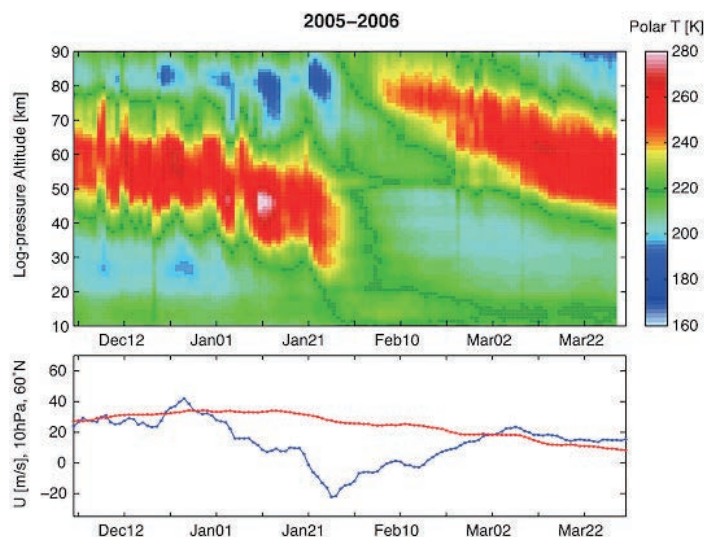


The dynamics of the mesosphere and lower thermosphere: a brief review

Vincent R A

[Keywords] Atmospheric tides, Gravity waves, Planetary waves, Middle atmosphere, Mesosphere, Lower thermosphere, Wave coupling

The dynamics of the mesosphere-lower thermosphere (MLT) (60 to 110 km) is dominated by waves and their effects. The basic structure of the MLT is determined by momentum deposition by small-scale gravity waves, which drives a summer-to-winter pole circulation at the mesopause. Atmospheric tides are also an important component of the dynamics of the MLT. Observations from extended ground-based networks, satellites as well as numerical modelling show that non-migrating tidal modes in the MLT are more important than previously thought, with evidence for directly coupling into the thermosphere/ionosphere. Major disturbances lower in the atmosphere, such as wintertime sudden stratospheric warmings, temporarily disrupt the circulation pattern and thermal structure of the MLT. In the equatorial mesosphere, gravity wave driving leads to oscillations in the zonal wind on semiannual time scales, although variability on quasi-biennial time scales is also apparent. Planetary-scale waves such as the quasi-two-day wave temporarily dominate the dynamics of the summertime MLT, especially in the southern hemisphere. Impacts may include short-term changes to the thermal structure and physics of the high-latitude MLT. Here, we briefly review the dynamics of the MLT, with a particular emphasis on developments in the past decade.



The 2006 major sudden warming. Top: time-height cross-section of temperatures during the major SSW in late January 2006. Note the descent and disappearance of the stratopause at the peak of the warming and its subsequent reappearance and descent from the mesosphere. Bottom: the time variation of the zonal-mean zonal wind at 10 hPa and 60 N. The blue line shows the wind during the stratwarming, while the red line depicts the climatological seasonal cycle. Adapted from Figure one of Yamazaki et al. (2012).

Stratospheric warmings occur when large-scale planetary waves break in the middle atmosphere (10-100 km) in winter. This figure shows that the whole middle atmosphere is affected, so that the EW (zonal) winds and the temperature structure temporarily revert to summer-like conditions. The zonal means winds in the stratosphere (blue line in bottom figure) become westward (negative) for a short time while those above 70 km (the mesosphere) become eastward. In turn, this change in the prevailing wind affects the vertical propagation of atmospheric gravity waves and changes their impact on the middle atmosphere. The effects of stratospheric warmings can also be observed in the ionosphere, impacting on radiowave propagation.

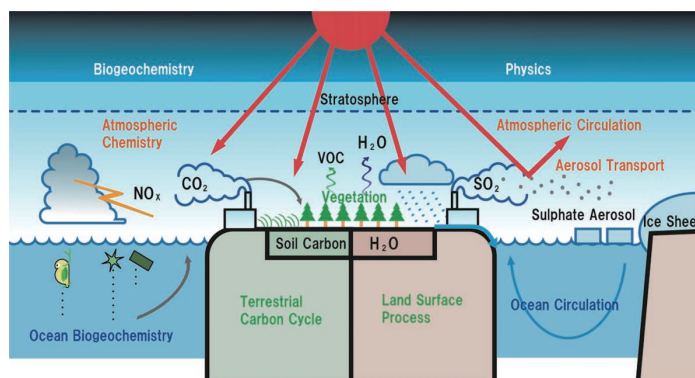


Modeling in Earth system science up to and beyond IPCC AR5

Hajima T, Kawamiya M, Watanabe M, Kato E, Tachiiri K, Sugiyama M, Watanabe S, Okajima H, Ito A

[Keywords] Earth system science, Earth system model, Carbon and nitrogen cycle, Land and ocean CO₂ uptake, Ocean acidification, Land-use and land-cover change, EMICs, Geoengineering, Iron deposition

Changes in the natural environment that are the result of human activities are becoming evident. Since these changes are interrelated and can not be investigated without interdisciplinary collaboration between scientific fields, Earth system science (ESS) is required to provide a framework for recognizing anew the Earth system as one composed of its interacting sub-systems. The concept of ESS has been partially realized by Earth system models (ESMs). In this paper, we focus on modeling in ESS,



Schematic diagram of Earth system models

review related findings mainly from the latest assessment report of the Intergovernmental Panel on Climate Change, and introduce tasks under discussion for the next phases of the following areas of science: the global nitrogen cycle, ocean acidification, land-use and land-cover change, ESMs of intermediate complexity, climate geoengineering, ocean CO₂ uptake, and deposition of bioavailable iron in marine ecosystems. Since responding to global change is a pressing mission in Earth science, modeling will continue to contribute to the cooperative growth of diversifying disciplines and expanding ESS, because modeling connects traditional disciplines through explicit interaction between them.

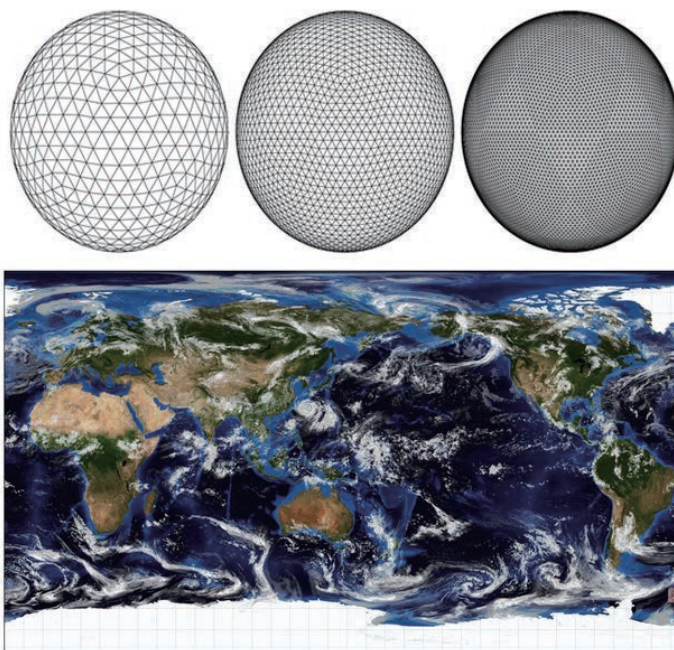


The Non-hydrostatic Icosahedral Atmospheric Model: Description and Development

Satoh M, Tomita H, Yashiro H, Miura H, Kodama C, Seiki T, Noda A, Yamada Y, Goto D, Sawada M, Miyoshi T, Niwa Y, Hara M, Ohno Y, Iga S, Arakawa T, Inoue T, Kubokawa H

[Keywords] Global non, hydrostatic model, Icosahedral grid, Global cloud-resolving simulations

This article reviews the development of a global non-hydrostatic model, focusing on the pioneering research of the Non-hydrostatic Icosahedral Atmospheric Model (NICAM). Very high resolution global atmospheric circulation simulations with horizontal mesh spacing of approximately 0.1 (km) were conducted using recently developed supercomputers. These types of simulations were conducted with a specifically designed atmospheric global model based on a quasi-uniform grid mesh structure and a non-hydrostatic equation system. This review describes the development of each dynamical and physical component of NICAM, the assimilation strategy and its related models, and provides a scientific overview of NICAM studies conducted to date.



Icosahedral grids for grid division levels of 3, 4, and 5 (from left to right) (horizontal mesh spacings of approximately 893, 446 and 223 km).

Cloud distribution simulated by the NICAM 870 m grid spacing experiment.



Review

Human geosciences

Biogeosciences

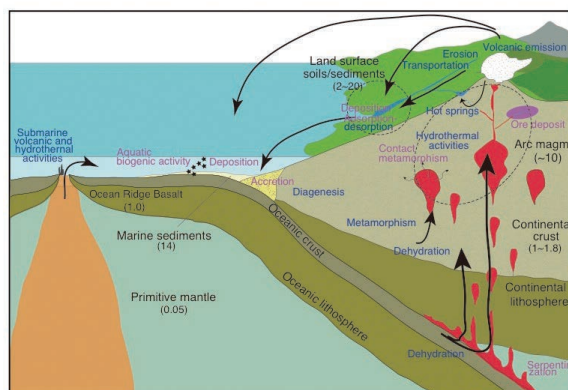
Arsenic cycling in the Earth's crust and hydrosphere: interaction between naturally occurring arsenic and human activities

Masuda H

[Keywords] Arsenic contamination, geologic cycle, plate tectonics, reduction, oxidation

Field-based research on naturally occurring arsenic contamination of surface waters and groundwaters and the mechanisms of contamination are reviewed. The distribution of arsenic is strongly related to areas of active plate tectonics, magmatism and associated hydrothermal activity, and high rates of erosion. Sources of arsenic contamination are mainly hydrothermal water, sulfide and arsenide minerals, volcanic ash, and iron oxyhydroxide/oxide as weathering products. The promotion of the reduction and oxidation of arsenic source minerals by in situ microbial activity is an important secondary mechanism that often determines arsenic levels in groundwater. Anthropogenic activities, such as geothermal and mining operations, as well as excess pumping of shallow groundwaters, disperse arsenic in the environment, thereby expanding areas of arsenic contamination.

Masuda, Figure 4



Geologic cycle concerning arsenic transportation in the geosphere and surface of the Earth shows the arsenic recycles in association with active tectonics.

Digit in parenthesis gives the average concentrations of each geologic body. Purple and blue colored letters indicate the releasing and fixing mechanisms of arsenic in the cycle.



Perspective on the response of marine calcifiers to global warming and ocean acidification – Behavior of corals and foraminifera in a high CO₂ world “hot house”

Kawahata H, Fujita K, Iguchi A, Inoue M, Iwasaki S, Kuroyamagi A, Maeda A, Manaka T, Moriya K, Takagi H, Toyofuku T, Yoshimura T, Suzuki A

[Keywords] Partial pressure of CO₂, Global warming, Ocean acidification, Coral, Foraminifera, Bleaching, Calcite, Aragonite, Saturation state, Organic matter, Alkalinity, Carbon cycle

The CO₂ concentration of air has increased over the last two centuries and recently surpassed 400 ppm. Carbon cycle models project CO₂ concentrations of 720 to 1000 ppm for the IPCC intermediate scenario (RCP 6.0), resulting in an increase in global mean temperature of ~2.6 °C and a decrease in seawater pH of ~0.3. Together, global warming and ocean acidification are often referred to as the “evil twins” of climate change, potentially inducing severe threats in the near future. In this paper, our discussion is focused on the response of two major calcifiers, foraminifera and corals, which contribute much to the global carbonate burial rate. Photosymbiosis is regarded as an adaptive ecology for living in warm and oligotrophic oceans, especially for reef-building corals and larger reef-dwelling benthic foraminifera. As a consequence of global warming, bleaching may be a global threat to algal symbiont-bearing marine calcifying organisms under conditions of high temperature and light intensity. If CO₂ is dissolved in seawater, the partial pressure of CO₂ in seawater (*p*CO₂) and dissolved inorganic carbon (DIC) increases while pH and the saturation state of carbonate minerals decreases without any change in total alkalinity. Generally, marine calcifying organisms show decreases in calcification rates in response to acidified seawater. However, the response often differs depending on situations, species, and life-cycle stage. Some benthic foraminifera showed a positive response to low pH conditions. The *Acropora digitifera* coral calcification of adult branches was not reduced markedly at higher *p*CO₂ conditions, although calcification tended to decrease versus *p*CO₂ in both aposymbiotic and symbiotic polyps. New analytical technologies help identify important constraints on calcification processes. Based upon Ca isotopes, the transport path of Ca²⁺ and the degree of its activity would predominantly control the carbonate precipitation rate. Visualization of the extracellular pH distribution shows that proton pumping produces the high internal pH and large internal–external pH gap in association with foraminiferal calcification. From the perspective of a long-term change in the Earth’s surface environment, foraminifera seem to be more adaptive and robust than corals in coping with ocean warming and acidification but it is necessary to further understand the mechanisms underlying variations in sensitivity to heat stress and acidified seawater for future prediction. Since CO₂ is more soluble in lower temperature seawater, ocean acidification is more critical in the polar and high-latitude regions. Additionally, older deep-water has enhanced acidity owing to the addition of CO₂ from the degradation of organic matter via a synergistic effect with high pressure. With current ocean acidification, pH and the saturation state of carbonate minerals are decreasing without any change in total alkalinity. However, in the Earth’s history, it is well known that alkalinity has fluctuated significantly. Therefore, it is necessary to quantitatively reconstruct alkalinity, which is another key factor determining the saturation state of carbonate minerals. The rapid release of anthropogenic CO₂ (in the present day and at the Paleocene/Eocene boundary) induces severe ocean acidification, whereas in the Cretaceous, slow environmental change, even at high levels of *p*CO₂, could raise alkalinity, thereby neutralizing ocean acidification.

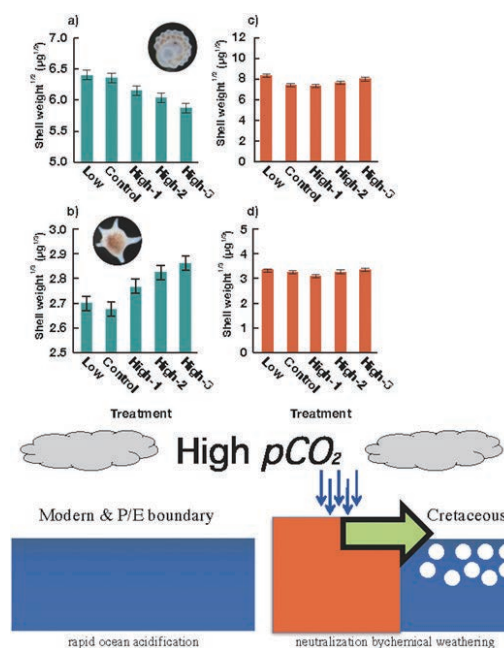


Fig. 1. Comparison of an acidification condition experiment and the growth weight of foraminifera.

Fig. 2. Schematic diagram of ocean acidification and the buffering system in the Earth’s surface system.

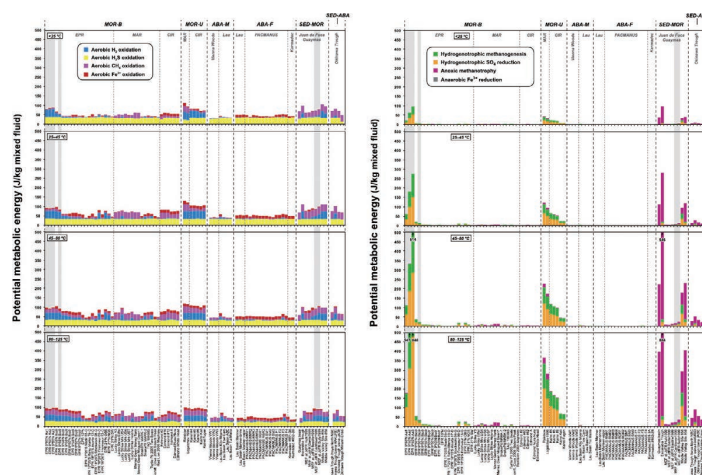


Theoretical constraints of physical and chemical properties of hydrothermal fluids on variations in chemolithotrophic microbial communities in seafloor hydrothermal systems.

Nakamura K, Takai K

[Keywords] Deep-sea hydrothermal systems, Chemosynthetic ecosystems, Hydrothermal fluid chemistry, Host rock geochemistry, Geochemical modeling, Bioavailable energy yield

In the past few decades, chemosynthetic ecosystems at deep-sea hydrothermal vents have received attention as plausible analogues to the early ecosystems of Earth, as well as to extraterrestrial ecosystems. These ecosystems are sustained by chemical energy obtained from inorganic redox substances (e.g., H_2S , CO_2 , H_2 , CH_4 , and O_2) in hydrothermal fluids and ambient seawater. The chemical and isotope compositions of the hydrothermal fluid are, in turn, controlled by subsurface physical and chemical processes, including fluid–rock interactions, phase separation and partitioning of fluids, and precipitation of minerals. We hypothesized that specific physicochemical principles describe the linkages among the living ecosystems, hydrothermal fluids, and geological background in deep-sea hydrothermal systems. We estimated the metabolic energy potentially available for productivity by chemolithotrophic microorganisms at various hydrothermal vent fields. We used a geochemical model based on hydrothermal fluid chemistry data compiled from 89 globally distributed hydrothermal vent sites. The model estimates were compared to the observed variability in extant microbial communities in seafloor hydrothermal environments. Our calculations clearly show that representative chemolithotrophic metabolisms (e.g., thiotrophic, hydrogenotrophic, and methanotrophic) respond differently to geological and geochemical variations in the hydrothermal systems. Nearly all of the deep-sea hydrothermal systems provide abundant energy for organisms with aerobic thiotrophic metabolisms; observed variations in the H_2S concentrations among the hydrothermal fluids had little effect on the energetics of thiotrophic metabolism. Thus, these organisms form the base of the chemosynthetic microbial community in global deep-sea hydrothermal environments. In contrast, variations in H_2 concentrations in hydrothermal fluids significantly impact organisms with aerobic and anaerobic hydrogenotrophic metabolisms. Particularly in H_2 -rich ultramafic rock-hosted hydrothermal systems, anaerobic and aerobic hydrogenotrophy is more energetically significant than thiotrophy. The CH_4 concentration also has a considerable impact on organisms with aerobic and anaerobic methanotrophic metabolisms, particularly in sediment-associated hydrothermal systems. Recently clarified patterns and functions of existing microbial communities and their metabolisms are generally consistent with the results of our thermodynamic modeling of the hydrothermal mixing zones. These relationships provide important directions for future research addressing the origin and early evolution of life on Earth as well as for the search for extraterrestrial life.



Metabolic energies available from each (Left) aerobic and (Right) anaerobic reactions for chemolithoautotrophy considered in this study

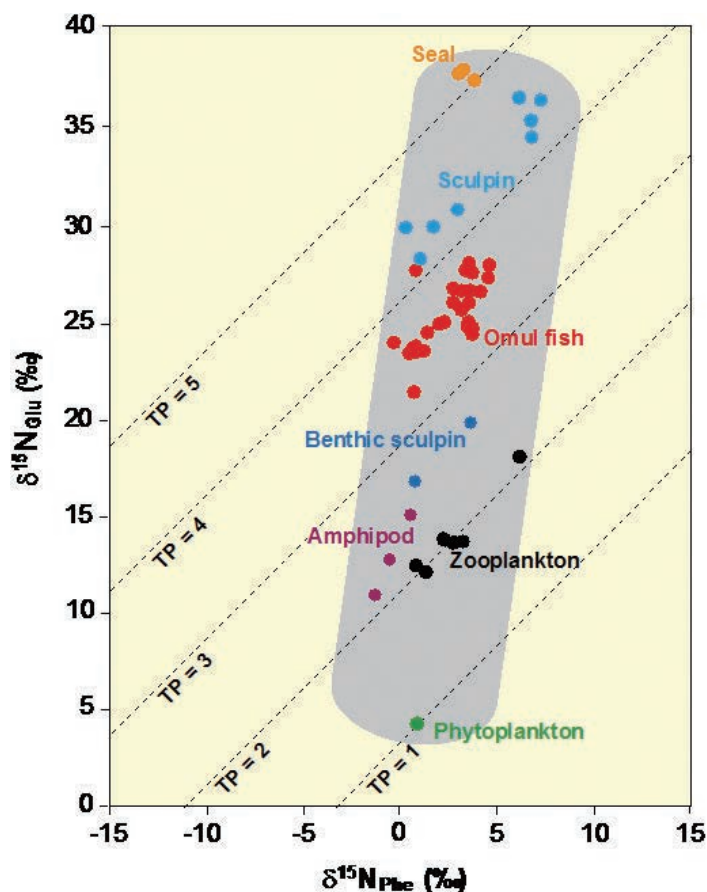


Biochemical and physiological bases for the use of carbon and nitrogen isotopes in environmental and ecological studies

Ohkouchi N, Ogawa N O, Chikaraishi Y, Tanaka H, Wada E

[Keywords] Carbon isotopic composition, Nitrogen isotopic composition, Ecosystem, Food web, Chlorophyll, Trophic position, Amino acid, Animal organ

We review the biochemical and physiological bases of the use of carbon and nitrogen isotopic compositions as an approach for environmental and ecological studies. Biochemical processes commonly observed in the biosphere, including the decarboxylation and deamination of amino acids, are the key factors in this isotopic approach. The principles drawn from the isotopic distributions disentangle the complex dynamics of the biosphere and allow the interactions between the geosphere and biosphere to be analyzed in detail. We also summarize two recently examined topics with new datasets: the isotopic compositions of individual biosynthetic products (chlorophylls and amino acids) and those of animal organs for further pursuing the basis of the methodology. As a tool for investigating complex systems, compound-specific isotopic analysis compensates the intrinsic disadvantages of bulk isotopic signatures. Chlorophylls provide information about the particular processes of various photoautotrophs, whereas amino acids provide a precise measure of the trophic positions of heterotrophs. The isotopic distributions of carbon and nitrogen in a single organism as well as in the whole biosphere are strongly regulated, so that their major components such as amino acids are coordinated appropriately rather than controlled separately.



Trophic positions of organisms from Lake Baikal based on the nitrogen isotopic composition of amino acids (glutamic acid and phenylalanine). "TP" denotes trophic position.



Review

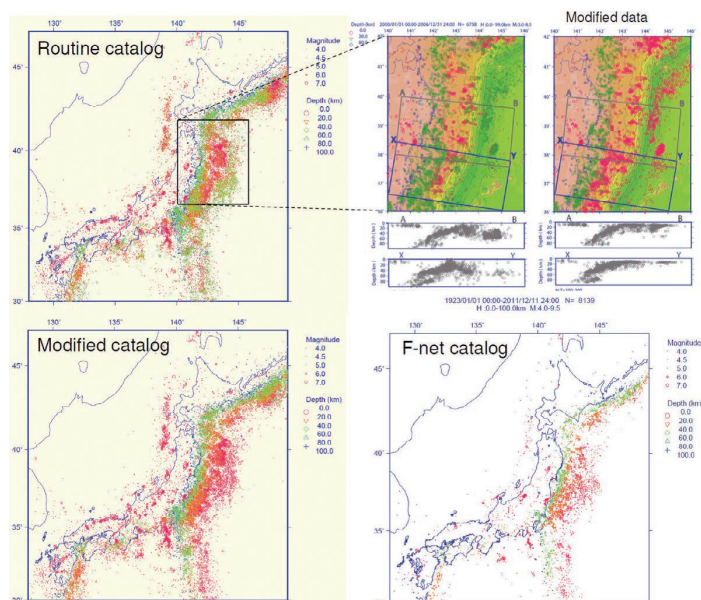
Solid earth sciences

Visualizing heterogeneities of earthquake hypocenter catalogs: modeling, analysis, and compensation

Ogata Y

[Keywords] ABIC, Bias compensation, Detection rate function, Empirical Bayesian method, Data heterogeneity, Hypocenter catalogs, Location corrections, MAP solutions, Magnitude-shift, Smoothness constraints

As basic data for seismic activity analysis, hypocenter catalogs need to be accurate, complete, homogeneous, and consistent. Therefore, clarifying systematic errors in catalogs is an important discipline of seismicity research. This review presents a systematic model-based methodology to reveal various biases and the results of the following analyses. (1) It is critical to examine whether there is a non-stationary systematic estimation bias in earthquake magnitudes in a hypocenter catalog. (2) Most earthquake catalogs covering long periods are not homogeneous in space, time, and magnitude ranges. Earthquake network structures and seismometers change over time, and therefore, earthquake detection rates change over time and space. Even in the short term, many aftershocks immediately following large earthquakes are often undetected, and the detection rate varies, depending on the elapsed time and location. By establishing a detection rate function, the actual seismic activity and the spatio-temporal heterogeneity of catalogs can be discriminated. (3) Near real-time correction of source locations, far from the seismic observation network, can be implemented based on better determined source location comparisons of other catalogs using the same identified earthquakes. The bias functions were estimated using an empirical Bayes method. I provide examples showing different conclusions about the changes in seismicity from different earthquake catalogs. Through these analyses, I also present actual examples of successful modifications as well as various misleading conclusions about changes in seismic activity. In particular, there is a human made magnitude shift problem included in the global catalog of large earthquakes in the late nineteenth and early twentieth centuries.



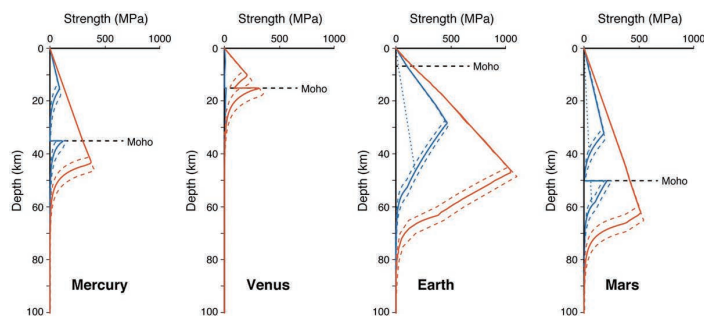
Strength models of the terrestrial planets and implications for their lithospheric structure and evolution

Ikuo Katayama

[Keywords] Rheological structure, Lithosphere, Elastic thickness, Terrestrial planets

Knowledge of lithospheric strength can help to understand the internal structure and evolution of the terrestrial planets, as surface topography and gravity fields are controlled mainly by deformational features within the lithosphere. Here, strength profiles of lithosphere were calculated for each planet using a recently updated flow law and taking into account the effect of water on lithospheric deformation. Strength is controlled predominantly by brittle deformation at shallow depths, whereas plastic deformation

becomes dominant at greater depths through its sensitivity to temperature. Incorporation of Peierls creep, in which strain rate is exponentially dependent on stress, results in the weakening of plastic strength at higher stress levels, and the transition from brittle to ductile deformation shifts to shallower depths than those calculated using conventional power-law creep. Strength in both the brittle and ductile regimes is highly sensitive to the presence of water, with the overall strength of the lithosphere decreasing markedly under wet conditions. The markedly low frictional coefficient of clay minerals results in a further decrease in brittle strength and is attributed to expansion of the brittle field. As plastic strength is influenced by lithology, a large strength contrast can occur across the crust–mantle boundary if deformation is controlled by ductile deformation. Effective elastic thickness for the terrestrial planets calculated from the rheological models indicates its close dependence on spatiotemporal variations in temperature and the presence of water. Although application of the strength models to observed large-scale surface deformational features is subject to large extrapolation and uncertainties, I emphasize the different sensitivity of these features to temperature and water, meaning that quantifying these features (e.g., by data from orbiting satellites or rovers) should help to constrain the internal structure and evolution of the terrestrial planets.



Strength models of terrestrial planets calculated under dry (red lines) and wet (blue lines) conditions.



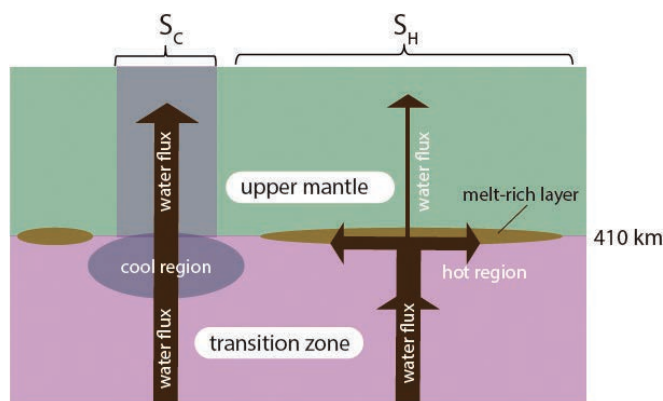
Deep mantle melting, global water circulation and its implications for the stability of the ocean mass

Shun-ichiro Karato, Bijaya Karki, Jeffrey Park

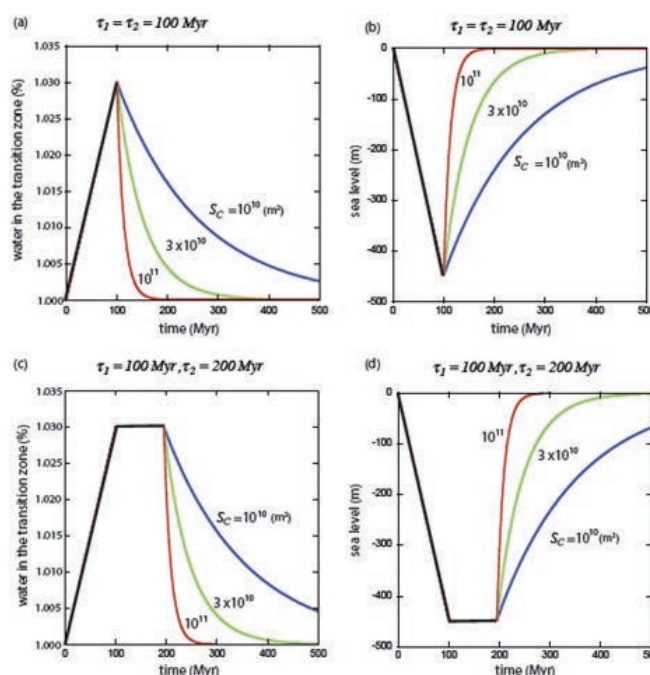
[Keywords] habitability, ocean mass, sea-level variations, mantle transition zone, water in the mantle, deep mantle melting, water valve

Oceans on Earth are present as a result of dynamic equilibrium between degassing and regassing through the interaction with Earth's interior. We review mineral physics, geophysical, and geochemical studies related to the global water circulation and conclude that the water content has a peak in the mantle transition zone (MTZ) with a value of 0.1–1 wt% (with large regional variations). When water-rich MTZ materials are transported out of the MTZ, partial melting occurs. Vertical direction of melt migration is determined by the density contrast between the melts and coexisting minerals. Because a density change associated with a phase transformation occurs sharply for a solid but more gradually for a melt, melts formed above the phase transformation depth are generally heavier than solids, whereas melts formed below the transformation depth are lighter than solids. Consequently, hydrous melts formed either above or below the MTZ return to the MTZ, maintaining its high water content. However, the MTZ water content cannot increase without limit. The melt-solid density contrast above the 410 km depends on the temperature. In cooler regions, melting will occur only in the presence of very water-rich materials. Melts produced in these regions have high water content and hence can be buoyant above the 410 km, removing water from the MTZ. Consequently, cooler regions of melting act as a water valve to maintain the water content of the MTZ near its threshold level (~0.1–1.0 wt%). Mass-balance considerations explain the observed near-constant

sea-level despite large fluctuations over Earth history. Observations suggesting deep-mantle melting are reviewed including the presence of low-velocity anomalies just above and below the MTZ and geochemical evidence for hydrous melts formed in the MTZ. However, the interpretation of long-term sea-level change and the role of deep mantle melting in the global water circulation are non-unique and alternative models are reviewed. Possible future directions of studies on the global water circulation are proposed including geodynamic modeling, mineral physics and observational studies, and studies integrating results from different disciplines.



Processes of water transport across the 410-km with heterogeneous temperature



Results of model calculations on ocean mass history



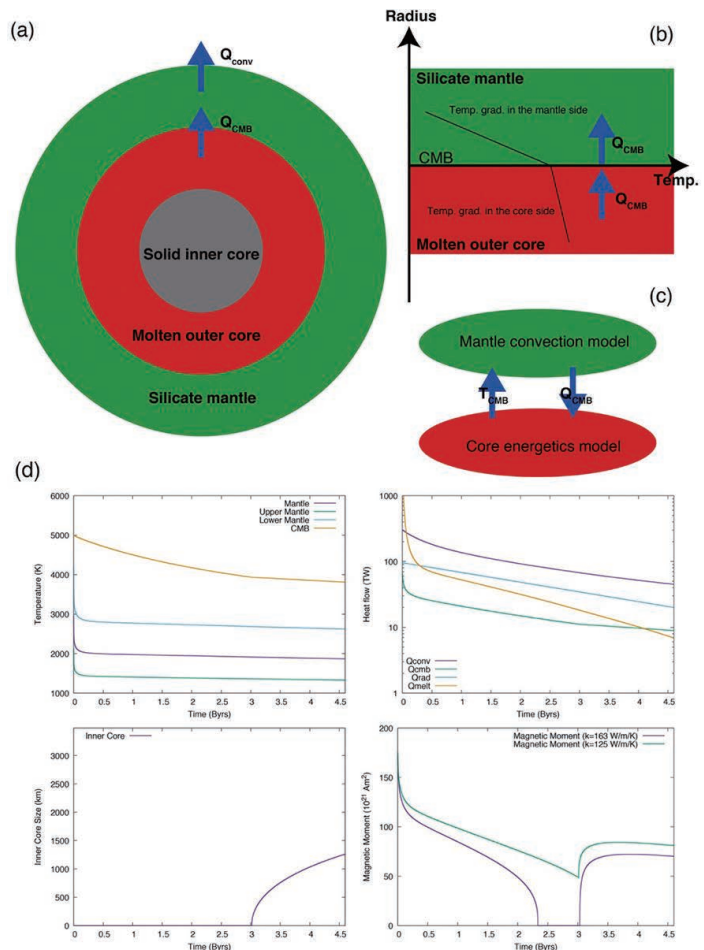
A coupled core-mantle evolution: Review and future prospects

Takashi Nakagawa

[Keywords] Geomagnetic field, Earth's core, Deep mantle, Long-term evolution

In this review, I provide the current status and future prospects for the coupled core-mantle evolution and specifically summarize the constraints arising from geomagnetism and paleomagnetism on the long-term secular variations of the geomagnetic field. The heat flow across the core-mantle boundary (CMB) is essential for determining the best-fit scenario that explains the observational data of geomagnetic secular variations (e.g., onset timing of the inner core growth, geomagnetic polarity reversals, and westward drift) and should include the various origins of the heterogeneous structures in the deep mantle that have affected the heat transfer across the CMB for billions of years. The coupled core-mantle evolution model can potentially explain the onset timing of the inner core and its influence on the long-term geomagnetic secular variations, but it is still controversial among modeling approaches on the core energetics because the paleomagnetic data contains various uncertainties. Additionally, with the coupled core-mantle evolution model in geodynamo simulations, the frequency of the geomagnetic polarity reversals can be explained with the time variations of the heat flow across the CMB. Additionally, the effects of the stable region in the outermost outer core to the magnetic evolution are also crucial but there would be still uncertain for their feasibility.

However, despite this progress in understanding the observational data for geomagnetic secular variations, there are several unresolved issues that should be addressed in future investigations: (1) initial conditions—starting with the solidification of the global magma ocean with the onset timing of plate tectonics and geodynamo actions and (2) planetary habitability—how the dynamics of the Earth's deep interior affects the long-term surface environment change that has been maintained in the Earth's multisphere coupled system.



(a) Schematic illustration of the coupled core-mantle evolution system; (b) Zoom-up of the thermal structure across the core-mantle boundary; (c) Schematic illustration of the feedback mechanism between core and mantle evolution; (d) An example result on the coupled core-mantle evolution model in parameterized mantle convection computation (Upper left: Thermal structure of the mantle; Upper right: Heat budget in the mantle; Lower left: Size of the inner core as a function of time; Lower right: Magnetic moment). On the magnetic moment, two values of the thermal conductivity of the Earth's core are assumed (163 W/m/K and 125 W/m/K).



Some remarks on hydrogen-assisted electrical conductivity in olivine and other minerals

Shun-ichiro Karato

[Keywords] Electrical conductivity, Hydrogen, Water in the mantle, Point defects

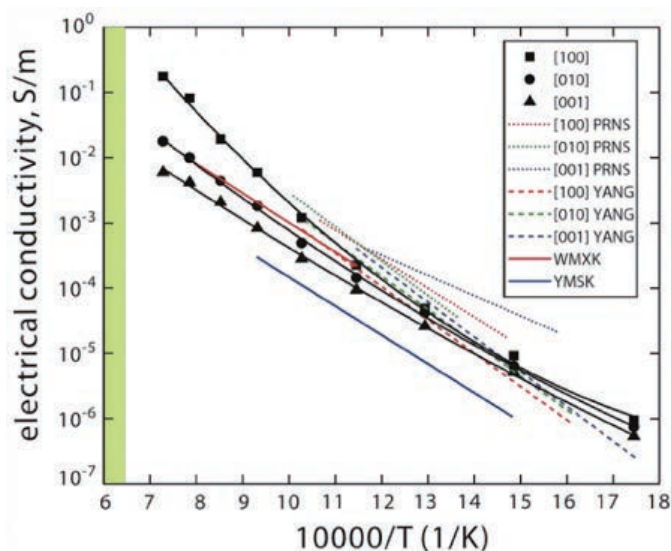
Electrical conductivity in minerals is sensitive to hydrogen content, and therefore, it is a potentially important property from which one can infer hydrogen (water) distribution in the mantle. However, there has been much confusion in the reported results on hydrogen-assisted conductivity. In this paper, I review the existing experimental observations on hydrogen-enhanced electrical conductivity in olivine and other minerals to identify the causes of confusion. Hydrogen loss as well as hydrogen gain could occur during a conductivity measurement at high pressures and temperatures. Particularly important is the unrecognized hydrogen gain during an experiment that could lead to a large degree of error. Many experiments were conducted under the conditions where specimens were super-saturated with hydrogen making the validity of those results unclear. A model for hydrogen loss is developed showing a strategy by which hydrogen loss can be minimized.

When one selects the experimental results in which the influence of hydrogen loss/gain are carefully examined, there is no major discrepancy among the results from different laboratories except differences between the results from low and high temperatures. Differences between low-temperature and high-temperature results are caused by the change in conduction mechanism. At low temperatures, conduction is due to the migration of interstitial (“free”) proton and is nearly isotropic, whereas conduction at high temperatures is due to the migration of two protons at M-site that is highly anisotropic. There is no evidence for substantial concentration dependence of activation enthalpy. Observed exceptionally large concentration dependence reported by Poe et al. (Phys Earth Planet Inter 181:103-111, 2010) is inconsistent with all other reports and is likely caused by some experimental artifact.

Experimental results in the high-temperature regime explain a majority of geophysical observations on the conductivity of the oceanic asthenosphere: partial melting is not needed in most regions and is rather inconsistent with the observations on the matured oceanic mantle. Exception is the asthenosphere near the ridge and/or near the trench where very high conductivity (~ 0.1 S/m) is reported at the top of the asthenosphere. Partial melting might play some role in these regions.

Electrical conductivity in the continental lithosphere cannot be attributed entirely to olivine. An important role of orthopyroxene and/or other minor materials (graphite, sulfide) is needed to explain high conductivity reported in some regions such as Bushveld in South Africa.

The largest remaining uncertainty is the degree to which hydrogen affects electrical conductivity in the lower mantle minerals. Determining the influence of hydrogen on electrical conductivity in lower mantle minerals is critical to make progress in understanding the global water circulation.



Electrical conductivity of hydrogen-bearing olivine. There is a systematic difference between low temperature and high temperature data. High temperature data are consistent with geophysically inferred electrical conductivity in the asthenosphere.



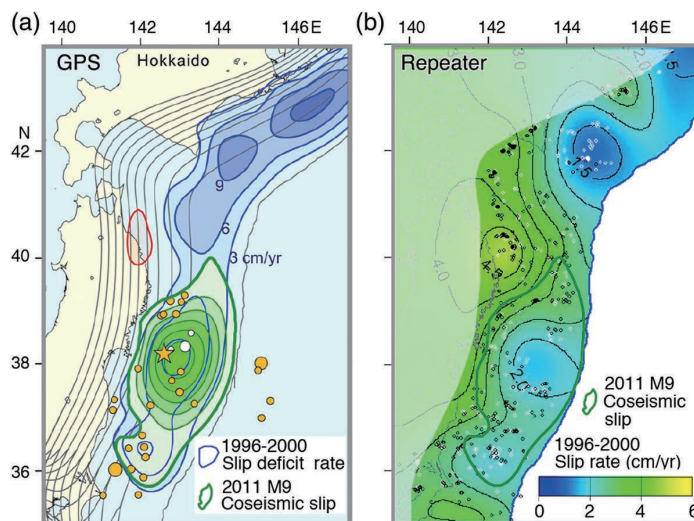
Detection of repeating earthquakes and their application in characterizing slow fault slip

Naoki Uchida

[Keywords] Repeating earthquake, Interplate slip, Fault creep, Aseismic slip

Repeating earthquakes (repeaters) that rupture the same fault area (patch) are interpreted to be caused by repeated accumulation and release of stress on the seismic patch in a creeping area. This relationship between repeaters with fault creep can be exploited for tracking the fault creep (slow slip) based on the repeaters' activity. In other words, the repeaters can be used as creepmeters embedded on a fault. To do this, it is fundamentally important to select earthquakes that definitely re-rupture in the same area. The selections are usually done based on waveform similarity or hypocenter location. In hypocenter-location based detection, the precision of the relative location compared with the dimension of earthquake sources

is critical for confirming the co-location of the source area. On the other hand, waveform-similarity-based detection needs to use appropriate parameters including high enough frequency components to distinguish neighboring sources. Inter-event timing (recurrence interval) and/or the duration of a sequence's activity are good diagnostic features for finding appropriate detection parameters and eliminating non-repeating events, which are important because an inappropriate selection leads to including triggered sequences that do not re-rupture the same area. Repeaters provide an independent estimation of creep from geodetic data and such estimations are mostly in good agreement when both kinds of data are available. Repeater data are especially useful in the deeper part of strike-slip faults and in near-trench areas of subduction zones where geodetic data's resolution is usually limited. The repeaters also have an advantage with geodetic data analysis because they are not contaminated by viscoelastic deformation or poroelastic rebound which are prominent postseismic process for large earthquakes and occur outside of faults. On the other hand, the disadvantages of repeater analysis include their uneven spatial distribution and the uncertainty of the estimates of slip amount requiring a scaling relationship between earthquake size and slip. There are considerable variations in the inferred slip amounts from different relationships. Applications of repeater analysis illuminate the spatial distribution of interplate stable slip, after slip, and spontaneous and cyclic slow slip events that represent important components of interplate slip processes in addition to major earthquakes.



Estimation of interplate coupling based on repeating earthquake data (b) and GPS data (a) (after Nomura et al., 2017).

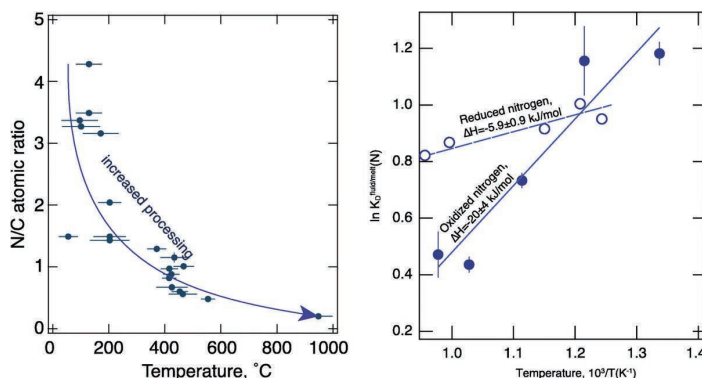


Nitrogen in the Earth: abundance and transport

Bjorn Mysen

[Keywords] Nitrogen, Recycling, Redox, Speciation, Solubility

The terrestrial nitrogen budget, distribution, and evolution are governed by biological and geological recycling. The biological cycle provides the nitrogen input for the geological cycle, which, in turn, feeds some of the nitrogen into the Earth's interior. A portion of the nitrogen also is released back to the oceans and the atmosphere via N_2 degassing. Nitrogen in silicate minerals (clay minerals, mica, feldspar, garnet, wadsleyite, and bridgmanite) exists predominantly as NH_4^+ . Nitrogen also is found in graphite and diamond where it occurs in elemental form. Nitrides are stable under extremely reducing conditions such as those that existed during early planetary formation processes and may still persist in the lower mantle. From experimentally determined nitrogen solubility in such materials, the silicate Earth is nitrogen undersaturated. The situation for the core is more uncertain, but reasonable Fe metal/silicate nitrogen partition coefficients (>10) would yield nitrogen contents sufficient to account for the apparent nitrogen deficiency in the silicate Earth compared with other volatiles. Transport of nitrogen takes place in silicate melt (magma), water-rich fluids, and as a minor component in silicate minerals. In melts, the N solubility is greater for reduced nitrogen, whereas the opposite appears to be the case for N solubility in fluids. Reduced nitrogen species (NH_3 , NH_2^- , and NH_2^+) dominate in most environments of the modern Earth's interior except the upper ~ 100 km of subduction zones where N_2 is the most important species. Nitrogen in magmatic liquids in the early Earth probably was dominated by NH_3 and NH_2^- , whereas in the modern Earth, the less reduced, NH_2^+ functional group is more common. N_2 is common in magmatic liquids in subduction zones. Given the much lower solubility of N_2 in magmatic liquids compared with other nitrogen species, nitrogen dissolved as N_2 in subduction zone magmas is expected to be recycled and returned to the oceans and the atmosphere, whereas nitrogen in reduced form(s) likely would be transported to greater depths. This solubility difference, controlled primarily by variations in redox conditions, may be a factor resulting in increased nitrogen in the Earth's mantle and decreasing abundance in its oceans and atmosphere during the Earth's evolution. Such an abundance evolution has resulted in the decoupling of nitrogen distribution in the solid Earth and the hydrosphere and atmosphere.

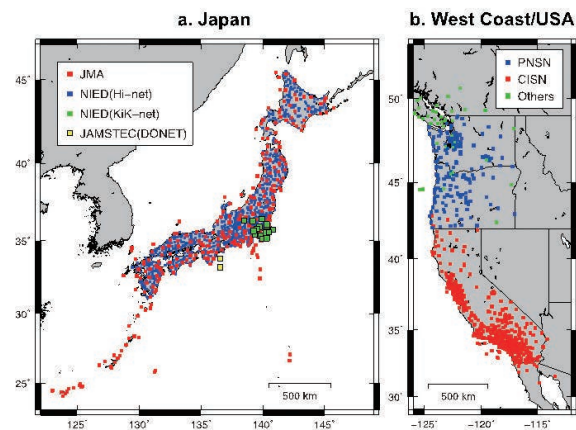
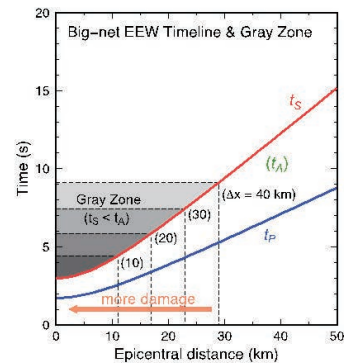


Earthquake Early Warning: what does “seconds before a strong hit” mean?

Tajima F, Hayashida T.

[Keywords] Earthquake early warning, effective preparation for seismic safety at recipients' sites, short-wavelength ground motion variation

An earthquake early warning (EEW) system is designed to detect an event, determine its parameters (hypocenter, magnitude, and origin time), and issue an alert to sites/areas where necessary actions should be taken before destructive seismic energy arrivals. At present, large-scale EEW systems are operational in several countries around the world. The most extensive nationwide EEW system has been operating in Japan since 2007, and was able to issue alerts broadly when the moment magnitude (M_w) 9 Tohoku-Oki earthquake hit in 2011. The casualties caused by this event were far less than those caused by other deadly earthquakes ($M_w \geq 6.6$) in this century. Many other countries attributed the fewer death victims to the advanced large-scale EEW system, and plan to install systems similar to Japan's model. However, the historical and environmental background in Japan, both in terms of earthquake hazards and safety preparation, differs considerably from other countries. In addition, EEW systems that use data from a large-scale network (i.e., “a big-net” hereafter) still have limitations. There are thus numerous factors that other countries should consider to benefit from installing a Japan-styled EEW. In this article, we review how research and development associated with EEW have been carried out, and how EEW systems presently function. We then show short-wavelength variation of ground motions within the typical station interval of a big-net using data recorded by a dense local seismic network in Japan. However, it is not particularly meaningful to attempt detailed modeling of varieties of ground motion within the station interval for a big-net EEW operation, because the possible combinations of earthquake sources, paths of wave propagation, and recipient sites are infinite. We emphasize that in all circumstances, for recipients to benefit from EEW, seismic safety preparations must be implemented. Necessary preparations at sites do not diminish in importance after incremental improvements in station coverage and/or algorithms in a big-net operation. Further, scientists and engineers involved in EEW projects should strive to publically disseminate how big-net EEW systems work, and also why, to achieve maximum benefit, these systems should always be supplemented by preparations at recipients' sites.



(top)

Big-net timeline of EEW alert issuance at t_A and gray zones where strong shaking may arrive at t_S before t_A . The vertical axis is the time relative to an earthquake origin time, and the horizontal axis the epicentral distance (D). Gray zones are illustrated for networks of different station spacing $\Delta x = 10, 20, 30,$ and 40 km. For example, for a network of $\Delta x = 20$ km, the gray zone radius is ~ 17 km from the epicenter, where the ground shaking may arrive before an alert and is likely to be stronger, causing more damage than outside of it.

(bottom)

Big-net station distributions: a. the station spacing in Japan is ~ 20 km or less over the country. This implies that the average gray zone radius is ~ 17 km from a hypo-center; b. the station spacing in the West Coast/USA is not homogeneous, i.e., it is ~ 10 km in the populated metropolitan areas such as around Los Angeles, San Francisco Bay and Seattle whereas it is larger in less populated areas.

Published: 2018/10/10

<https://doi.org/10.1186/s40645-018-0221-6>



Redox-controlled mechanisms of C and H isotope fractionation between silicate melt and COH fluid in the Earth's interior

Mysen B

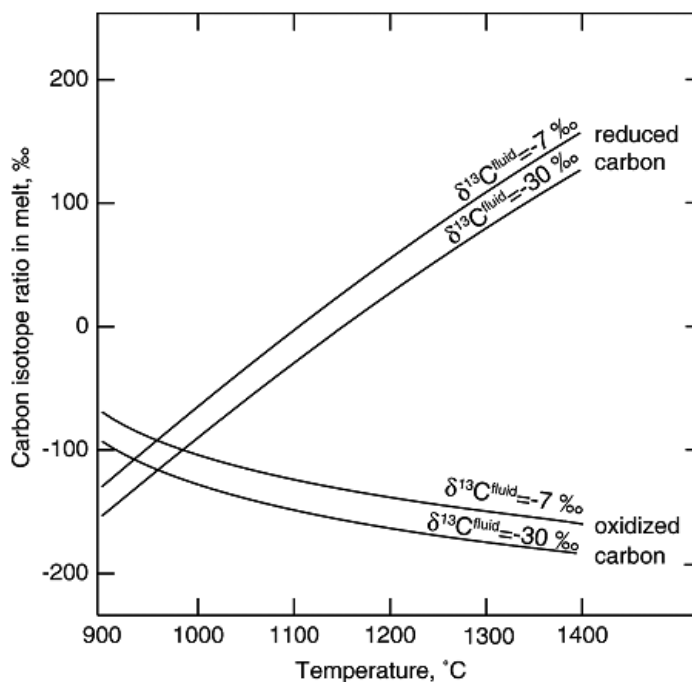
[Keywords] Fluid, Solubility, Structure, Spectroscopy, Redox, Stable isotopes

The behavior of COH fluids, their isotopes (hydrogen and carbon), and their interaction with magmatic liquids are at the core of understanding formation and evolution of the Earth. Experimental data are needed to aid our understanding of how COH volatiles affect rock-forming processes in the Earth's interior. Here, I present a review of experimental data on structure of fluids and melts and an assessment of how structural factors govern hydrogen and carbon isotope partitioning within and between melts and fluids as a function of redox conditions, temperature, and pressure.

The solubility of individual COH components in silicate melts can differ by several orders of magnitude and ranges from several hundred ppm to several wt%. Silicate solubility in fluid can reach several molecular at mantle temperatures and pressures. Different solubility of oxidized and reduced C-bearing species in melts reflects different solution equilibria. These equilibria are $2\text{CH}_4 + \text{Q}^n = 2\text{CH}_3^- + \text{H}_2\text{O} + \text{Q}^{n+1}$ and $2\text{CO}_3^{2-} + \text{H}_2\text{O} + 2\text{Q}^{n+1} = \text{HCO}_3^- + 2\text{Q}^n$, under reducing and oxidizing conditions, respectively. In the Q^n -notations, the superscript, n , denotes the number of bridging oxygen in the silicate species (Q-species).

The structural changes of carbon and silicate in magmatic systems (melts and fluids) with variable redox conditions result in hydrogen and carbon isotope fractionation factors between melt, fluid, and crystalline materials that depend on redox conditions and can differ significantly from 1 even at magmatic temperatures. The ΔH of D/H fractionation between aqueous fluid and magma in silicate–COH systems is between -5 and 25 kJ/mol depending on redox conditions. The ΔH values for $^{13}\text{C}/^{12}\text{C}$ fractionation factors are near -3.2 and 1 kJ/mol under oxidizing and reducing conditions, respectively. These differences are because energetics of O–D, O–H, O– ^{13}C , and O– ^{12}C bonding environments are governed by different solution mechanisms in melts and fluids.

From the above data, it is suggested that (COH)-saturated partial melts in the upper mantle can have δD values 100%, or more, lighter than coexisting silicate-saturated fluid. This effect is greater under oxidizing than under reducing conditions. Analogous relationships exist for $^{13}\text{C}/^{12}\text{C}$. At magmatic temperatures in the Earth's upper mantle, $^{13}\text{C}/^{12}\text{C}$ of melt in equilibrium with COH-bearing mantle in the -7 to -30 ‰ range increases with temperature from about 40 to >100 ‰ and 80–120‰ under oxidizing and reducing conditions, respectively.



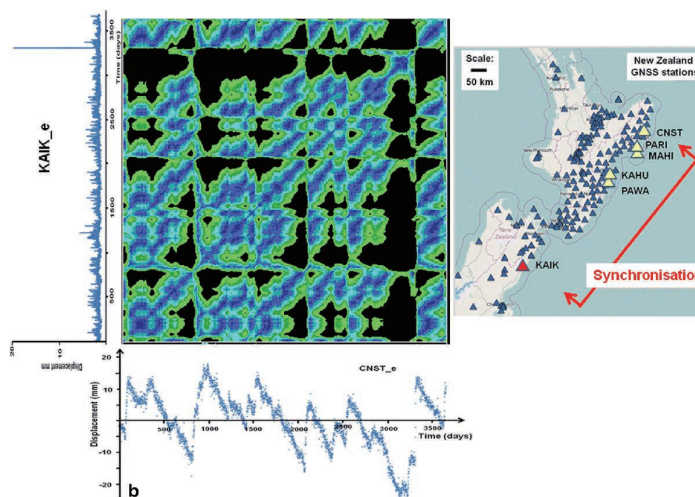
Nonlinear dynamical analysis of GNSS data: quantification, precursors and synchronization

Hobbs B, Ord A

[Keywords] GNSS time series, Nonlinear analysis, Dynamical systems, Recurrence plots, Recurrence quantification analysis (RQA), Cross and joint recurrence plots, Crustal deformation, Precursors, Synchronisation

The goal of any nonlinear dynamical analysis of a data series is to extract features of the dynamics of the underlying physical and chemical processes that produce that spatial pattern or time series; a by-product is to characterise the signal in terms of quantitative measures. In this paper, we briefly review the methodology involved in nonlinear analysis and explore time series for GNSS crustal displacements with a view to constraining the dynamics of the underlying tectonic processes responsible for the kinematics. We use recurrence plots and their quantification to extract the invariant measures of the tectonic system including the embedding dimension, the maximum Lyapunov exponent and the entropy and characterise the system using recurrence quantification analysis (RQA). These measures are used to develop a data

model for some GNSS data sets in New Zealand. The resulting dynamical model is tested using nonlinear prediction algorithms. The behaviours of some RQA measures are shown to act as precursors to major jumps in crustal displacement rate. We explore synchronisation using cross- and joint-recurrence analyses between stations and show that generalised synchronisation occurs between GNSS time series separated by up to 600 km. Synchronisation between stations begins up to 250 to 400 days before a large displacement event and decreases immediately before the event. The results are used to speculate on the coupled processes that may be responsible for the tectonics of the observed crustal deformations and that are compatible with the results of nonlinear analysis. The overall aim is to place constraints on the nature of the global attractor that describes plate motions on the Earth.



Synchronisation of GNSS data in New Zealand. Colored map is a joint recurrence plot of detrended coordinate time series (E-W component) at CNST (below) and KAIK (left) sites. Correlation concentrates along the diagonal line 250–400 days before large slow slip events (~800, =2100, and 3300 days), indicating synchronisation.

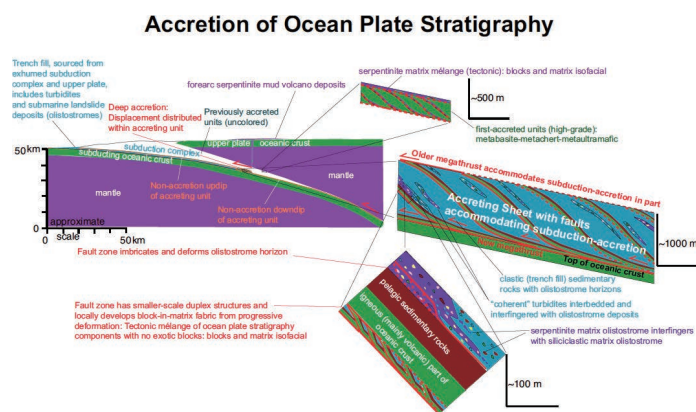


Structural context and variation of ocean plate stratigraphy, Franciscan Complex, California: insight into mélangé origins and subduction-accretion processes

John Wakabayashi

[Keywords] Ocean plate stratigraphy, Subduction complex evolution, Subduction megathrust slip accommodation, tectonic and sedimentary mélanges

The transfer (accretion) of materials from a subducting oceanic plate to a subduction-accretionary complex has produced rock assemblages recording the history of the subducted oceanic plate from formation to arrival at the trench. These rock assemblages, comprising oceanic igneous rocks progressively overlain by pelagic sedimentary rocks (chert and/or limestone) and trench-fill clastic sedimentary rocks (mostly sandstone, shale/mudstone), have been called ocean plate stratigraphy (OPS). During accretion of OPS, megathrust slip is accommodated by imbricate faults and penetrative strain, shortening the unit and leading to tectonic repetition of the OPS sequence, whereas OPS accreted at different times are separated by non-accretionary megathrust horizons. The Franciscan subduction complex of California accreted episodically over a period of over 150 million years and incorporated OPS units with a variety of characteristics separated by non-accretionary megathrust horizons. Most Franciscan OPS comprises MORB (mid-ocean-ridge basalt) progressively overlain by chert and trench-fill clastic sedimentary rocks that are composed of variable proportions of turbidites and siliciclastic and serpentinite-matrix olistostromes (sedimentary mélanges). Volumetrically, the trench-fill component predominates in most Franciscan OPS, but some units have a significant component of igneous and pelagic rocks. Ocean island basalt (OIB) overlain by limestone is less common than MORB-chert assemblages, as are abyssal serpentinitized peridotite slabs. The earliest accreted OPS comprises metabasite of supra-subduction zone affinity imbricated with smaller amounts of metaultramafic rocks and metachert, but lacking a clastic component. Most deformation of Franciscan OPS is localized along discrete faults rather than being distributed in the form of penetrative strain. This deformation locally results in block-in-matrix tectonic mélanges, in contrast to the sedimentary mélanges making up part of the clastic OPS component. Such tectonic mélanges may include blocks and matrix derived from the olistostromes. Franciscan subduction and OPS accretion initiated in island arc crust at about 165–170 Ma, after which MORB and OIB were subducted and accreted following a long (tens of mega-ampere) gap with little or no accretion. Following subduction initiation, a ridge crest approached the trench but probably went dormant prior to its subduction (120–125 Ma), after which the subducted oceanic crust became progressively older until about 95 Ma. From 95 Ma, the age of subducted oceanic crust decreased progressively until arrival of the Pacific-Farallon spreading center led to termination of subduction and conversion to a transform plate boundary.



Cross sectional cartoon showing accretion of OPS and the connection between this process and the rock assemblages found in subduction complexes, including different types of mélanges. This schematic also illustrates that olistostromes of serpentinite and/or siliciclastic matrix comprise part of the clastic part of OPS.

The Franciscan subduction complex of California accreted episodically over a period of over 150 million years and incorporated OPS units with a variety of characteristics separated by non-accretionary megathrust horizons. Most Franciscan OPS comprises MORB (mid-ocean-ridge basalt) progressively overlain by chert and trench-fill clastic sedimentary rocks that are composed of variable proportions of turbidites and siliciclastic and serpentinite-matrix olistostromes (sedimentary mélanges). Volumetrically, the trench-fill component predominates in most Franciscan OPS, but some units have a significant component of igneous and pelagic rocks. Ocean island basalt (OIB) overlain by limestone is less common than MORB-chert assemblages, as are abyssal serpentinitized peridotite slabs. The earliest accreted OPS comprises metabasite of supra-subduction zone affinity imbricated with smaller amounts of metaultramafic rocks and metachert, but lacking a clastic component. Most deformation of Franciscan OPS is localized along discrete faults rather than being distributed in the form of penetrative strain. This deformation locally results in block-in-matrix tectonic mélanges, in contrast to the sedimentary mélanges making up part of the clastic OPS component. Such tectonic mélanges may include blocks and matrix derived from the olistostromes. Franciscan subduction and OPS accretion initiated in island arc crust at about 165–170 Ma, after which MORB and OIB were subducted and accreted following a long (tens of mega-ampere) gap with little or no accretion. Following subduction initiation, a ridge crest approached the trench but probably went dormant prior to its subduction (120–125 Ma), after which the subducted oceanic crust became progressively older until about 95 Ma. From 95 Ma, the age of subducted oceanic crust decreased progressively until arrival of the Pacific-Farallon spreading center led to termination of subduction and conversion to a transform plate boundary.



Seismic imaging of slab metamorphism and genesis of intermediate-depth intraslab earthquakes

Hasegawa A, Nakajima J

[Keywords] Internal slab structure, slab metamorphism, dehydration-related embrittlement, intermediate-depth earthquake, intraslab earthquake, earthquake generation mechanism, subduction zone

We review studies of intermediate-depth seismicity and seismic imaging of the interior of subducting slabs in relation to slab metamorphism and their implications for the genesis of intermediate-depth earthquakes. Intermediate-depth events form a double seismic zone in the depth range of c. 40–180 km, which occur only at locations where hydrous minerals are present, and are particularly concentrated along dehydration reaction boundaries. Recent studies have revealed detailed spatial distributions of these events and a close relationship with slab metamorphism. Pressure–temperature paths of the crust for cold slabs encounter facies boundaries with large H₂O production rates and positive total volume change, which are expected to cause highly active seismicity near the facies boundaries. A belt of upper-plane seismicity in the crust nearly parallel to 80–90 km depth contours of the slab surface has been detected in the cold Pacific slab beneath eastern Japan, and is probably caused by slab crust dehydration with a large H₂O production rate. A seismic low-velocity layer in the slab crust persists down to the depth of this upper-plane seismic belt, which provides evidence for phase transformation of dehydration at this depth. Similar low-velocity subducting crust closely related with intraslab seismicity has been detected in several other subduction zones. Seismic tomography studies in NE Japan and northern Chile also revealed the presence of a P-wave low-velocity layer along the lower plane of a double seismic zone. However, in contrast to predictions based on the serpentinized mantle, S-wave velocity along this layer is not low. Seismic anisotropy and pore aspect ratio may play a role in generating this unique structure. Although further validation is required, observations of these distinct low P-wave velocities along the lower seismic plane suggest the presence of hydrated rocks or fluids within that layer. These observations support the hypothesis that dehydration-derived H₂O causes intermediate-depth intraslab earthquakes. However, it is possible that dual mechanisms generate these earthquakes; the initiation of earthquake rupture may be caused by local excess pore pressure from H₂O, and subsequent ruptures may propagate through thermal shear instability. In either case, slab-derived H₂O plays an important role in generating intermediate-depth events.

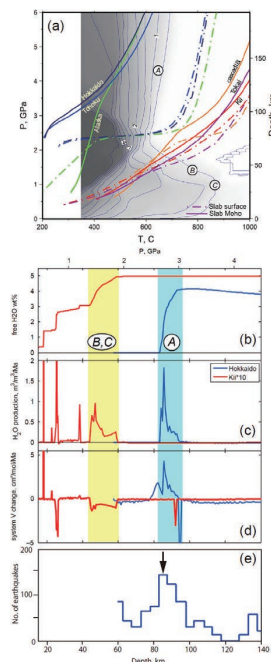


Fig. 1 (a) P–T paths of the subducting crust for six subduction zones. Shading shows maximum H₂O contents in wt%. (b) Accumulated dehydration-derived H₂O content in wt%, (c) rate of H₂O production and (d) total system (solid + H₂O) volume for Hokkaido (blue lines) as a representative cold slab, and for Kii (red lines) as a representative warm slab. In (c), Kii is scaled by a factor of 10. (e) Frequency of upper-plane earthquakes beneath central Hokkaido as a function of depth.

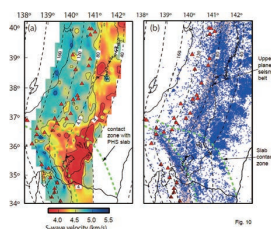


Fig. 2 (a) S-wave velocity distribution and (b) earthquake hypocenters within the crust of the Pacific slab. A belt of upper-plane seismicity is shown in pink. Broken black curves denote iso-depth contours of the upper plate surface. The slab–slab contact zone between the Pacific and Philippine Sea slabs is enclosed by two green broken curves.

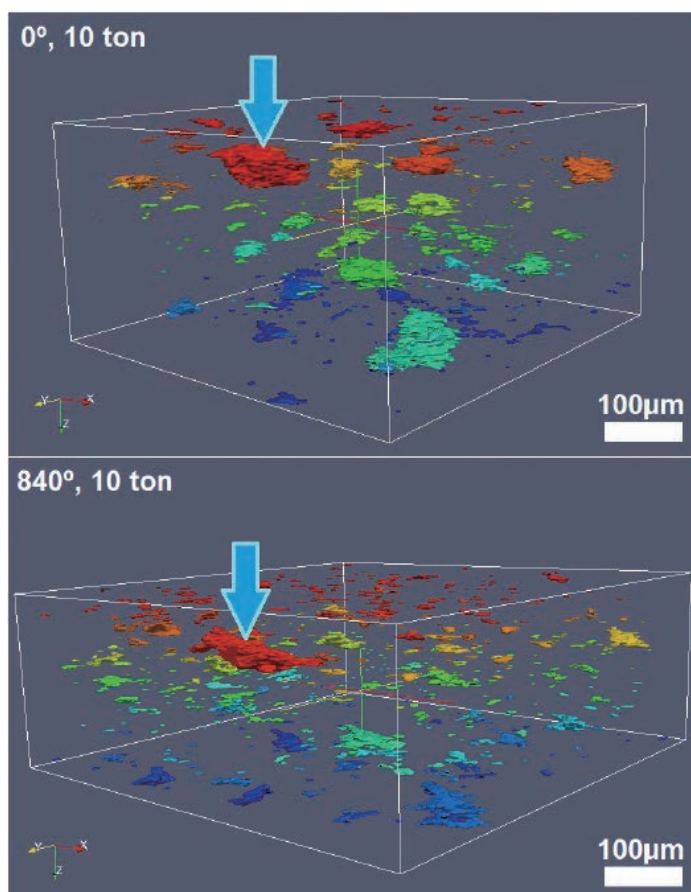


Imaging in 3D under pressure: a decade of high-pressure X-ray microtomography development at GSECARS

Yu T, Wang Y, Rivers M L

[Keywords] High pressure, Tomography, Synchrotron, Density, Rotation, Shear, Non-crystalline, Elasticity

The high-pressure X-ray microtomography (HPXMT) apparatus has been operating at the GeoSoilEnviroCARS (GSECARS) bending magnet beamline at the Advanced Photon Source since 2005. By combining the powerful synchrotron X-ray source and fast switching between white (for X-ray diffraction) and monochromatic (for absorption imaging) modes, this technique provides the high-pressure community with a unique opportunity to image the three-dimensional volume, texture, and microstructure of materials under high pressure and temperature. The ability to shear the sample with unlimited strain by twisting the two opposed anvils in the apparatus allows shear deformation studies under extreme pressure and temperature to be performed. HPXMT is a powerful tool for studying the physical properties of both crystalline and non-crystalline materials under high pressure and high temperature. Over the past 10 years, continuous effort has been put into technical development, modifications to improve the overall performance, and additional probing techniques to meet users' needs. Here, we present an up-to-date report on the HPXMT system, a brief review of some of its many exciting scientific applications, and a discussion of future developments.



Evolution of FeS melt distribution in the olivine matrix by shear deformation.



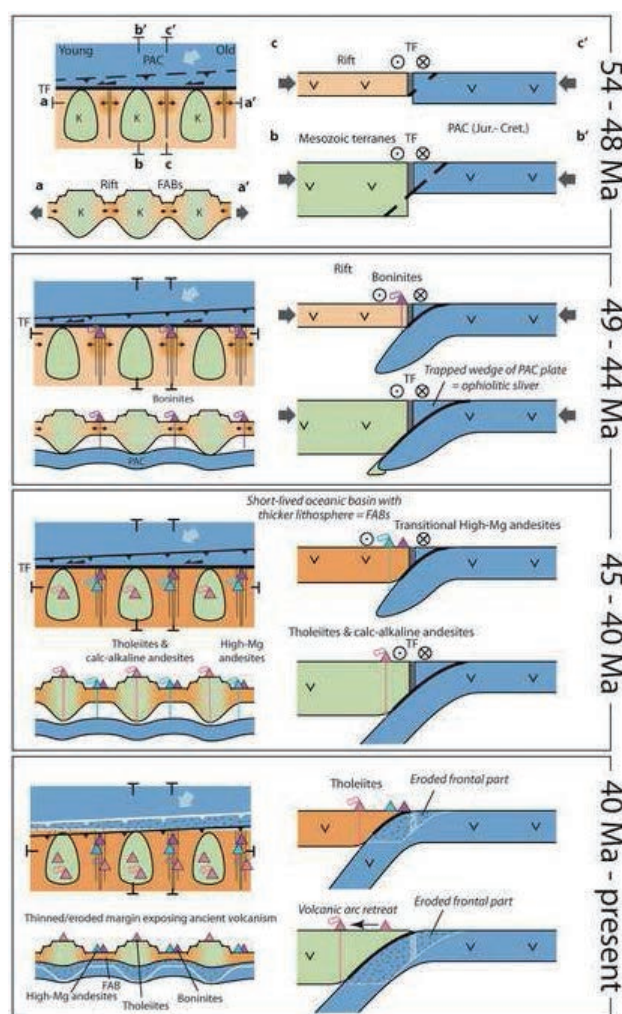
Philippine Sea Plate inception, evolution and consumption with special emphasis on the early stages of Izu-Bonin-Mariana subduction

Lallemand S

[Keywords] Philippine Sea Plate, Izu-Bonin-Mariana, subduction initiation, boninite, fore-arc basalt, serpentinite mud volcano, back-arc basin, transform fault, arc terrane, plume-ridge interaction

We compiled the most relevant data acquired throughout the Philippine Sea Plate (PSP) from the early expeditions to the most recent. We also analyzed the various explanatory models in light of this updated dataset. The following main conclusions are discussed in this study.

(1) The Izanagi slab detachment beneath the East Asia margin around 60–55 Ma likely triggered the Okidaito plume occurrence, Mesozoic proto-PSP splitting, shortening and then failure across the paleo-transform boundary between the proto-PSP and the Pacific Plate, Izu-Bonin-Mariana subduction initiation and ultimately PSP inception. (2) The initial splitting phase of the composite proto-PSP under the plume influence at ~54–48 Ma led to the formation of the long-lived West Philippine Basin and short-lived oceanic basins, part of whose crust has been ambiguously called “fore-arc basalts” (FABs). (3) Shortening across the paleo-transform boundary evolved into thrusting within the Pacific Plate at ~52–50 Ma, allowing it to subduct beneath the newly formed PSP, which was composed of an alternance of thick Mesozoic terranes and thin oceanic lithosphere. (4) The first magmas rising from the shallow mantle corner, after being hydrated by the subducting Pacific crust beneath the young oceanic crust near the upper plate spreading centers at ~49–48 Ma were boninites. Both the so-called FABs and the boninites formed at a significant distance from the incipient trench, not in a fore-arc position as previously claimed. The magmas erupted for 15 m.y. in some places, probably near the intersections between back-arc spreading centers and the arc. (5) As the Pacific crust reached greater depths and the oceanic basins cooled and thickened at ~44–45 Ma, the composition of the lavas evolved into high-Mg andesites and then arc tholeiites and calc-alkaline andesites. (6) Tectonic erosion processes removed about 150–200 km of frontal margin during the Neogene, consuming most or all of the Pacific ophiolite initially accreted to the PSP. The result was exposure of the FABs, boninites, and early volcanics that are near the trench today. (7) Serpentinite mud volcanoes observed in the Mariana fore-arc may have formed above the remnants of the paleo-transform boundary between the proto-PSP and the Pacific Plate.



Schematic tectono-magmatic model of IBM subduction initiation and early evolution. Special emphasis has been done on the geodynamic context of various magma1 eruptions. The white lines in stage “40 Ma - present” represent the former positions of plate boundaries or the base of the upper plate in stage “45-40 Ma”.

TF = transform fault, PAC = Pacific, FAB = Forearc basalts



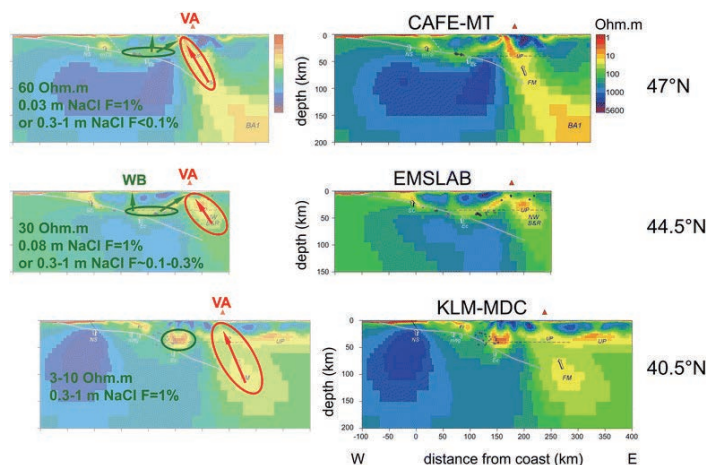
Mantle hydration and Cl-rich fluids in the subduction forearc

Reynard B

[Keywords] Subduction, Fluids, Forearc mantle, Salinity, Chlorine

In the forearc region, aqueous fluids are released from the subducting slab at a rate depending on its thermal state. Escaping fluids tend to rise vertically unless they meet permeability barriers such as the deformed plate interface or the Moho of the overriding plate. Channeling of fluids along the plate interface and Moho may result in fluid overpressure in the oceanic crust, precipitation of quartz from fluids, and low Poisson ratio areas associated with tremors. Above the subducting plate, the forearc mantle wedge is the place of intense reactions between dehydration fluids from the subducting slab and ultramafic rocks leading to extensive serpentinization. The plate interface is mechanically decoupled, most likely in relation to serpentinization, thereby isolating the forearc mantle wedge from convection as a cold, potentially serpentinized and buoyant, body. Geophysical studies are unique probes to the interactions between fluids and rocks in the forearc mantle, and experimental constraints on rock properties allow inferring fluid migration and fluid-rock reactions from geophysical data.

Seismic velocities reveal a high degree of serpentinization of the forearc mantle in hot subduction zones, and little serpentinization in the coldest subduction zones because the warmer the subduction zone, the higher the amount of water released by dehydration of hydrothermally altered oceanic lithosphere. Interpretation of seismic data from petrophysical constrain is limited by complex effects due to anisotropy that needs to be assessed both in the analysis and interpretation of seismic data. Electrical conductivity increases with increasing fluid content and temperature of the subduction. However, the forearc mantle of Northern Cascadia, the hottest subduction zone where extensive serpentinization was first demonstrated, shows only modest electrical conductivity. Electrical conductivity may vary not only with the thermal state of the subduction zone, but also with time for a given thermal state through variations of fluid salinity. High-Cl fluids produced by serpentinization can mix with the source rocks of the volcanic arc and explain geochemical signatures of primitive magma inclusions. Signature of deep high-Cl fluids was also identified in forearc hot springs. These observations suggest the existence of fluid circulations between the forearc mantle and the hot spring hydrothermal system or the volcanic arc. Such circulations are also evidenced by recent magnetotelluric profiles.



Potential location of high-salinity fluids in the forearc mantle and pathways of mixing with hot springs and the volcanic arc. Magnetotelluric profiles in the Cascadia subduction (Wannamaker, et al. 2014) are shown on the right and are interpreted on the left. The southernmost section shows the highest conductivity in the forearc (green ellipse) that is interpreted as up to 1 m NaCl fluids using diagrams in Fig. 2. Lower forearc conductivities (green ellipses) on the other two sections indicate dilution by more than one order of magnitude by low-salinity dehydration fluids from the slab or a decrease by more than one order of magnitude of the fluid fraction. This is attributed drainage to shallow aquifers above the forearc region (e. g., the Willamette basin in Oregon, WB) or to the volcanic arc (VA) region (green arrows). High-conductivity regions further east are ascribed to melt-rich regions under the volcanic arc (red ellipses)

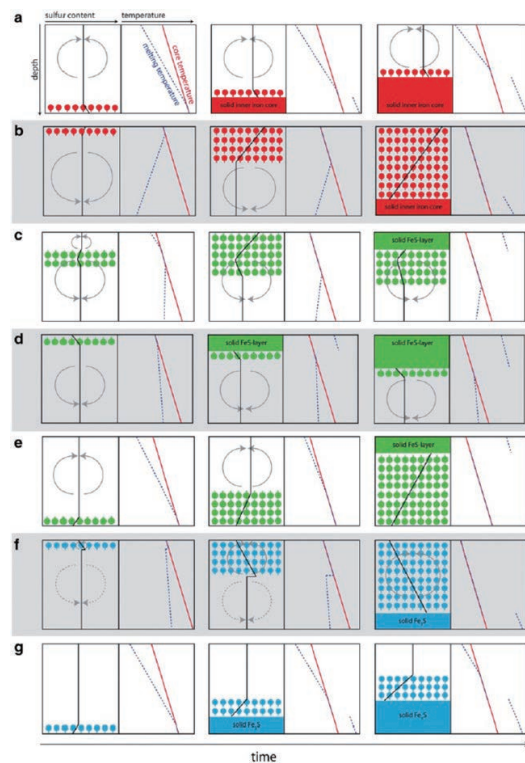


Iron snow, crystal floats, and inner-core growth: modes of core solidification and implications for dynamos in terrestrial planets and moons

Breuer D, Rueckriemen T, Spohn T

[Keywords] Core crystallization, Dynamo generation, Iron snow, Terrestrial planets, Thermal evolution

Recent planetary space missions, new experimental data, and advanced numerical techniques have helped to improve our understanding of the deep interiors of the terrestrial planets and moons. In the present review, we summarize recent insights into the state and composition of their iron (Fe)-rich cores, as well as recent findings about the magnetic field evolution of Mercury, the Moon, Mars, and Ganymede. Crystallizing processes in iron-rich cores that differ from the classical Earth case (i.e., Fe snow and iron sulfide (FeS) crystallization) have been identified and found to be important in the cores of terrestrial bodies. The Fe snow regime occurs at pressures lower than that in the Earth's core on the iron-rich side of the eutectic, where iron freezes first close to the core–mantle boundary rather than in the center. FeS crystallization, instead, occurs on the sulfur-rich side of the eutectic. Depending on the core temperature profile and the pressure range considered, FeS crystallizes either in the core center or close to the core–mantle boundary. The consequences of the various crystallizing mechanisms for core dynamics and magnetic field generation are discussed. For the Moon, revised paleomagnetic data obtained with advanced techniques suggest a peculiar history of its internal dynamo, with an early strong field persisting between 4.25 and 3.5 Ga, and subsequently a much weaker field. In addition, the long-lasting dynamo and the possible presence of an inner core, as inferred from a revised interpretation of Apollo seismic data, suggest core crystallization as a viable process of magnetic field generation for a substantial period during lunar evolution. The present-day magnetic fields of Mercury and Ganymede (if they occur on the iron-rich side of the Fe–FeS eutectic) and the related dynamo action are likely generated in the Fe snow regime and seem to be recent features. An earlier dynamo in Mercury would have been powered differently. For Mercury, MESSENGER data further suggest core formation under reducing conditions that may have resulted in an Fe–S–Si composition, further complicating the core crystallization process. Mars, with its early and strong paleo-field, likely has not yet started to freeze out an inner iron core.



Crystallization scenarios in the Fe–FeS system. **a** Earth-like, Fe-rich inner core grows from the center. Sulfur is enriched in the outer core and drives chemical convection. **b** Iron snow forms at the CMB, sinks, and remelts at depth and drives chemical convection. The stable snow zone grows in time. When it reaches the center, an inner solid core will form. **c** Floating FeS crystals form a stable zone growing toward the CMB where eventually a solid FeS layer will form. The fluid below is enriched in iron and unstable to convection. **d** A solid FeS layer grows from the CMB. Expulsion of Fe results in chemical convection in the fluid below as in (c). **e** FeS crystals rise from the center and remelts at lower depths. The liquid above the FeS zone is convectively unstable. When the FeS crystal zone reaches the CMB, a solid FeS layer will form. **f** Fe₃S snow forms at the CMB and the chemically unstable snow zone grows until it comprises the entire core where a solid Fe₃S inner core will form. The layer below is chemically homogeneous but may convect thermally. **g** A solid Fe₃S inner core grows with time without the release of chemical buoyancy to the outer core and convection above. *Red, green, and blue dots* indicate solid iron, solid FeS, and Fe₃S, respectively. *Short dashes* show the direction of sinking or rising. *Red solid lines* are the core temperature, *blue dashed lines* the core melting temperature, and *black solid lines* the concentration of sulfur, respectively. *Solid arrows* indicate chemical and *dashed arrows* thermal convection, respectively. For further explanation, see text.

Published: 2015/11/16

<https://doi.org/10.1186/s40645-015-0069-y>



Liquid Sodium Models of the Earth's Core

Adams M M, Stone D R, Zimmerman D S, Lathrop D P

[Keywords] Magnetic dynamos, Fluid experiments, Geodynamo, Magnetic induction, Zonal flows, Turbulence, Experimental fluid dynamos, Spherical Couette flow

Our understanding of the dynamics of the Earth's core can be advanced by a combination of observation, experiments, and simulations. A crucial aspect of the core is the interplay between the flow of the conducting liquid and the magnetic field this flow sustains via dynamo action. This non-linear interaction, and the presence of turbulence in the flow, precludes direct numerical simulation of the system with realistic turbulence. Thus, in addition to simulations and observations (both seismological and geomagnetic), experiments can contribute insight into the core dynamics. Liquid sodium laboratory experiments can serve as models of the Earth's core with the key ingredients of conducting fluid, turbulent flow, and overall rotation, and can also approximate the geometry of the core. By accessing regions of parameter space inaccessible to numerical studies, experiments can benchmark simulations and reveal phenomena relevant to the Earth's core and other planetary cores. This review focuses on the particular contribution of liquid sodium spherical Couette devices to this subject matter.



Rendering of the 3 m experiment. The inner sphere and the outer spherical shell can be driven independently by their two respective motors (*top*). Liquid sodium serves as the working fluid for hydromagnetic experiments

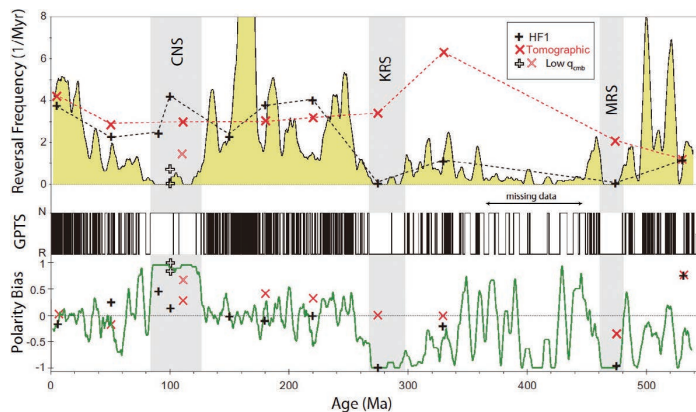


Towards more realistic core-mantle boundary heat flux patterns: a source of diversity in planetary dynamos

Amit H, Choblet G, Olson P, Monteux J, Deschamps F, Langlais B, Tobie G

[Keywords] Magnetic field, Dynamo, Core-mantle boundary, Heat flux

Mantle control on planetary dynamos is often studied by imposing heterogeneous core-mantle boundary (CMB) heat flux patterns on the outer boundary of numerical dynamo simulations. These patterns typically enter two main categories: Either they are proportional to seismic tomography models of Earth's lowermost mantle to simulate realistic conditions, or they are represented by single spherical harmonics for fundamental physical understanding. However, in reality the dynamics in the lower mantle is much more complicated and these CMB heat flux models are most likely oversimplified. Here we term *alternative* any CMB heat flux pattern imposed on numerical dynamos that does not fall into these two categories, and instead attempts to account for additional complexity in the lower mantle. We review papers that attempted to explain various dynamo-related observations by imposing alternative CMB heat flux patterns on their dynamo models. For present-day Earth, the alternative patterns reflect non-thermal contributions to seismic anomalies or sharp features not resolved by global tomography models. Time-dependent mantle convection is invoked for capturing past conditions on Earth's CMB. For Mars, alternative patterns account for localized heating by a giant impact or a mantle plume. Recovered geodynamo-related observations include persistent morphological features of present-day core convection and the geomagnetic field as well as the variability in the geomagnetic reversal frequency over the past several hundred Myr. On Mars the models aim at explaining the demise of the paleodynamo or the hemispheric crustal magnetic dichotomy. We report the main results of these studies, discuss their geophysical implications, and speculate on some future prospects.



Top: Geomagnetic reversal frequency (yellow and barcode below) based on the Geomagnetic Polarity Time Scale (GPTS) database vs. reversal frequency in dynamo models with time-dependent CMB heat flux (black pluses) and fixed present-day tomographic pattern (red crosses). The Creteaceous Normal Superchron (CNS), Kiaman Reversed Superchron (KRS) and Moyero Reversed Superchron (MRS) are grey shaded.

Bottom: Polarity bias, i.e. the difference between time spent in normal and reversed polarities normalized by their sum.



Sound velocity of hcp-Fe at high pressure: experimental constraints, extrapolations and comparison with seismic models

Antonangeli D, Ohtani E

[Keywords] Sound velocity measurements, High pressure, hcp-Fe, Extrapolation schemes, Earth's inner core, Comparison with seismic models

Determining the sound velocity of iron under extreme thermodynamic conditions is essential for a proper interpretation of seismic observations of the Earth's core but is experimentally challenging. Here, we review techniques and methodologies used to measure sound velocities in metals at megabar pressures, with specific focus on the compressional sound velocity of hexagonal close-packed iron. A critical comparison of literature results, coherently analyzed using consistent metrology (pressure scale, equation of state), allows us to propose reference relations for the pressure and density dependence of the compressional velocity of hexagonal close-packed iron at ambient temperature. This provides a key base line upon which to add complexity, including high-temperature effects, pre-melting effects, effects of nickel and/or light element incorporation, necessary for an accurate comparison with seismic models, and ultimately to constrain Earth's inner core composition.

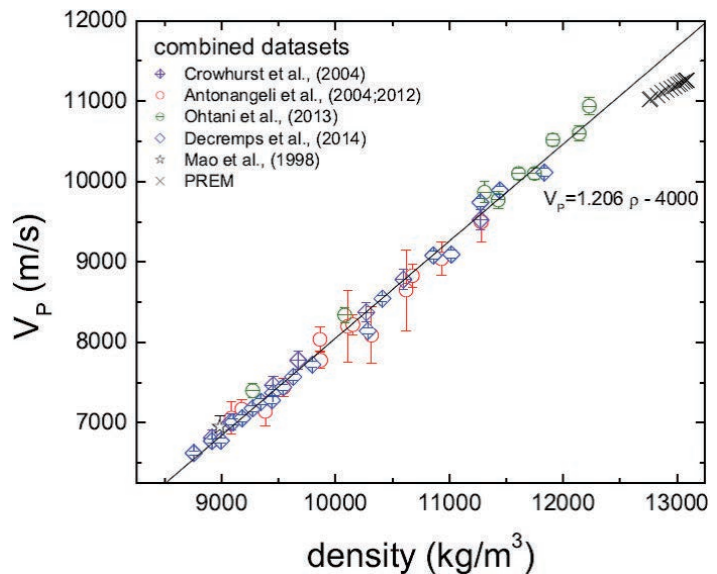


Figure 1: Various previous experimental data on sound velocity and density of hcp-Fe are corrected based on the same pressure scale and the equation of state of hcp-Fe. Most of previous data are consistent with each other.

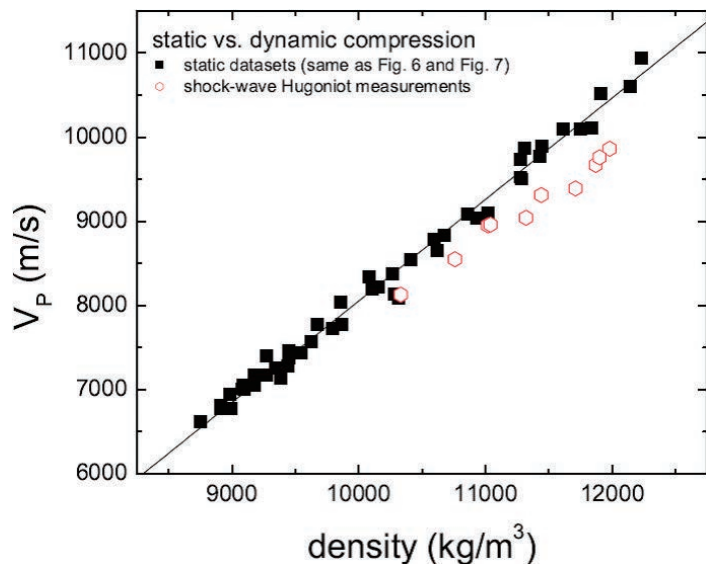


Figure 2: Compressional sound velocity as a function of density under static compression at 300 K is compared with the shock wave data along Hugoniot. The temperature effect on the Birch's law is clearly observed in this figure.



Earthquake faulting in subduction zones: insights from fault rocks in accretionary prisms

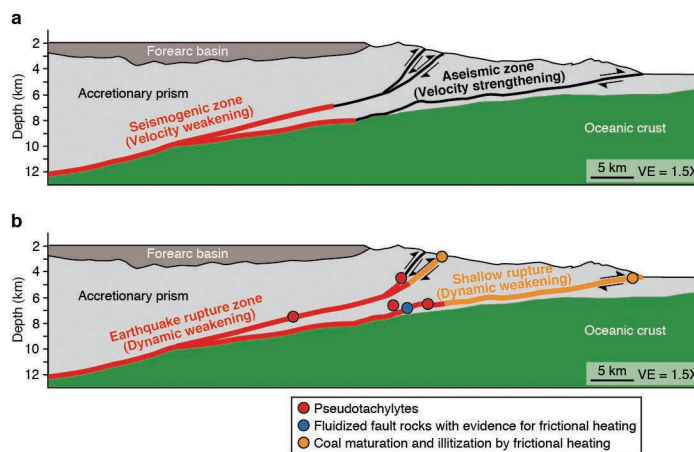
Ujiie K, Kimura G

[Keywords] Subduction earthquake, Accretionary prism, Fault rock, NanTroSEIZE

Subduction earthquakes on plate-boundary megathrusts accommodate most of the global seismic moment release, frequently resulting in devastating damage by ground shaking and tsunamis. As many earthquakes occur in deep-sea regions, the dynamics of earthquake faulting in subduction zones is poorly understood. However, the Integrated Ocean Drilling Program (IODP) Nankai Trough Seismogenic Zone Experiment (NanTroSEIZE) and fault rock studies in accretionary prisms exhumed from source depths of subduction earthquakes have greatly improved our understanding of earthquake faulting in subduction zones. Here, we review key advances that have been made over the last decade in the studies of fault rocks and in

laboratory experiments using fault zone materials, with a particular focus on the Nankai Trough subduction zone and its on-land analog, the Shimanto accretionary complex in Japan. New insights into earthquake faulting in subduction zones are summarized in terms of the following: (1) the occurrence of seismic slip along velocity-strengthening materials both at shallow and deep depths; (2) dynamic weakening of faults by melt lubrication and fluidization, and possible factors controlling coseismic deformation mechanisms; (3) fluid-rock interactions and mineralogical and geochemical changes during earthquakes; and (4) geological and experimental aspects of slow earthquakes.

Ujiie and Kimura, Fig. 17



Concept of earthquake faulting in subduction zones shown in schematic profile of the Nankai accretionary prism.



Published: 2014/6/3

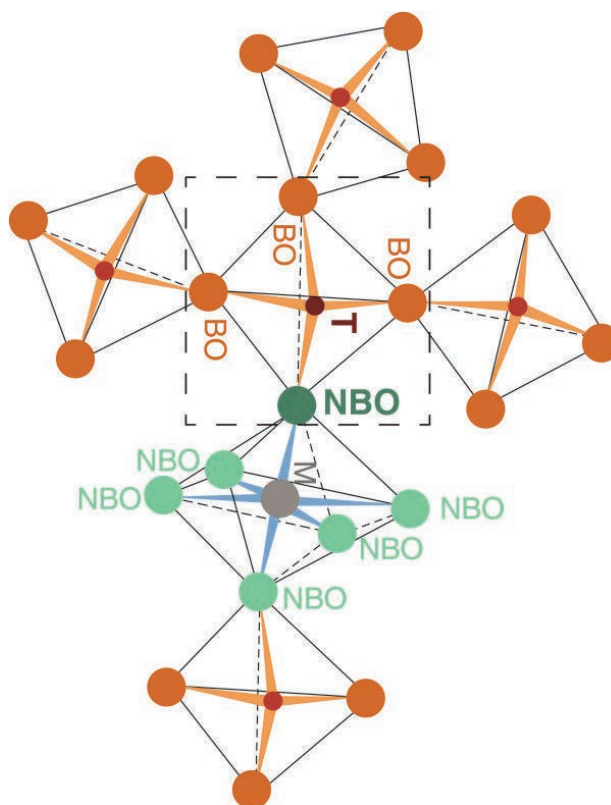
<https://doi.org/10.1186/2197-4284-1-7>

Water-melt interaction in hydrous magmatic systems at high temperature and pressure

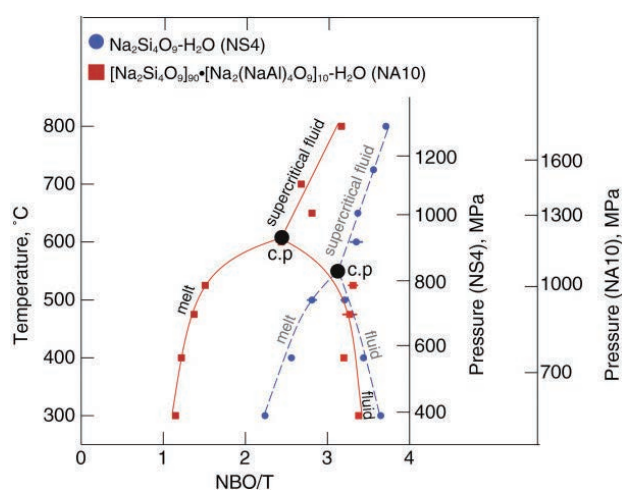
Bjorn Mysen

[Keywords] Hydrous magma, Aqueous fluid, Melt structure, Viscosity, Isotope partitioning, Partial melting, Water solubility, Silicate solubility, Glass transition, Solution mechanism

Experimental data on the structure and properties of melts and fluids relevant to water-melt interaction in hydrous magmatic systems in the Earth's interior have been reviewed. Complex relationships between water solubility in melts and their bulk composition [Al/Si-ratio, metal oxide/(Al + Si) and electron properties of metal cations] explain why water solubility in felsic magmas such as those of rhyolite and andesite composition is significantly greater than the water solubility in basalt melts. The silicate solubility in aqueous fluid is also significantly dependent on composition with metal oxide/(Al + Si) and electron properties of the metal cations, the dominant variables. Hydrogen bonding is not important in hydrous fluids and melts at temperatures above 500°C to 550°C and does not, therefore, play a role in hydrous magmatic systems. The properties of hydrous melts and aqueous solutions are governed by how the silicate speciation (Q^n species, where n is the number of bridging oxygen in an individual species) varies with bulk composition, silicate composition, temperature, and pressure. The reactions that describe the interactions are similar in melts, fluids, and supercritical fluids. The degree of melt polymerization caused by dissolved water varies with melt composition and total water content. Silicate- and alkali-rich felsic magmatic melts are more sensitive to water content than more mafic magmas. Transport and configurational properties of hydrous magmatic melts can be modeled with the aid of the Q^n speciation variations. Liquidus and melting phase relations of hydrous systems also can be described in such terms, as can minor and trace element partition coefficients. Stable isotope fractionation (e.g., D/H) can also be rationalized in this manner. Critical to these latter observations is the high silicate concentration in aqueous fluids. These components can enhance solubility of minor and trace elements by orders of magnitude and change the speciation of H and D complexes so that their fractionation factors change quite significantly. Data from pure silicate-H₂O systems cannot be employed for these purposes.



Schematic representation of the concept of bridging (BO) and nonbridging (NBO) oxygen



Degree of silicate polymerization, NBO/T. In silicate in hydrous melts, silicate-saturated aqueous fluid, and supercritical fluid in a hydrous Na-aluminosilicate system

Published: 2014/4/22

<https://doi.org/10.1186/2197-4284-1-4>

Review

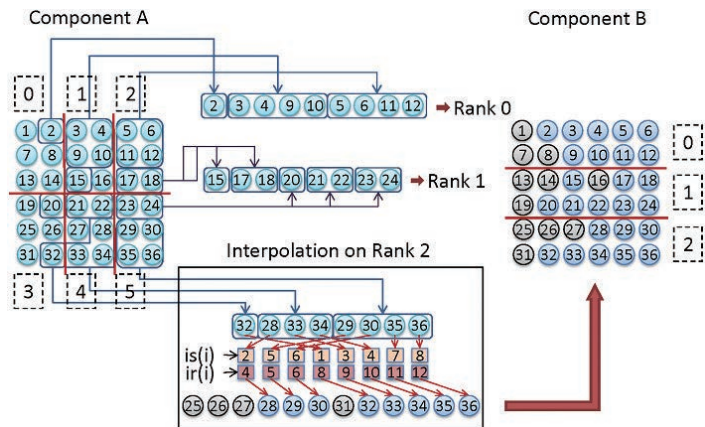
Interdisciplinary research

Coupling library Jcup3: its philosophy and application

Arakawa T, Inoue T, Yashiro H, Satoh M

[Keywords] Earth system modeling, Coupler, Coupled simulation

In this paper, we describe the design of the coupling library, Jcup, and report its various applications, including the coupling between global atmospheric and oceanic models of different grid systems. Jcup is a software library mainly focused on weather/climate models and was developed for coupling the components of various models. Jcup has the flexibility to be applied to an unspecified number of components of earth system models. To achieve a high level of safety and versatility, we classified the processes of the general coupling software into processes that change the value of the data and those that do not and placed the former outside of the program and under the control of the user. Consequently, Jcup exhibits two features: (1) the correspondence relationship between grid indexes is used as input information, and (2) the user can implement an arbitrary interpolation code. Jcup was applied to atmosphere-ocean coupling, IO component coupling, and the coupling between the seismic model and structure model, and the validity and usefulness of the design were demonstrated.



Data exchange diagram. The gray circles represent masked value. Therefore, only the grid point value indicated by the blue circle is passed from Component A to Component B.

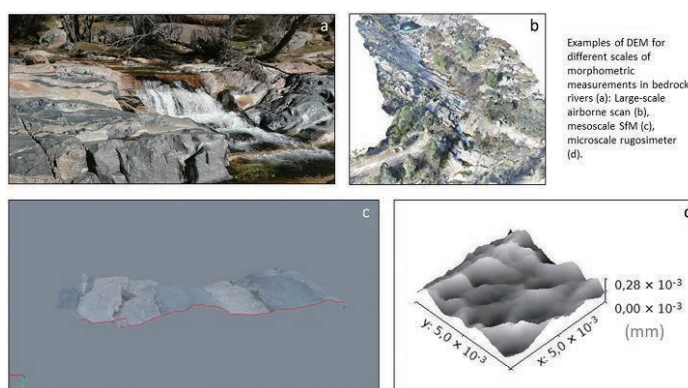


Morphometric measurements of bedrock rivers at different spatial scales and applications to geomorphological heritage research

Gomez-Heras M, Ortega-Becerril JA, Garrote J, Fort R, Lopez-Gonzalez L

[Keywords] Bedrock rivers, Geomorphological heritage, Non-destructive techniques, Digital elevation models, LiDAR, SfM, Photogrammetry, Microroughness

Morphometric characterisation is particularly relevant in the study of geomorphological heritage. 3D modelling techniques have been proven as very useful tools to recognise, characterise and valorise geomorphosites. Bedrock rivers account for one of the most outstanding aspects within geomorphological heritage due to the amount of distinctive and attractive geomorphological features associated to them and the high preservation of sculpted forms. Digital elevation models (DEMs) have made it increasingly possible to establish accurate morphometric indices and establish clearer connections between forms and processes. This paper reviews different methodologies to obtain DEMs on bedrock rivers. This review goes from DEM analysis at multiple spatial scales to introduce optical microrugosimeter as the latest technical development to facilitate micromorphometric analysis. Micromorphometric analysis opens the scope for improving the knowledge we have on trans-scale issues in bedrock rivers. Micromorphometric analysis also opens a new layer of information that enriches the public's valuation of geodiversity of geomorphosites by increasing its didactic and interpretative potential.



(a) Example of DEM for different scales of morphometric measurements in bedrock rivers, (b) Large-scale airborne scan, (c) mesoscale SfM, (d) microscale rugosimeter

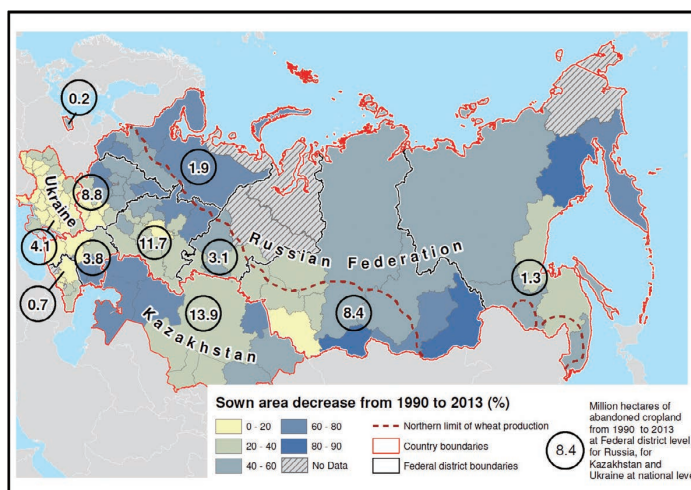


Northern Eurasia Future Initiative (NEFI): facing the challenges and pathways of global change in the twenty-first century

Pavel Groisman et al.

[Keywords] Environmental Changes, Northern Eurasia, Ecosystems dynamics, Terrestrial water cycle, Cryosphere retreat, Extreme and inclement environmental conditions, Sustainable development, Land-cover and land-use change, Integrated assessment models for decision-makers

During the past several decades, the Earth system has changed significantly, especially across Northern Eurasia. Changes in the socio-economic conditions of the larger countries in the region have also resulted in a variety of regional environmental changes that can have global consequences. The Northern Eurasia Future Initiative (NEFI) has been designed as an essential continuation of the Northern Eurasia Earth Science Partnership Initiative (NEESPI), which was launched in 2004. NEESPI sought to elucidate all aspects of ongoing environmental change, to inform societies and, thus, to better prepare societies for future developments. A key principle of NEFI is that these developments must now be secured through science-based strategies co-designed with regional decision-makers to lead their societies to prosperity in the face of environmental and institutional challenges. NEESPI scientific research, data, and models have created a solid knowledge base to support the NEFI program. This paper presents the NEFI research vision consensus based on that knowledge. It provides the reader with samples of recent accomplishments in regional studies and formulates new NEFI science questions. To address these questions, nine research foci are identified and their selections are briefly justified. These foci include warming of the Arctic; changing frequency, pattern, and intensity of extreme and inclement environmental conditions; retreat of the cryosphere; changes in terrestrial water cycles; changes in the biosphere; pressures on land use; changes in infrastructure; societal actions in response to environmental change; and quantification of Northern Eurasia's role in the global Earth system. Powerful feedbacks between the Earth and human systems in Northern Eurasia (e.g., megafires, droughts, depletion of the cryosphere essential for water supply, retreat of sea ice) result from past and current human activities (e.g., large-scale water withdrawals, land use, and governance change) and potentially restrict or provide new opportunities for future human activities. Therefore, we propose that integrated assessment models are needed as the final stage of global change assessment. The overarching goal of this NEFI modeling effort will enable evaluation of economic decisions in response to changing environmental conditions and justification of mitigation and adaptation efforts.



Changes in sown areas across the former Soviet Union (Russia, Ukraine, and Kazakhstan) from 1990 to 2013. Areas of abandoned sown areas for this period are 40 Mha in Russia (Rosstat 2016), 5.4 Mha in Ukraine (Ukrstat 2014), and 13 Mha in Kazakhstan (Kazstat 2014).



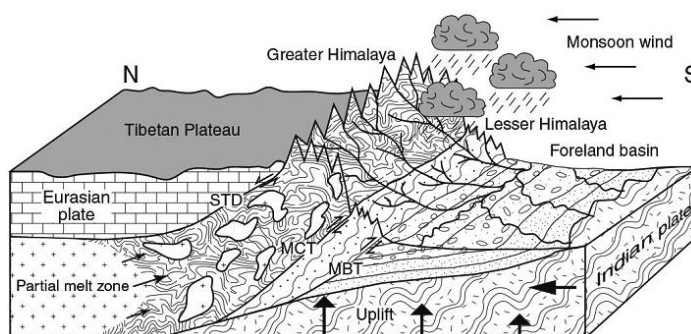
Cenozoic sedimentary records of climate-tectonic coupling in the Western Himalaya

Clift P D

[Keywords] Monsoon, Climate-tectonic, Himalaya, Erosion, Exhumation, Arabian Sea, Foreland basin, Provenance, Geochemistry, Cenozoic, Weathering

Sedimentary archives in the Himalayan foreland basin and Indus submarine fan provide the most detailed records of how changing monsoon strength may have affected erosion and the development of tectonic structures in the western Himalaya during the Neogene. Muscovite Ar-Ar ages show that fast exhumation of the Greater Himalaya was earlier in the west (20–35 Ma) than in the central Himalaya (10–25 Ma), probably driven by progressive lithospheric slab tearing that caused both rock uplift and an intensified summer monsoon to start earlier in the western Himalaya.

Rates of exhumation reduced after ~17 Ma as uplift also slowed, apparently unrelated to climate change. However, further reduction at 6–8 Ma coincided with a time of weakening summer rains, as shown by carbon isotope data from the foreland and hematite-goethite records from ODP Site 730 on the Oman margin. Coming at a time of stronger winds, this drying was linked to global climatic cooling. Weakening of Late Miocene monsoon rains coincided with a southward migration of the ITCZ and faster erosion of the Lesser rather than Greater Himalaya. Unroofing of the Inner Lesser Himalaya, starting after 9 Ma, followed as a consequence of duplex formation enabled by focused erosion, although widespread exposure of that range was delayed until after 6 Ma. Inner Lesser Himalayan exposure, combined with unroofing of the Nanga Parbat Massif, caused a decrease in average ϵ_{Nd} values of Indus River sediment after 5 Ma, rather than large-scale drainage capture.



The correlation between the uplift of the Himalaya-Tibetan Plateau and the Asian monsoon

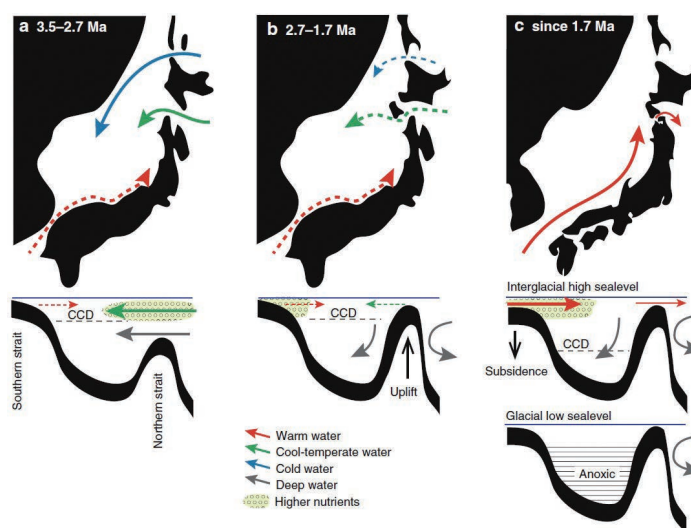


Transitional changes in microfossil assemblages in the Japan Sea from the Late Pliocene to Early Pleistocene related to global climatic and local tectonic events

Itaki T

[Keywords] Radiolaria, Diatom, Calcareous nannofossil, Foraminifera, Ostracoda, Productivity, Paleoceanography, Northern Hemisphere glaciation, Tectonics, Tsushima Warm Current

Many micropaleontological studies based on data from on-land sections, oil wells, and deep-sea drilling cores have provided important information about environmental changes in the Japan Sea that are related to the global climate and the local tectonics of the Japanese Islands. Here, major changes in the microfossil assemblages during the Late Pliocene to Early Pleistocene are reviewed. Late Pliocene (3.5–2.7 Ma) surface-water assemblages were characterized mainly by cold-temperate planktonic flora and fauna (nannofossils, diatoms, radiolarians, and planktonic foraminifera), suggesting that nutrient-rich North Pacific surface waters entered the Japan Sea via northern straits. The common occurrence of Pacific-type deep-water radiolarians during this period also suggests that deep water from the North Pacific entered the Japan Sea via the northern straits, indicating a sill depth >500 m. A weak warm-water influence is recognized along the Japanese coast, suggesting a small inflow of warm water via a southern strait. Nannofossil and sublittoral ostracod assemblages record an abrupt cooling event at 2.75 Ma that correlates with the onset of the Northern Hemisphere glaciation. Subsequently, cold intermediate- and deep-water assemblages of ostracods and radiolarians increased in abundance, suggesting active ventilation and the formation of the Japan Sea Proper Water, associated with a strengthened winter monsoon. Pacific-type deep-water radiolarians also disappeared around 2.75 Ma, which is attributed to the intermittent occurrence of deep anoxic environments and limited migration from the North Pacific, resulting from the near-closure or shallowing of the northern strait by a eustatic fall in sea level and tectonic uplift of northeastern Japan. A notable reduction in primary productivity from 2.3 to 1.3 Ma also suggests that the nutrient supply from the North Pacific was restricted by the near-closure of the northern strait. An increase in the abundance of subtropical surface fauna suggests that the inflow of the Tsushima Warm Current into the Japan Sea via a southern strait began at 1.7 Ma. The opening of the southern strait may have occurred after the subsidence of southwestern Japan.



Schematic maps showing paleogeographic changes in the Japan Sea during three stages. Solid arrows show major inflows of oceanic water, and dashed arrows indicate restricted inflows.

Subsequently, cold intermediate- and deep-water assemblages of ostracods and radiolarians increased in abundance, suggesting active ventilation and the formation of the Japan Sea Proper Water, associated with a strengthened winter monsoon. Pacific-type deep-water radiolarians also disappeared around 2.75 Ma, which is attributed to the intermittent occurrence of deep anoxic environments and limited migration from the North Pacific, resulting from the near-closure or shallowing of the northern strait by a eustatic fall in sea level and tectonic uplift of northeastern Japan. A notable reduction in primary productivity from 2.3 to 1.3 Ma also suggests that the nutrient supply from the North Pacific was restricted by the near-closure of the northern strait. An increase in the abundance of subtropical surface fauna suggests that the inflow of the Tsushima Warm Current into the Japan Sea via a southern strait began at 1.7 Ma. The opening of the southern strait may have occurred after the subsidence of southwestern Japan.

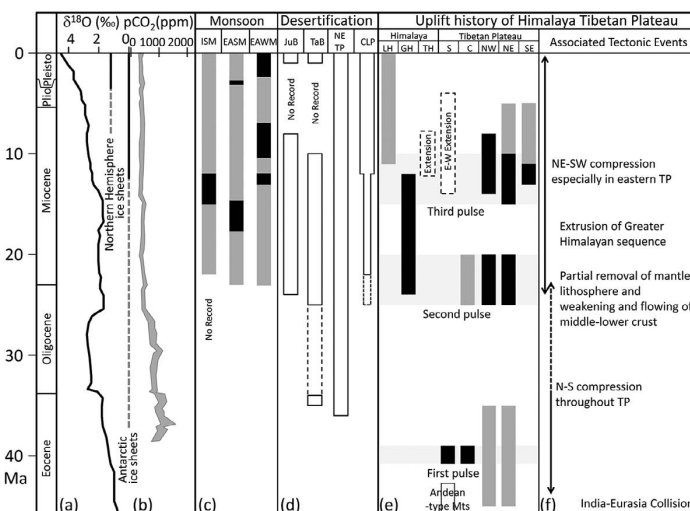


Evolution and variability of the Asian monsoon and its potential linkage with uplift of the Himalaya and Tibetan Plateau

Tada R, Zheng H, Cliff P D

[Keywords] East Asian summer monsoon, East Asian winter monsoon, Indian summer monsoon, Himalaya, Tibetan Plateau, Chinese Loess Plateau, Climate model, Tectonic–climate linkage, Westerly jet, Desertification

In the densely populated region of East Asia, it is important to know the mechanism, scale, and frequency of heavy precipitation brought about during the monsoons and typhoons. However, observational data, which cover only several decades, are insufficient to examine the long-term trend of extreme precipitation and its background mechanism. In humid areas, the transport flux of a suspended detrital material through a river system is known to have an empirical power relationship with precipitation. Thus, the sedimentation flux of a fine detrital material could potentially be used as a proxy for reconstructing past heavy precipitation events. To test the idea that the sedimentation flux of detrital materials records past heavy precipitation events (e.g., typhoons), we focused on the detrital flux estimated from the annually laminated sediment of Lake Suigetsu, central Japan, which is capable of accurately correlating the age of detrital flux with the precipitation record. We first established a precise age model (error within ± 1 year in average) beginning in 1920 A.D. on the basis of varve counting fine-tuned by correlation between event layers with historical floods. The flux of the detrital material ($\text{g}/\text{cm}^2/\text{year}$) was estimated on the basis of Al_2O_3 content (wt%), dry bulk density (g/cm^3), and sedimentation rate (cm/year) calculated from the age model. The detrital flux of background sedimentation showed a weak positive correlation with annual and monthly (June and September) precipitation excluding heavy precipitation that exceeded 100 mm/day. Furthermore, the thickness of instantaneous event layers, which corresponds to several maxima of detrital flux and is correlated with floods that occurred mainly during typhoons, showed a positive relationship with the total amount of precipitation that caused a flood event. This result suggests that the detrital flux maxima (deposition of event layers) record past extreme precipitation events that were likely associated with typhoons that hit the middle part of Honshu Island. Based on this result, the record of typhoon-caused flood events can go back to older period (e.g., last glacial period) on the basis of the occurrence, and thickness, or mass flux of event layers using long sediment cores from Lake Suigetsu.

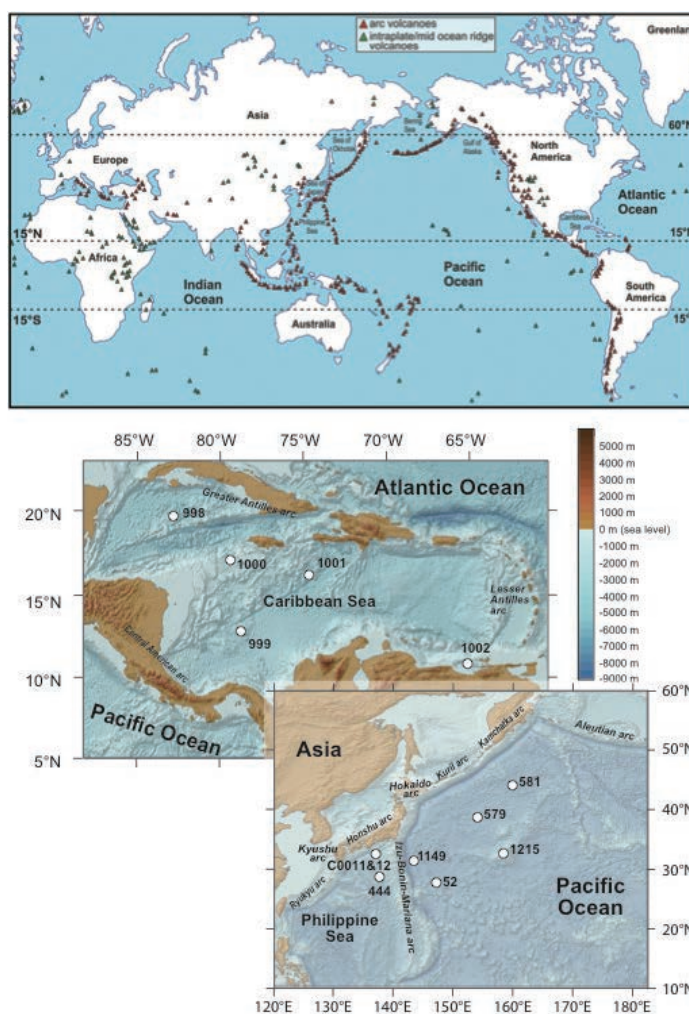


Evolution of Asian monsoons, desertification, HTP uplift, and their relation with global changes during Cenozoic. Temporal changes of a $\delta^{18}\text{O}$ of benthic foraminifera (modified from Zachos et al. 2001) and b pCO_2 (modified from Zhang et al. 2013) are compared with temporal evolution of c Asian monsoons, d desertification, e HTP uplift, and f associated tectonic events. In c and e, gray bars represent weak phases and black bars represent strong phases. In d, JuB and TaB indicate Jungger Basin and Tarim Basin, respectively.



Geochemical approaches to the quantification of dispersed volcanic ash in marine sediment**Scudder R P, Murray R W, Schindlbeck J C, Kutterolf S, Hauff F, Underwood M B, Gwizd S, Lauzon R, McKinley C C****[Keywords]** Dispersed ash, Caribbean Sea, Equatorial Pacific Ocean, Northwest Pacific Ocean, Ash layers, Volcanic eruptions, DSDP, ODP, IODP

Volcanic ash has long been recognized in marine sediment, and given the prevalence of oceanic and continental arc volcanism around the globe in regard to widespread transport of ash, its presence is nearly ubiquitous. However, the presence/absence of very fine-grained ash material, and identification of its composition in particular, is challenging given its broad classification as an “aluminosilicate” component in sediment. Given this challenge, many studies of ash have focused on discrete layers (that is, layers of ash that are of millimeter-to-centimeter or greater thickness, and their respective glass shards) found in sequences at a variety of locations and timescales and how to link their presence with a number of Earth processes. The ash that has been mixed into the bulk sediment, known as dispersed ash, has been relatively unstudied, yet represents a large fraction of the total ash in a given sequence. The application of a combined geochemical and statistical technique has allowed identification of this dispersed ash as part of the original ash contribution to the sediment. In this paper, we summarize the development of these geochemical/statistical techniques and provide case studies from the quantification of dispersed ash in the Caribbean Sea, equatorial Pacific Ocean, and northwest Pacific Ocean. These geochemical studies (and their sedimentological precursors of smear slides) collectively demonstrate that local and regional arc-related ash can be an important component of sedimentary sequences throughout large regions of the ocean.



Top: Global distribution of subaerial volcanoes in different tectonic settings. Map has been modified after <http://d-maps.com> and volcano positions are taken from the Smithsonian Global Volcanism Program (<http://www.volcano.si.edu>).

Bottom: Locations of sites highlighted in this paper. Data from GeoMapApp (<http://www.geomapp.org>); GMRT-Global Multi-Resolution Topography; Ryan et al., 2009)



Sea surface temperature proxies (alkenones, foraminiferal Mg/Ca, and planktonic foraminiferal assemblage) and their implications in the Okinawa Trough

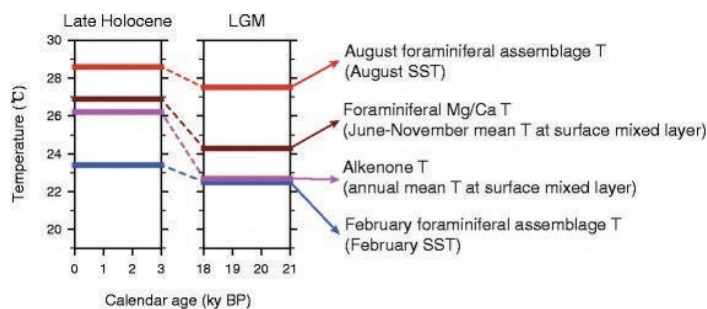
Kim R A, Lee K E, Bae S W

[Keywords] Sea surface temperature, Okinawa Trough, Alkenone, Planktonic foraminiferal Mg/Ca ratio, Planktonic foraminiferal assemblages

We reviewed three sea surface temperature (SST) proxies in the Okinawa Trough (OT): alkenones, planktonic foraminiferal Mg/Ca, and planktonic foraminiferal assemblages. The seasonal and vertical distribution patterns of each proxy-related organism in the water column were reviewed to confirm the applicability of each proxy. In addition, current SSTs (Japan Oceanographic Data Center dataset from 1906 to 2003) were compared with core-top sediment temperatures reconstructed using the proxies.

Temperatures calculated using the alkenone unsaturation index represent annual mean SSTs, and temperatures calculated using Mg/Ca of *Globigerinoides ruber* capture summer to autumn (June–November) SSTs. Core-top August SSTs calculated from planktonic foraminiferal assemblages corresponded well with the observed SSTs, but core-top February temperatures were ~3.6 °C warmer than the observed SSTs. SST proxy estimates from marine sediments dating back to the late Holocene (0–3 cal kyr BP) and the last glacial maximum (18–21 cal kyr BP) were compared. Comparisons between proxy SST estimates show that foraminiferal assemblage-based August SSTs were the warmest. Alkenone-based temperature estimates were lower than Mg/Ca-based temperature estimates, probably because the alkenone-based temperature represents the annual mean temperature, whereas the Mg/Ca-based temperature represents the summer–autumn mean temperature. February assemblage SSTs seem to be greatly affected by the statistical technique and/or database used. These results suggest that seasonality should be considered in past SST reconstruction using alkenone and Mg/Ca in the OT. The planktonic foraminiferal assemblage technique does not appear to be promising with respect to accurately reconstructing past SSTs (especially winter) in the OT. Habitat depth may not be an issue because both alkenone producers and *G. ruber* live at the upper surface mixed layer in the area.

Glacial–interglacial changes in the surface hydrography of the OT reconstructed based on the SST and salinity proxies were also reviewed here. The surface hydrography of the OT has been influenced by changes in the Kuroshio Current and the East Asian monsoon system during the late Quaternary. Comparisons of the hydrography records from the OT with records of stalagmites in China, the Tropical Pacific, and the North Atlantic show that there is a teleconnection between them.



Schematic diagram of SST proxy data in the OT. SST proxy data are given for periods during the late Holocene (0–3 cal kyr BP) and LGM (18–21 cal kyr BP). T indicates temperature.



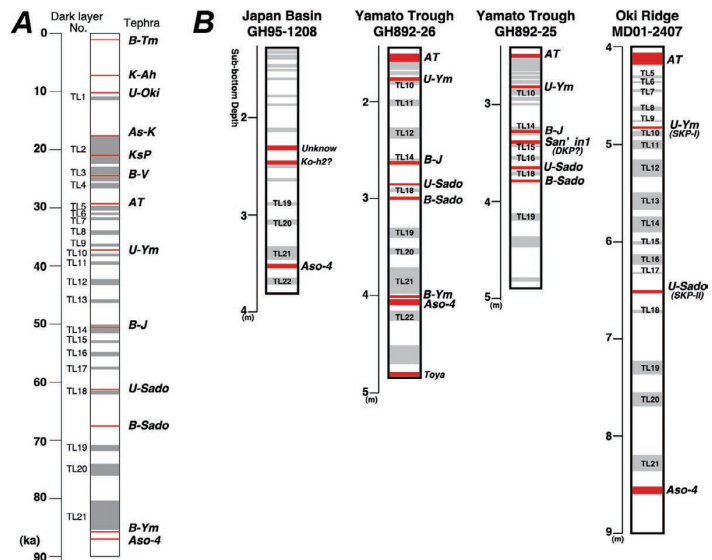
Marine tephra in the Japan Sea sediments as a tool for paleoceanography and paleoclimatology

Ikehara K

[Keywords] Tephra, Key bed, Japan Sea, Stratigraphy, Chronology, Paleoceanography

Tephra is a product of large and explosive volcanic events and can travel thousands of kilometers before deposition. Consequently, tephra deposits are common in terrestrial, lacustrine, marine, and glacial environments. Because tephra deposition is a geologically synchronous event, tephra deposits constitute important isochrones in the Quaternary sequence, not only in Japan but also throughout the northwest Pacific and its marginal seas. As a result, establishing the chronostratigraphic order of tephra deposits is an effective tool for assessing local and regional stratigraphies and for correlating events among sites. For example, tephrostratigraphy can provide precise chronological constraints for other stratigraphic data, such as magneto- and biostratigraphic data. Spatiotemporal variability in the occurrence and geochemistry of tephra

can also be used to trace the magmatic evolution of island arcs and their relationships to regional tectonics. In a paleoclimatic context, tephra deposits allow the correlation of past climate events among terrestrial, lacustrine, and marine environments. Tephrochronology is also a fundamental element used in reconstructing the marine reservoir effect, where the ages of tephra in marine and terrestrial settings are compared. Therefore, tephra is a valuable tool not only in stratigraphy, chronology, and volcanology but also in paleoceanography and paleoclimatology.



Dark-layer stratigraphy and tephra occurrences in the late Quaternary Japan Sea sediments (A) and tephra occurrences in marine sediment cores during MIS 3–5.3 (B)



The Pliocene to Recent History of the Kuroshio and Tsushima Currents: a multi-proxy approach

Gallagher S J, Kitamura A, Iryu Y, Itaki T, Koizumi I, Hoiles P

[Keywords] Kuroshio Current, Tsushima Current, Pliocene, Pleistocene, Holocene, Paleoceanographic proxies, Biogeography, Microfossils, Macrofossils, Geochemistry

The Kuroshio Current is a major western boundary current controlled by the North Pacific Gyre. It brings warm subtropical waters from the Indo-Pacific Warm Pool to Japan exerting a major control on Asian climate. The Tsushima Current is a Kuroshio offshoot transporting warm water into the Japan Sea. Various proxies are used to determine the paleohistory of these currents. Sedimentological proxies such as reefs, bedforms, sediment source and sorting reveal paleocurrent strength and latitude. Proxies such as coral and mollusc assemblages reveal past shelfal current activity. Microfossil assemblages and organic/inorganic geochemical analyses determine paleo-sea surface temperature and salinity histories. Transportation of tropical palynomorphs and migrations of Indo-Pacific species to Japanese waters also reveal paleocurrent activity. The stratigraphic distribution of these proxies suggests the Kuroshio Current reached its present latitude (35 °N) by ~3 Ma when temperatures were 1 to 2 °C lower than present. At this time a weak Tsushima Current broke through Tsushima Strait entering the Japan Sea. Similar oceanic conditions persisted until ~2 Ma when crustal stretching deepened the Tsushima Strait allowing inflow during every interglacial. The onset of stronger interglacial/glacial cycles ~1 Ma was associated with increased North Pacific Gyre and Kuroshio Current intensity. This triggered Ryukyu Reef expansion when reefs reached their present latitude (~31 °N), thereafter the reef front advanced (~31 °N) and retreated (~25 °N) with each cycle. Foraminiferal proxy data suggests eastward deflection of the Kuroshio Current from its present path at 24 °N into the Pacific Ocean due to East Taiwan Channel restriction during the Last Glacial Maximum. Subsequently Kuroshio flow resumed its present trajectory during the Holocene. Ocean modeling and geochemical proxies show that the Kuroshio Current path may have been similar during glacials and interglacials, however the glacial mode of this current remains controversial. Paleohistorical studies form important analogues for current behavior with future climate change, however, there are insufficient studies at present in the region that may be used for this purpose. Modeling of the response of the Kuroshio Current to future global warming reveals that current velocity may increase by up to 0.3 m/sec associated with a northward migration of the Kuroshio Extension.

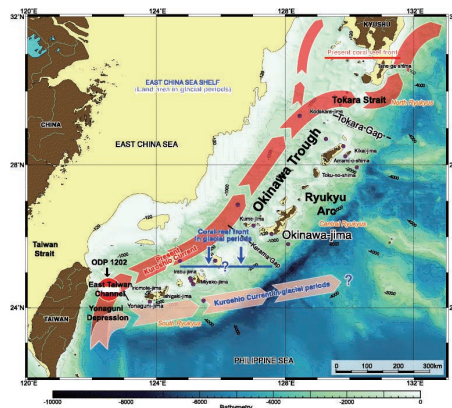


Figure 1: The southern path of the Kuroshio Current showing the inferred extent of the Ryukyu Reefs in glacial and interglacial periods (adapted from Iryu et al. [2006])

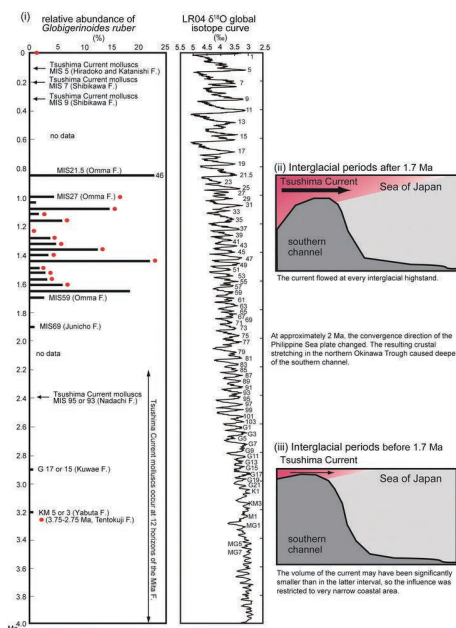
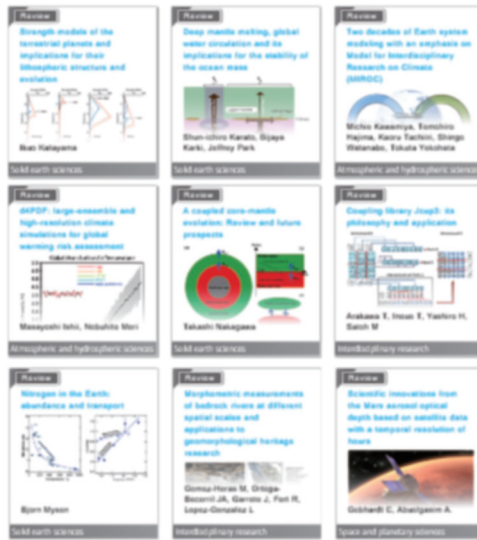


Figure 2: (i) The distribution of *G. ruber* and Tsushima Current molluscs in interglacials of the Omma Formation (adapted from Kitamura and Kimoto [2006]) correlated to the LR04 benthic stack of Lisiecki and Raymo ([2005]). The red dots (1.6 to 1 Ma) are interglacials where migratory Indo-Pacific Warm Pool benthic foraminifera are present (Hoiles et al. [2012]). Red dots at 0 and ~3 Ma are Warm Pool benthic foram ingressions described in Gallagher et al. ([2009]). Reconstructions of the paleogeography of the Tsushima Strait after 1.6 Ma (ii) and prior to 1.7 Ma (iii) adapted from Kitamura and Kimoto ([2006])





Date of Issue: April, 2021